



K.L.E Society's

S.NIJALINGAPPA COLLEGE

Re-accredited by NAAC at 'A+' grade with 3.53 CGPA

College with UGC-STRIDE Component-I

II Block, Rajajinagar, Bengaluru. Karnataka-560010. INDIA



Proceedings

IQAC Initiated UGC- STRIDE Sponsored



TWO DAY INTERNATIONAL e - CONFERENCE

on

“APPLIED MATERIALS AND TECHNOLOGY - 2020”

held on 9th & 10th October 2020

An Approach to Trans-Disciplinary Research

Organised By

Department of Physics

ISBN: 978-93-5437-097-7



E-mail: phyconference@klesnc.org

website: www.klesnc.org



KLE Society's
S. Nijalingappa College
IInd Block, Rajajinagar, Bengaluru-560010
Re-accredited by NAAC at 'A' grade with 3.53 CGPA
College with UGC STRIDE Component -I

Title:

Proceedings of IQAC Initiated UGC-STRIDE Sponsored Two Days International e-Conference on "Applied Materials & Technology – 2020" An approach to Trans-disciplinary Research

Author's Name: Dr. Arunkumar B. Sonappanavar

Editorial Committee Details:

Sl.No.	Author Details	Designation	Contributor Details
1	Dr. Arunkumar B. Sonappanavar	Principal	Scientific Editor
2	Prof. K. Nagi Reddy	Associate Professor	Associate Editor
3	Dr. Shivananda C S	Assistant Professor	Associate Editor
4	Mrs. Saroja R. Savadatti	Assistant Professor	Member
5	Dr. Indudhar P. Vali	Assistant Professor	Member
6	Mrs. Shreeshmal Bhavya	Assistant Professor	Member
7	Mr. Parameshwar G Gouda	Assistant Professor	Member
8	Mr. Vishal S V	Assistant Professor	Member
9	Ms. Meghana H N	Assistant Professor	Member
10	Mr. Santhosh Kumar M	Assistant Professor	Member

Published By: Self Published

Publisher's Address,

Dr. Arunkumar B. Sonappanavar, Principal, K.L.E. Society's S. Nijalingappa College, 2nd Block, Rajajinagar, Bengaluru, Karnataka -560010.

Email: klesncphysics@gmail.com Website: <http://www.klesnc.org> Tel: 080 2352 6055

Publisher's Details,

Dr. Arunkumar B. Sonappanavar, Principal, K.L.E. Society's S. Nijalingappa College, 2nd Block, Rajajinagar, Bengaluru, Karnataka -560010.

Email: klesncphysics@gmail.com Mobile: +919483946362

Printer's Details,

Principal, K.L.E. Society's S. Nijalingappa College, 2nd Block, Rajajinagar, Bengaluru, Karnataka -560010.

Edition Details: 1 (First Edition), 2020

ISBN: 978-93-5437-097-7

Copyright ©2021 All rights reserved. No part of this publication may be reproduced, stored in retrieval system or transmitted in any form or by any means, electronic, mechanical, photocopying, recording, otherwise, without the prior written permission of the publishers.

Editorial Committee



Dr. Arun Kumar B. Sonappanavar Principal

Prof. K. Nagi Reddy

Dr. Shivananda C. S.

Mrs. Saroja R. Savadatti

Dr. Indudhar P. Vali

Mrs. Shreeshmal Bhavya

Mr. Parameshwar G. Gouda

Mr. Vishal S. V.

Ms. Meghana H. N .

Mr. Santhosh Kumar M.

Scientific Editor

Associate Editor

Associate Editor

Member

Member

Member

Member

Member

Member

Member

CONTENTS

Title Page	i
Committees	ii - iv
About Society	iv
About College	iv - v
About Department	v
About Conference	v
Themes/Subthemes	v - vi
Participants/Beneficiaries	vi
Awards	vi
Mentoring & Monitoring Committee of UGC STRIDE Component – I	vi
Conference Schedule	vii - viii
Messages	ix - xvi
Author Index	xvii - xviii

KLE Society's
S. Nijalingappa College
II Block, Rajajinagar, Bengaluru-560010
Re-accredited by NAAC at 'A+' grade with 3.53 CGPA
College with UGC STRIDE Component –I

PROCEEDINGS

**UGC – STRIDE Sponsored Two Day International
e-Conference Organized by Department of Physics**

ON

**“Applied Materials and Technology 2020,
An Approach to Trans-Disciplinary Research”
2020-2021**

Chief Patron

Dr. Prabhakar B. Kore Ex. MP

Chairman, Board of Management, KLE Society, Belagavi

Advisors

Sri. Mahantesh M. Kavatagimath

Chief Whip, Government of Karnataka

Director, Board of Management, KLE Society, Belagavi

Shri. Shankaranna I. Munavalli

Director, Board of Management, KLE Society, Belagavi

Shri. Jayanand M. Munavalli

Director, Board of Management, KLE Society, Belagavi

Local Organizing Committees

Chairperson:	Dr. Arunkumar B. Sonappanavar
Coordinator:	Dr. Mahananda B. Chittawadagi
Convener:	Prof. K. Nagi Reddy.
Organising Secretary:	Dr. Shivananda C. S.
Joint Secretaries:	Dr. Tejaswini Nandi Mrs. Chaya M. R.
Organising Committee:	Mrs. Saroja R. Savadatti Dr. Indudhar P. Vali Dr. Manohar P. Mr. Vishal S. V. Mrs. Shreeshmal Bhavya Mr. Parameshwar G. Gouda

Master of Ceremony (MOC) Mrs. Shreeshmal Bhavya

Paper Review Committee (Online and Print Publication)

Dr. Arunkumar B. Sonappanavar	Convener
Prof. K. Nagi Reddy	Member
Dr. Shivananda C. S.	Member
Dr. Indudhar P. Vali	Member
Dr. Manohar P.	Member
Dr. Lakshmeesha Rao B.	Member
Dr. Jagadish Angadi V.	Member
Dr. Fakruddin K.	Member

Inaugural and Key note lecture

Prof. K. Nagi Reddy	Convener
Mrs. Chaya M. R.	Member

Technical Session-I Committee

Dr. Shivananda C. S.	Convener
Mr. Vishal S. V.	Member

Technical Session-II Committee

Dr. Jagadish Angadi V.	Convener
Mrs. Saroja R. Savadatti	Member

Technical session-III Committee

Mr. Paramshwar G Gouda	Convener
Mr. Vishal S. V.	Member

Technical session-IV Committee

Prof. K. Nagi Reddy	Convener
Dr. Manohar P.	Member

Technical session-V Committee

Dr. Tejaswini Nandi V	Convener
Mr. Parameshwar G Gouda	Member

Technical session-V Committee

Dr. Indudhar P. Vali	Convener
Mrs. Saroja R. Savadatti	Member

Technical session-VI Committee

Dr. Manohar P.	Convener
----------------	----------

Dr. Indudhar P. Vali Member

Valedictory Committee

Prof. Rajaiah B. Convener

Prof. K. Nagi Reddy Member

Dr. Shivananda C. S. Member

Background Preparation and Technical Support

Mr. Vishal S. V. Convener

Mr. Parameshwar G. Gouda Member

About Society

The KLE Society, Belagavi, since its inception 1916, has been a model in parting quality education and upliftment of socioeconomic status. The KLE Society disseminates the knowledge in all spheres of education from pre nursery to PG, for overall personality development of the students. It promotes and encourages the student's community to opt for programmes like Medicine, Dentistry, Pharmacy, Nursing, Agriculture, Law, Business management, Hotel management, Engineering & Technology, Basic Arts, Science, Commerce and Education. Under the leadership of visionary chairman Dr. Prabhakar B. Kore, Ex-M.P., the number of institutions has elevated up to 270 in various fields of education including research in India & abroad with equality concept. The dynamism of our chairman has motivated the faculty & students in the process of exploring knowledge for the welfare of society at large.

About Our College

KLE Society's S. Nijalingappa College, established in the year 1963, is one of the premier institutions under KLE Society, and has been included under 2(f) and 12(b) of UGC. The college has seen phenomenal growth in terms of courses offered, quality enhancement, student and staff strength besides development in infrastructure. The college offers higher education to 3,685 students from all sections of the society. Over its glorious service of more than half a century to the community, the college has earned many significant laurels. The crowning one of these are: the rare distinction of having been re-accredited at 'A+' grade with CGPA of 3.53 on a 4 point scale in 2016; it has received the status of the 'College with Potential Excellence' Phase – 2 and STRIDE

Component – 1 by UGC in 2019. The college conducts a range of UG courses in BA, B.Sc., B.Com, BCA, BBA, BHM and PG Courses in M.Sc., M.Com., MCA, and Ph.D in Commerce to cater to the diverse needs of the evolving higher educational scenario at the national as well as global level. The college is also recognized as research centre in commerce by Bengaluru Central University.

About Department

The Department of Physics established in the year 1963 and currently affiliated to Bengaluru City University offers undergraduate and postgraduate programmes. The faculties of the department are involved in various research activities. The department is actively conducting seminars, workshop, lectures series, faculty development programs and conferences for students, research scholars and faculties

About Conference

Material science research in the last several decades has revolutionized modern day technologies and greatly contributed to the benefit of mankind. The development of new materials and their screening for desired application is always a quest for researchers. In the recent years, research activities on emerging materials including nanomaterials, spintronic materials, wide bandgap semiconductor materials, composite materials, amorphous materials, two-dimensional/low dimensional materials etc. have offered unique advantages for certain dedicated applications in the field of optoelectronics, micro and nanoelectronics, sensors, high-power, high-frequency, renewable energy (solar and thermoelectrics), imaging, display and memory technologies. However, most of the studies are still on scientific footing, far from being thoroughly described and understood, and overall hindering the cutting edge research advances. In this view, the present conference facilitates the students, researchers and faculties to uncover the progress and various challenges in the field of material science and technology.

Theme:

“Applied Materials and Technology 2020, An Approach to Trans-Disciplinary Research”

Subthemes:

- Nanomaterials
- 2D materials
- Spintronic materials

- Amorphous materials
- Biomaterials and bio-devices
- Solar energy and thermoelectric materials
- Semiconductor materials and devices
- Liquid crystals
- Composite materials
- Polymers
- Nanomedicine & Biotherapeutics

Participants/Beneficiaries:

Academicians, Research scholars, UG and PG students.

Awards:

Two best papers have been awarded to Faculty, Research Scholar and UG/PG students (One each) respectively, along with a certificate to be conferred at the valedictory.

Dr. Shivananda C S, Organizing Secretary shivanandacs@klesnc.org,
phyconference@klesnc.org, Mobile No. +91-9538715600

Mentoring and Monitoring Committee of UGC STRIDE Component-I

- Prof. V. Prakash, Former Director, CFTRI, Mysore, UGC STRIDE Nominee
- Dr. Arunkumar B. Sonappanavar, Principal
- Dr. (Smt) Mahananda Chittawadagi, Coordinator
- Prof. K. Nagi Reddy, Member
- Dr. Jayashree Kambar, Member
- Sri. Shivakumar Sajjan, Member
- Smt. Swapna, Member
- Sri. Rajeshwar Prasanna, Member
- Dr. Supraja, Member
- Sri. Rajeev Potdar, Member

Schedule of the TWO DAY INTERNATIONAL e - CONFERENCE			
Day 1: 09 October 2020			
Time	Session	Topic	Resource Person
10:00 AM to 11.30 AM	01	Semiconductor Nanowires for Optoelectronics Applications	Dr. Chennupati Jagadish A C Professor Department of Electronic Materials Engineering Australian National University, Canberra
11.30 AM to 01:00 PM	02	Interfacial Modification in Nanocomposites to Tailor Functionalities	Dr. Sabu Thomas FRSC Vice Chancellor, Mahatma Gandhi University Kottayam, Kerala, India
02.00 PM to 03:00 PM	03	Insights into Magnetic Nanoparticles by DFT Calculations	Dr. Renan Augusto Pontes Ribeiro Professor State University of Minas Gerais Belo Horizonte, Brazil
03:00 PM to 04:30 PM	04	Oral Presentations	Session Chair Dr. Lakshmeesha Rao B Assistant Professor Department of Physics Poornapragna Degree College, Udupi
Day 2: 10 October 2020			
10:00 AM to 11.30 AM	01	The Ubiquitous GaN Nanowall Network	Dr. Shivaprasad S.M. Director, Karnataka State Higher Education Academy Dharwad and Professor, International Centre for Materials Science Jawaharlal Nehru Centre for Advanced Scientific Research Bengaluru
11.30 AM to 01:00 PM	02	Oral Presentations	Session Chair Dr. K. Fakruddin Professor & Head of Physics Gousia Engineering College, Ramanagar, Karnataka, India
02.00 PM to 03:00 PM		Smart Materials and Devices for Better Future	Dr. D. Haranath Associate Professor Department of Physics National Institute of Technology, Warangal, India

03:00 PM to 04:30 PM		Translational Nano-medicine: An Overview	Dr. Sarasija Suresh Project Director IDBR Bengaluru, India Co-founder, RJV Research and Innovations Pvt. Ltd.
----------------------------	--	---	--

Valedictory: 10 October 2020 @ 4.30 PM

Chief Guest

Dr. Sarasija Suresh

Project Director, IDBR

Bengaluru, India

Co-founder,

RJV Research and Innovations Pvt. Ltd.

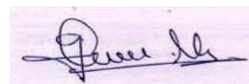
Presided By

Dr. Arunkumar B. Sonappanavar, Principal



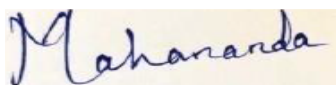
Organizing Secretary

Dr. Shivananda C S



Convener

Prof. K. Nagi Reddy



Coordinator

Dr. M.B. Chittawadagi



Principal

Dr. Arunkumar B. Sonappanavar



Message by

Dr. Prabhakar B. Kore
Chairman
KLE Society Belagavi
Karnataka

I am so delighted to know that IQAC of KLE Society's S Nijalingappa College, Bengaluru is organising UGC-STRIDE Sponsored two day International conference on "Applied Materials and Technology 2020- An Approach to Trans-Disciplinary Research" on 9th & 10th October 2020 and has invited eminent resource personalities. I am confident that the conference will enrich the knowledge of academicians and administrators of higher education institutions across the nation. Congratulations to the organisers and I wish the international conference an epic magnificent success.



Message by

Shri. Mahantesh M. Kavatagimath
Chief Whip, Government of Karnataka
Member,
Board of Management
KLE Society Belagavi
KLE Society's S Nijalingappa College
Rajajinagar, Bengaluru-560010

Greetings!

Being in the framework of this international conference, I take immense pleasure to welcome all the attendees of the conference on “Applied Materials and Technology 2020 - An Approach to Trans-Disciplinary Research”. This is a timely arranged international level platform organised to offer novel scientific thoughts and research findings of academicians, administrators, industrialists and students. I hearty congratulate the principal and his team for their timely organisation of this international conference and providing an easy and safe platform.

I wish the conference a huge hit and thought provoking informative proceedings that disseminate knowledge to all the stakeholders of this organisation.



Message by

Shri. Shankaranna I. Munavalli
Member,
Board of Management
KLE Society Belagavi
KLE Society's S Nijalingappa College
Rajajinagar, Bengaluru-560010

This is my privilege and I am so enthusiastic to welcome you all for UGC-STRIDE Sponsored two day international conference on “Applied Materials and Technology 2020, An Approach to Trans-Disciplinary Research” 9th & 10th October 2020 organised by KLE Society’s S Nijalingappa College, Bengaluru. It is worth mentioning that the topic of the conference is related to the Trans-Disciplinary Research in Applied Materials and Technology at international level. The conference will help in understanding the concept of applied materials and latest innovation/technology in the field of physics. I am very sure that this international conference including keynote address, special talk and academic/research work presentations will be helpful for the participants across the globe.



Message by

Dr. Arunkumar B Sonappanavar
Principal
KLE Society's S Nijalingappa College
Rajajinagar, Bengaluru-560010

It gives me immense pleasure to welcome all the eminent speakers and delegates to the IQAC initiated UGC-STRIDE sponsored Two-days International Conference on “Applied Materials and Technology – 2020, An Approach to Trans-Disciplinary Research” 9th and 10th October 2020 organised by Department of Physics, KLE Society's S Nijalingappa College, Bengaluru.

The conference covers a keynote address followed by eight technical sessions over the course of two days by eminent speakers, research scholars and students across the globe. I hope the two-day academic deliberations in the conference will enlighten the faculty, researchers and students on recent strides in material science research and its applications for the benefit of humanity and encourage them to take up further research in these crucial fields of study.

On this occasion, I extend a heartfelt welcome to all the delegates to KLE Society's S Nijalingappa College, Bengaluru. The college will bring out proceedings of the conference. I congratulate the organising committee members of conference on conducting such an event to boost the knowledge of faculty, researches and students.

Dr Arunkumar B. Sonappanavar

PRINCIPAL



Message by

Prof. K. Nagi Reddy

Convener

Associate Professor and HOD of Physics

KLE Society's S Nijalingappa College

Rajajinagar, Bengaluru-560010

We are grateful to organise Two Day International e-Conference on “Applied Materials and Technology – 2020” (AMT-2020). The conference is sponsored by UGC-STRIDE Component I and organised by Department of Physics, KLE Society's S. Nijalingappa College, Bengaluru. The subthemes of the conference are nanomaterials, spintronic materials, wide bandgap semiconductor materials, composite materials, amorphous materials, two-dimensional/low dimensional materials etc. These materials have led to new innovations in the field of optoelectronics, micro and nanoelectronics, sensors, high-power, high-frequency, renewable energy (solar and thermoelectric), imaging, display and memory technologies.

The conference in particular highlights the need for trans-disciplinary approach to uncover the progress and various challenges in the field of material science technology. In this International e-Conference, technical talks were delivered by Dr. Chanupati Jagadish A C, Professor, Australian National University, Canberra, Dr. Sabu Thomas, FRSC, Vice Chancellor, Mahatma Gandhi University, Kottayam, Dr. Renan Augusto Pontes Riberio, Professor, State University of Minas Gerais, Brazil, Dr. Shivaprasad S M, Director, Karnataka State higher Education Academy, Dharwad, and Professor, Jawaharlal Nehru Centre for Advanced Scientific Research, Bangalore, and Dr. D Haranath, Associate Professor, National Institute of Technology, Warangal, and Dr. Sarasija Suresh, Project Director, IDBR, Bangalore and Co-founder, RJV Research and Innovations Pvt. Ltd. The first day oral presentation session was chaired by Dr. B Lakshmeesha Rao, Assistant Professor, Poornaprajna College, Udupi, and second day oral presentation was chaired by Dr. K Fakruddin, Professor, Gousia Engineering College, Ramanagar.

I take this opportunity to thank UGC-STRIDE Component-I for funding this conference. I thank our honourable chairman Dr. Prabhakar B Kore KLE Society's

Belagavi, all the members of board of management, the secretary, life members and Principal for extending their support and valuable guidance in successfully organizing this academic event. I extend my gratitude to my colleagues who extended their support in making this e-conference successful. I also thank the students, research scholars and faculties for submitting their research work in this e-conference.



Prof. K. Nagi Reddy

Convener



Message by

Dr. Shivananda C S
Organising Secretary
Assistant Professor and PG Coordinator of Physics
KLE Society's S. Nijalingappa College
Rajajinagar, Bengaluru

Material science research revolutionized modern day technology by contributing new inventions in various fields. The quest of researchers for the development of new materials and technologies yielded in benefit and betterment of mankind in all forms. Especially, the advancement in the area of nanomaterials, spintronic materials, wide bandgap semiconductor materials, composite materials, amorphous materials, two-dimensional/low dimensional materials etc, lead to the new innovations in the field of optoelectronics, micro and nanoelectronics, sensors, high-power, high-frequency, renewable energy (solar and thermoelectric), imaging, display and memory technologies. These aspects were covered in Two Day International e-Conference on “Applied Materials and Technology – 2020” (AMT-2020). The conference is sponsored by UGC-STRIDE Component I and organised by Department of Physics, KLE Society's S. Nijalingappa College, Bengaluru. This e-Conference facilitated the students, research scholars, faculties and scientists from various parts of the India as well as outside the India. The conference in particular highlights the need for trans-disciplinary approach to uncover the progress and various challenges in the field of material science technology. In this International e-Conference, we are privileged to listen to various technical talks from eminent personalities including Dr. Chanupati Jagadish A C, Professor, Australian National University, Canberra, Dr. Sabu Thomas, FRSC, Vice Chancellor, Mahatma Gandhi University, Kottayam, Dr. Renan Augusto Pontes Riberio, Professor, State University of Minas Gerais, Brazil, Dr. Shivaprasad S M, Director, Karnataka State higher Education Academy, Dharwad, and Professor, Jawaharlal Nehru Centre for Advanced Scientific Research, Bangalore, and Dr. D Haranath, Associate Professor, National Institute of Technology, Warangal, and Dr. Sarasija Suresh, Project Director, IDBR, Bangalore and Co-founder, RJV Research and Innovations Pvt. Ltd. As a result, the information about the e-Conference was largely spread throughout the Internet. A

record number of more than 500 participants have registered for conference and more than 45 research abstracts were received from research scholars, faculties and scientists from India and abroad. Out of these, 16 best abstracts were selected for the oral presentation. The first oral presentation session was chaired by Dr. B Lakshmeesha Rao, Assistant Professor, Poornaprajna College, Udupi, and second day oral presentation was chaired by Dr. K Fakruddin, Professor, Gousia Engineering College, Ramanagar. The papers submitted in the conference will be published in conference proceeding with ISBN after peer-review process. This proceeding will be prepared on a valuable document for guiding the young researchers and students to develop passion in research. I take this opportunity to thank UGC-STRIDE Component-I for funding this conference. I thank our honourable chairman Dr. Prabhakar B Kore KLE Society's Belagavi, all the members of board of management, the secretary, life members and Principal for extending their support and valuable guidance in successfully organizing this academic event. I extend my gratitude to my colleagues who extended their support in making this e-conference successful. I also thank the students, research scholars and faculties for submitting their research work in this e-conference.

Shivananda CS

Dr. Shivananda C S
Organising Secretary

Author Index

Sl. No	Title	Author/s	Page No.
1.	Structural Properties and Density of States of ZnO under Pressure	P. K. Saini and S. Daoud	1-11
2.	Nanomaterials InAlGaAs/InP Based Gain Studies Under Normal Strains	PyareLal	12-16
3.	Physical and Structural Studies of Nd ³⁺ -doped Lead Boro-Tellurite Glasses	N B Shigihalli1, Sushma V and Santhosh kumar M	17-27
4.	To Study AC Electrical Conductivity of PVC PMMA Polyblend Thin Films by using Pool of Mercury	S.D. Kharbade	28-33
5.	Carbon Based Nanostructures for Energy Storage	K. Sree latha	34-40
6.	Reduced graphene oxide Nano sheet Decorated Nb ₂ O ₅ composite for Advanced Energy Storage Material	R. Sandhya, M. Mylarappa, S. Kantharaju, Rajaiah B and Deepushree S.R	41-54
7.	Prospective Nanomaterial Applications for Various Fields	D.Rama Rao, M.V.K.Mehar, N.Srinivas and K. Ashok	55-62
8.	Polarizability And Diamagnetic Susceptibility Of Cyanobiphenyl Alkyl Aniline Benzylidene Liquid Crystalline Compound	Syed habeebullahassain1, K. Nagi Reddy, C.M. Subhan and K. Fakruddin,	63-68
9.	Fluorescence Quenching Studies of Nitroaromatics Employing sulphonic acids Doped polymers	Dr. Parvathi Patil and Dr. Jaishree Badiger	69-74
10.	Electrical Conductivity Study of Lithium-Borate Glasses containing Gd ³⁺ ions	Hanumantharaju. N, Sardar Pasha, K.R, Sriprakash. G and Veeranna Gowda	75-81
11.	Synthesis and Characterization of Zn Substituted Li–Ni Nano Ferrites	R. G. Kharabe and B. K. Chougule	82-88
12.	Effects of different radiation on the growth of strontium doped copper tartrate single crystals	Pradeepkumar K V, Jagannatha N, Rohith P S, Delma	89-97

		D'Souza and Susheela K L.	
13.	Effect of Barium Incorporation on Thermal and Optical Properties of Copper Mixed Cadmium Oxalate Single Crystals	P. S. Rohith, N.Jagannatha, K.V. Pradeep Kumar ,Delma D'Souza, K B Reema	98-108

Structural Properties and Density of States of ZnO under Pressure

P. K. Saini^{1,*}, S. Daoud²

¹Department of Physics, Government College, Hansi, 125033, India

²Laboratory of Materials and Electronic Systems (LMSE), Faculty of Sciences and Technology, Mohamed Elbachir El Ibrahimi, Bordj Bou Arreridj University, 34000 Bordj Bou Arreridj, Algeria

* Corresponding author E-mail: pawansaini2005@gmail.com

Abstract:

This work presents the study of structural parameters and density of states of ZnO using TB-LMTO and full-potential linear augmented plane wave method (FP-LAPW) as employed in the WIEN2k simulation code. We have used both the generalized gradient approximation and Engel-Vosko generalized gradient approximations (EV-GGA) for the exchange-correlation energy, based on the optimization of total energy and corresponding potential, respectively. Apart from ground state structural properties and density of states, the work is also reported on band structure, Fermi energy, band gap etc.. The calculated parameters are also analyzed and discussed under high pressure. The calculated value of equilibrium lattice constant, bulk modulus (B), its pressure derivative and (DOS) density of states are found well agreed with the experimental data and other results available in literature.

Keywords: Structural properties, density of states, band gap, DFT and EV-GGA

1. Introduction

In recent decades the semiconductors of group II-VI have been reviewed and studied due to having their important applications in various fields such as thin films, transparent conductors for photovoltaic flat panel displays, spintronics, optoelectronic devices and solar cells. They also have some major optical, electrical and photoconductive properties etc. [1-5]. ZnO is potential oxide inorganic materials for next generation short-wavelength optoelectronic

devices such as laser diodes, low-cost light-emitting diodes LEDs, transparent p-n junctions, large-area flat-panel displays and solar cells [6-8]. In addition, it has an tremendous chemical stability and specific electronic/optical properties of a wide band gap semiconductor. For over two decades, zinc oxide structure has been studied theoretically using well known local density approximation (LDA). The major limitations of LDA are that it always computes very small energy band gaps and it closely binds the Zn-3d semicore electrons upto 2-4 eV as comparison made with the experimental data [9]. Consequently, the relationships of the Zn-3d orbital electrons with the O -2p valence electrons are incorrectly enlarged which resulting in stronger hybridization in the compound. This may also affects on the O- 2p bandwidth and it can shifts unrealistically close to the conduction band. However, the above stated studies were accepted out experimentally and there were relatively smaller effort to understand the theoretical electronic and semi conducting properties which is significant for well understanding for this class of materials. Moreover, the problem of underestimating of LDA based considered band gap can be improved using the well known EV-GGA [10, 11], which strongly motivated us to take up this problem with EV-GGA approximation to improve the energy band gap. We also have worked out similar kind of computational work for various types of materials with using the different methods [12-13] and so, in the present work, we have examined and analyzed structural properties and density of states (DOS) of ZnO under pressure using efficient density functional theory (DFT). The paper is organized as: The section 2 explains the detail of calculation method. Further, results and discussion are specified in section 3. Finally, results are explained in section 4.

2. Method of Calculation

We have studied out theoretical computational work using density functional theory based TB-LMTO method with in the atomic sphere approximation (ASA) and full-potential linear augmented plane wave method [14] implemented in the WIEN2k code [15]. The exchange-correlation potential was considered using GGA within the parameterization of Perdew-Burke-Emzerhof (PBE) [16-17]. The unit cell was sub divided into two parts such as non-overlapping muffin-tin spheres around the atomic sites and the interstitial region. The potential and wave function were expended inside spherical harmonic functions under non overlapping spheres and a plane wave basis fixed in the interstitial region of the unit cell of our compound. The selected Rmt was taken in such a way that the spheres did not overlap

each other. The plane wave cut off of $K_{max} = 8.0/R$ (RMT is the smallest muffin-tin radius) was preferred for the wave functions for the existing the interstitial region. A special mesh of k-points (72) was considered in the irreducible Brillouin zone for the calculations of ZnO for both ambient & high pressure phases. We have considered the valence and semi core states as semi-relativistically (ignoring spin-orbit coupling) while the core states are considered fully relativistically in these calculations. The self-consistent cycle was converged for the energy 10^{-5} eV. The atomic positions, Zn atom is present at the location of (0,0,0) and O atom positioned at the (1/4,1/4,1/4) in primitive unit cell for zinc-blende structure while for the case of rock-salt structure, Zn atom situated at the position of (0,0,0) and O atom is fixed at the position of (1/2,1/2,1/2) in the respective unit cell.

3. Result and discussion

First of all we have computed the values of total energies and then fixed to Murnaghan or Birch's equation of state (EOS) [18] to get the equilibrium value of lattice constants. Fig. 1(a) & 1(b) represent the calculated total energy with different volume of ZnO for both phases (ZB) and (RS) respectively. The calculated value of optimized lattice constant at equilibrium for ZnO is well agreement with the experimental and theoretical value of lattice constant [19-22]. The calculated value of lattice constant of crystal, bulk modulus and pressure derivative of bulk modulus are displayed in Table 1. The lattice constant decreases with increase in pressure. Our calculated findings are found slightly overestimate as comparatively to earlier reported theoretical data and experimental results. This fact may be explained that the structural results using GGA always overestimate the values.

Table:1 Calculated value of lattice constant Bulk modulus and pressure derivative of bulk modulus

ZnO	Lattice constant Å	Bulk modulus	Pressure derivative of bulk modulus
ZB phase	4.63	133.27	4.49
RS Phase	4.29	178.66	5.54

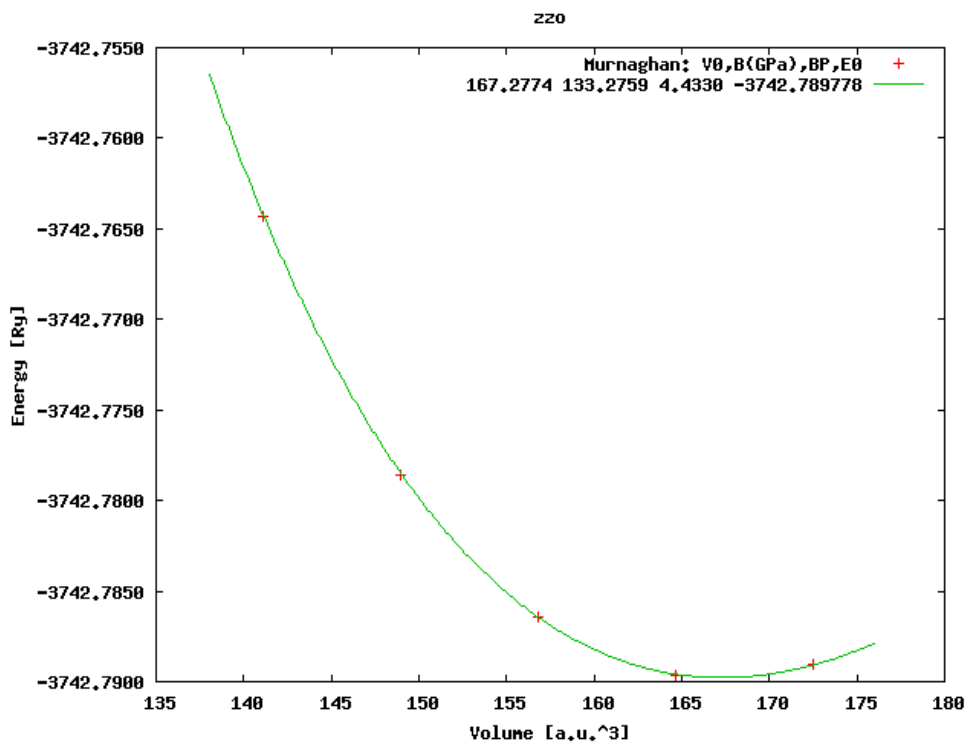


Fig. 1(a): Energy vs volume for ZnO at ambient pressure ZB phase

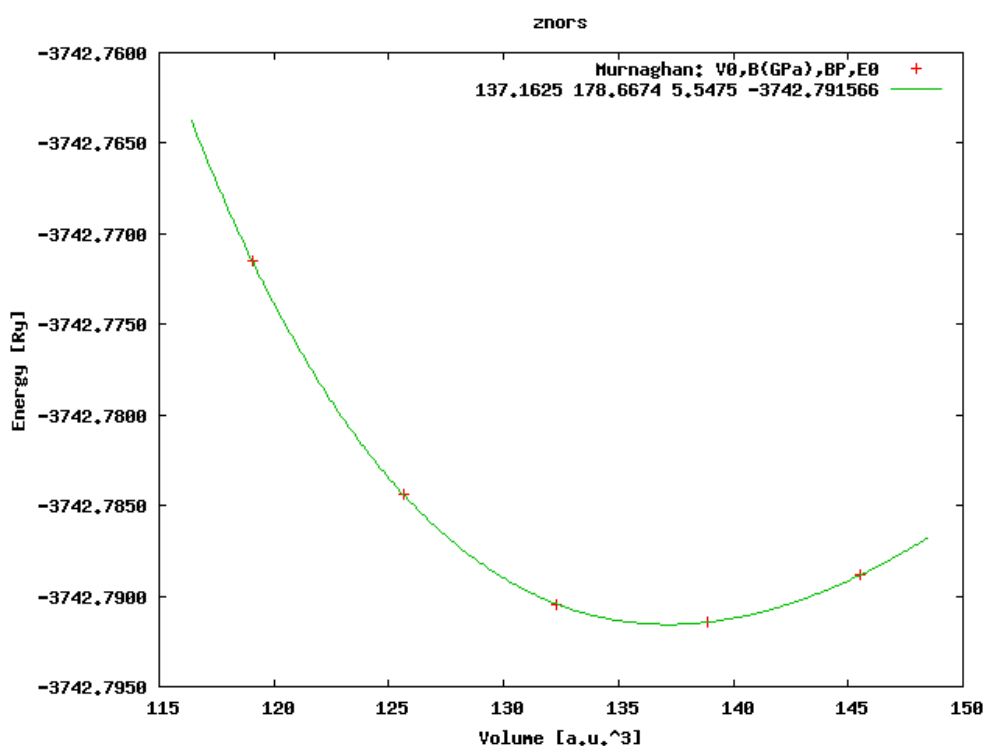


Fig. 1(b): Energy vs volume for ZnO at high pressure RS phase

Using lattice parameters we have calculated and plotted the electronic band structure of zinc blende (B3) phase as well as high pressure rock salt (B1) phase of ZnO, using the first principal tight-binding linear muffin-tin orbital method (TB-LMTO) and FP-LAPW within EV-GGA along with the concerned high symmetry directions associated in the Brillouin zone. The curve for band structure for ZnO at ambient (ZB) and high pressure (RS) phases as presented in fig.2 (a-b) using both methods TB-LMTO and FP-LAPW. The zero energy is considered for reference at the valence band maximum. The calculated profile of zinc oxide in ZB phase is found to be similar to the band structure of zinc oxide given in Ref.[23,24]. However, to our knowledge we did not find any experimental data available in the literature to compare the results corresponding to the high symmetry directions. But there exists some difference in the bands position in both structures plotted using TB-LMTO and FP-LAPW methods in ZB phase. It was noticed that the lowest lying region band existing in the valence band region appears around ~ -6.11 eV. Which mainly arises due to 2s states of O while the bands just below EF are in the valence region are predominantly arises due to Zn-4s and O-2p orbitals. The conduction band lying above EF is primarily arises due to 2p states of O interaction with 3p and 3d states of Zn. The dotted line shown in the center of curve is Fermi energy.

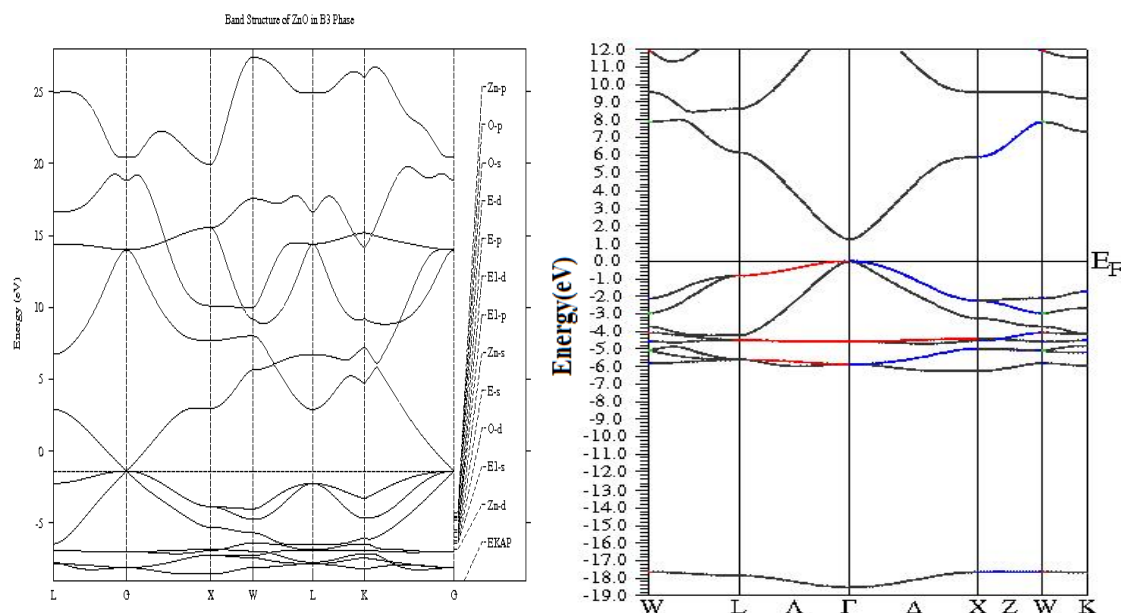


Fig. 2(a) Band structures of ZnO in high pressure ZB phase using TB-LMTO and FP-LAPW methods

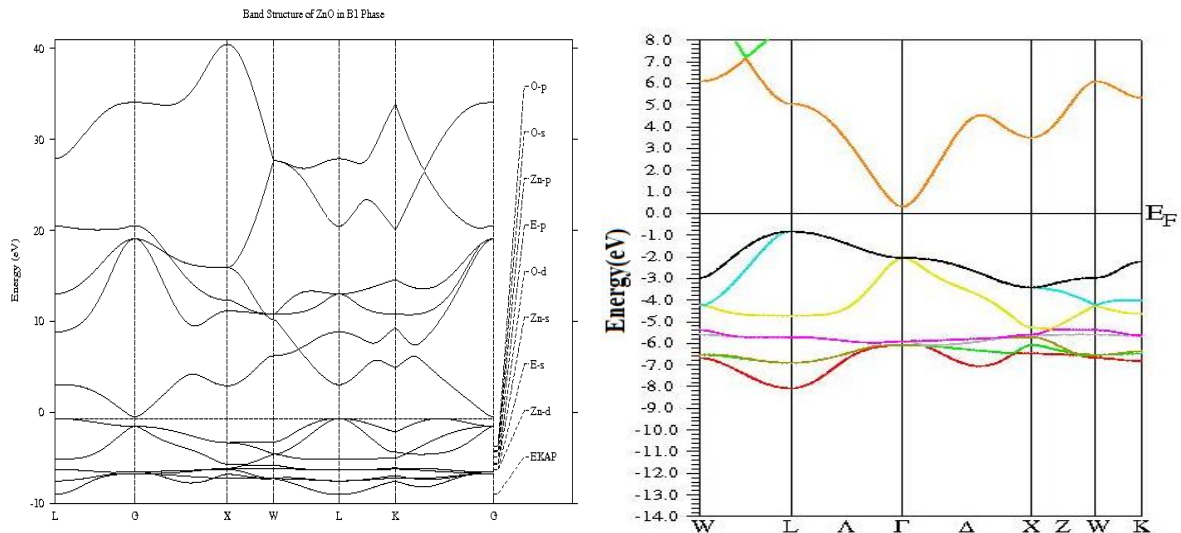
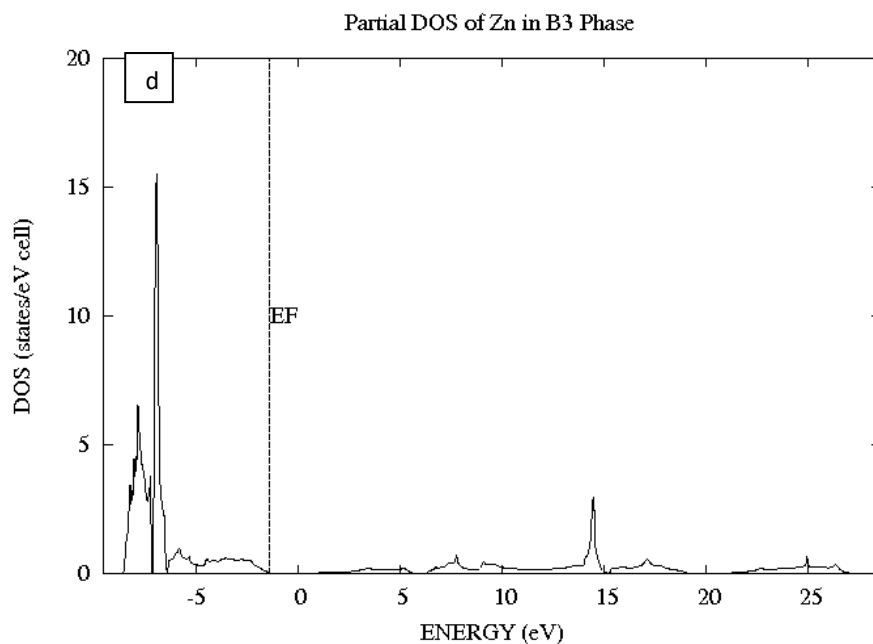
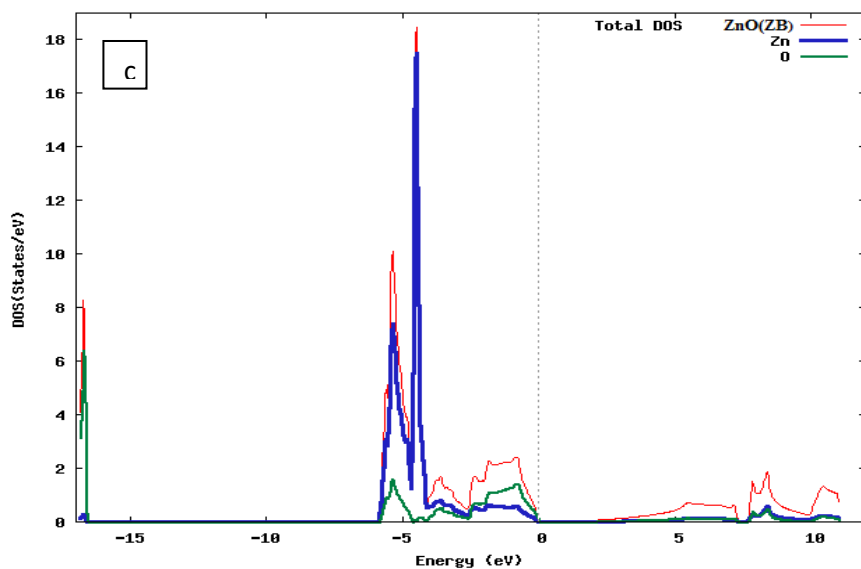


Fig. 2(b) Band structures of ZnO in high pressure RS phase using TB-LMTO and FP-LAPW methods

Similarly, we also have computed the electronic band structure for rock salt (RS) phase of ZnO using TB-LMTO and GGA based FP-LAPW methods along with the high symmetry directions in the existing Brillouin zone as plotted in Figure 2(b). The overall profile of band structure obtained from both methods is almost similar to the electronic band structure of with a little change related to the positions of the different bands [25]. However, due to lack of theoretical or experimental result of high pressure RS phase of ZnO, comparisons could not be possible. The low lying bands in the valence band region appears at ~ -6.99 eV mainly due the 4s states of O whereas the bands situated in valence region just below E_F are mainly due to Zn-4s and O-2p orbitals. The conduction band above E_F is generally arises due to 2p states of O with the hybridization of 3p and 3d states of Zn. However, the effect of high pressure is responsible for the increased width of the upper valence bands region and hence, O-2p states are pressed up in the energy towards the states Zn-4s resulting the change in the energy band gap. So at high pressure band gap decreases.

Density of state: Density of state is required to find out the electronic properties of solids. We have calculated and plotted the total and partial DOS for both ZB and RS phases of ZnO using both TB-LMTO and FP-LAPW methods as shown in the Figure 2 (c, d, e, f, g). Fermi energy is represented by dotted type line and different peaks of the DOS have been identified with their related electronic states. The different total and partial DOS histograms that in both the phases, the peaks found in lowest energy region primarily arise from the 2s states of O while the peaks in next higher energy region just below E_F are mostly due to 4s and 3p orbital

of Zn. It can be seen that the conduction band lying above the fermi energy level E_F is primarily arises due to 2p states of O interaction with 3p and 3d states of Zn. The overall profiles of DOS histograms for both the phases are found almost similar except some peak positions and heights.



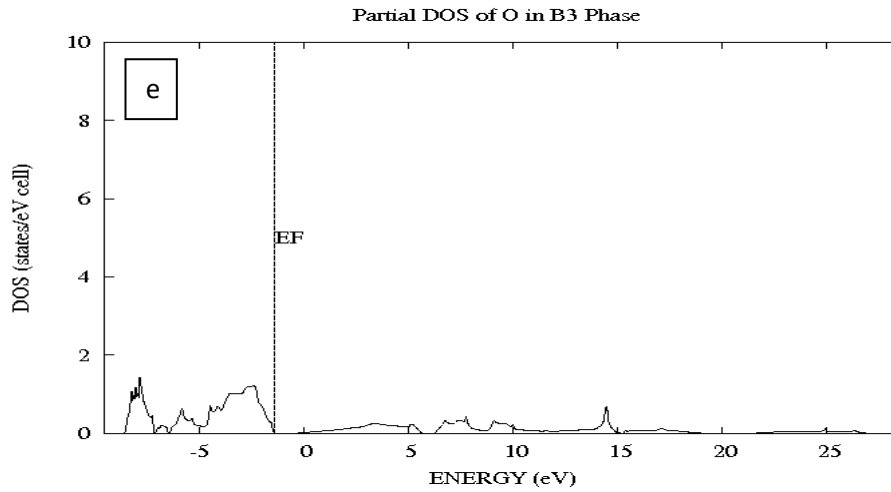


Fig. 3 (c-e): Total and partial density of state of ZnO in ZB phase using TB-LMTO and FP-LAPW methods

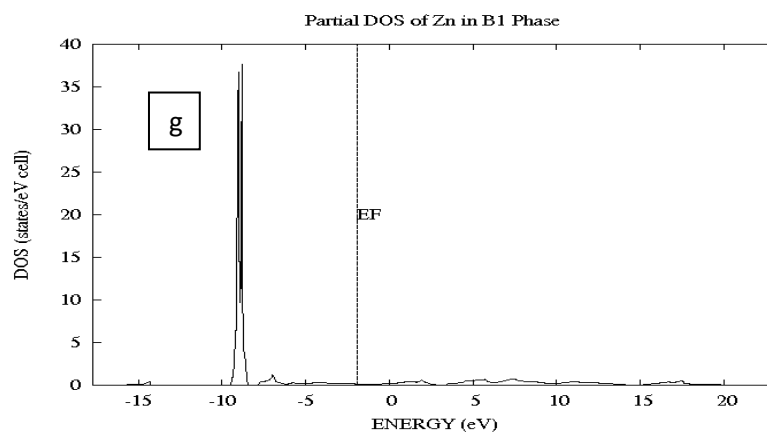
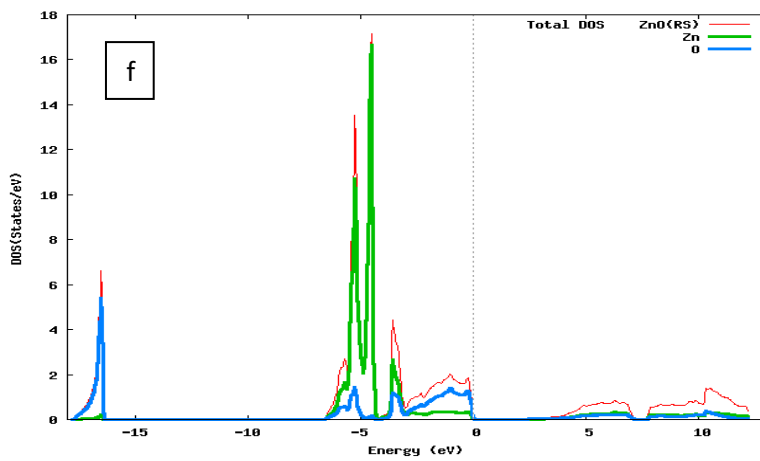


Fig.3 (f-g): Total and partial density of state of ZnO in RS phase using TB-LMTO and FP-LAPW methods

4. Conclusion

In summary, we have calculated and analyzed the lattice constant at equilibrium, bulk modulus and band structure of ZnO in both zincblende (ZB) and rocksalt (RS) phases using the TB-LMTO and FP-LAPW methods. We found that with the enhance of pressure in rocksalt phase the crossing of bands occurs which shows some metallic character of ZnO compound. The observed values of structural parameters have been found well agreement with the others available results in the literature. There is no data available of RS phase of ZnO in the literature. So comparison could not be possible.

References:

- [1] G.A. Samara, H. G. Drickamer :Pressure induced phase transitions in some II–VI compounds. *J. Phys. Chem. Solids* 23, 457(1962).doi:10.1016/0022-3697(62)90086-0
- [2] G. J. Piermarini, H. G. Block: Ultrahigh pressure diamond-anvil cell and several semiconductor phase transition pressures in relation to the fixed point pressure scale. *Rev. Sci. Instrum.* 46, 973(1975).doi.org/10.1063/1.1134381
- [3] B. A. Weinstein: Phonon dispersion of zinc chalcogenides under extreme pressure and the metallic transformation. *Solid State Commun.*24, 595(1977).doi.org/10.1016/0038-1098(77)90369-6
- [4] S. R. Tiong , M. Hiramastu, Y. Matsushima, E, Ito: The Phase Transition Pressures of Zinc sulfoselenide Single Crystals *JPN. J. Appl. Phys.* 28, 291(1989).doi.org/10.1143/JJAP.28.291
- [5] P. L. Smith, J. E. Martin, The high-pressure structures of zinc sulphide and zinc selenide. *Physics.Lett.*19, 541(1965).doi.org/10.1016/0031-9163(65)90766-3
- [6] J. R. Tuttle, M. A. Contreras, T. J. Gillespie, K. R. Ramanathan, A. L. Tennant, J. Keane, A. M. Gabor, R. Noufi, Prog : Accelerated publication 17.1% efficient Cu(In,Ga)Se₂-based thin-film solar cell. *Progress in Photovoltaics.*3, 235 (1995).doi.org/10.1002/pip.4670030404
- [7] H. J. Ko, Y. F. Chien, S. K. Hong, H. Wensch, T. Yao, D. C. Look : Ga-doped ZnO films grown on GaN templates by plasma-assisted molecular-beam epitaxy. *Appl. Phys. Lett.* 77, 3761 (2000).doi.org/10.1063/1.1331089
- [8] X. L. Guo, J. H. Choi, H. Tabata, T. Kawai: Fabrication and Optoelectronic Properties of a Transparent ZnOHomostructural Light-Emitting Diode. *Jpn. J. Appl. Phys.* 40, L177 (2001).doi.org/10.1143/JJAP.40.L177

- [9] D. Vogel, P. Krüger, J. Pollmann :*Ab initio* electronic-structure calculations for II-VI semiconductors using self- interaction-corrected pseudopotentials. Phys. Rev. B 52, R14316 (1995). doi.org/10.1103/PhysRevB.52. R14316
- [10] P. Blaha , K. Schwarz , G.K.H. Madsen , D. Kvasnicka and J. Luitz 2001 WIEN2k, An Augmented Plane Wave + Local Orbitals Program for Calculating Crystal Properties (Wein: Karlheinz Schwarz, Techn. University)
- [11] E. Engel, S.H. Vosko :Exact Exchange-only Potentials and the Virial relation as Microscopic Criteria for Generalized gradient approximations. Phys. Rev. 47,13164(1993). doi.org/10.1103/PhysRevB.47.13164
- [12] P.K.Saini, D.S.Ahlawat, S.Daoud, D,Singh : Electronic, Mechanical, Thermodynamic and Optical Properties of CdS Under Pressure. Indian journal of Pure & applied Physics,Vol. 57, Nov. 793(2019). <http://52.172.152.24/index.php/IndJPAP/article/view/190074>
- [13] P. K. Saini, D.S.Ahlawat, D,Singh: Calculations of the Structural, Elastic and Optical Properties of ZnSe at Ambient and High Pressure. Chalcogenide Letters,Vol.11, No.9,405(2014). http://chalcogen.ro/405_Saini.pdf
- [14] P. Hohenberg, W. Kohn :Inhomogeneous Electron Gas. Inhomogeneous Electron Gas ,Phys. Rev. B 136, 864 (1964). doi.org/10.1103/PhysRev.136.B864
- [15] P. Blaha, K. Schwarz, G.K.H. Madsen, D. Kvasnicka J. Luitz, WIEN2k, An Augmented Plane Wave Plus Local Orbitals Program for Calculating Crystal Properties, Vienna University of Technology, Vienna, Austria, (2001).
- [16] J. P. Perdew, K. Burke and M. Ernzerhof : Generalized Gradient Approximation Made Simple. Phys. Rev. Lett. 77, 3865 (1996).doi.org/10.1103/PhysRevLett.77.3865
- [17] M. Peterson, F. Wanger, L. Hufnagel, M. Scheffler, P.Blaha, K. Schwarz :Improving the efficiency of FP-LAPW calculations. Computer Physics Communications, 126, 294 (2000).doi.org/10.1016/S0010-4655(99)00495-6
- [18] F.D. Murnaghan :The Compressibility of Media under Extreme Pressures. Proc. Natl. Acad. Sci. USA 30 (1944) 5390.
- [19] J. E. Jaffe, J.A. Snyder, Z. Lin, A.C. Hess :LDA and GGA calculations for high-pressure phase transitions in ZnO and MgO. Phys. Rev. B 62, 1660(2000).doi.org/10.1103/PhysRevB.62.1660
- [20] S. Desgreniers :Structural and compressive parameters High-density phases of ZnO. Phys. Rev. B 58, 14102(1998).doi.org/10.1103/PhysRevB.58.14102

- [21] W. H. Bragg and J.A. Darbyshire, J. Meteorol. 6, 238(1954)
- [22] J. Serrano, A. H. Romero, F. J. Manjon , R. Lauck, M. Cardona, A. Rubio : Pressure dependence of the lattice dynamics of ZnO: An *ab initio* approach. Phys. Rev. B 69, 094306(2004). doi.org/10.1103/PhysRevB.69.094306
- [23] G. Zwicker, K. Jacobi : Solid state communications. Vol.54, issue 8, 701 (1985).doi.org/10.1016/0038-1098(85)90591-5
- [24] O.Madelung, Numerical Data and Functional Relationships in Science and Technology, New Series, Vol.17b (Springer-Verlag, Berlin, 1982).
- [25] P. Nozieres, D. Pines : Electron Interaction in Solids. Characteristic Energy Loss Spectrum. Phys. Rev. 113,1254(1959). doi.org/10.1103/PhysRev.113.1254

Nanomaterials InAlGaAs/InP Based Gain Studies Under Normal Strains

PyareLal

Department of Physics, Banasthali Vidyapith-304022 (Rajasthan) INDIA.

E-mail corresponding author: drpyarephysics@gmail.com

Abstract:

Under normal strains the studies of gains of light based on the nanomaterials InAlGaAs/InP have been investigated in this research letter. These type studies have an essential role in the present time to provide better telecommunications without any attenuation through the optic fibre by the process of TIR (Total Internal Reflection). In the results the achieved optical gains of higher values have wavelengths in the range of 1200 nm to 1600 nm. These type ranges of wavelengths have been essential utilised in the applications of NIR and SWIR radiations. Moreover, the ranges of wavelengths ~ 1550 nm and 1300 nm have better performance in the optically fibre based communications. Next, the normal strain controlled gain spectra with lasing wavelengths have been presented graphically. The behaviours of parameters of anti guiding and differential type gains with carrier densities for several effects of normal strains have also been illustrated and investigated.

Keywords: Gains, Differential type gain, Parameter of antiguiding, InAlGaAs, InP

1. Introduction

Among various heterostructures, the InAlGaAs/InP nanomaterials (grown on InP substrate) has been very popular due to emission of radiations of ~ 1.55 μm wavelength. This wavelength has been of great concern due to its potential applications in optical fiber communications because of very low attenuation [1-3]. These nanomaterials have been set up some additional reward such as gain stability at higher temperature, improved line width enhancement factor and tunable wavelength. The InAlGaAs/InP nanomaterials have also been reported as a platform on which the electronic devices can be fabricated. For example,

the electrical characteristics such as the current-voltage and capacitance–voltage characteristics of the Schottky diodes, which were fabricated on InGaAlAs/InP nanomaterials, have been studied under the variation of barrier heights, variation in the temperature (with the range 80–300 K) and variation in the Al mole fraction in the alloy [4]. Recently, the modeling of InAlGaAs/InPnanomaterials with the InGaAs material has been performed to show its usage in mode-locked quantum-well semiconductor laser [5].

2. Simulation

We have simulated the optical gain for the type-I InAlGaAs/InPnanomaterials which consists of single quantum well (SQW) of InAlGaAs quaternary material having graded index cladding profile. The whole structure is supposed be grown on InP substrate whose lattice is lattice matched with the QW material. The optical gain has been simulated with the help of following formula.

$$G(\hbar\omega) = \frac{2 \cdot \pi e^2}{nc\epsilon\omega Lm^2} \sum_{\sigma=U,L} \sum_{n,m} \int \left| \langle \hat{e} \cdot M_{nm}^{\eta\sigma}(k_t) \rangle \right|^2 \times \frac{(f_n^c(k_t) - f_{\sigma m}^v(k_t)) \left(\frac{\gamma}{\pi}\right) k_t dk_t}{(E_{\eta,\sigma nm}^{c,v}(k_t) - \omega\hbar)^2 + \gamma^2} \frac{1}{2\pi}$$

In the above expression, the detail of all the terms can be seen in ref. [6].

3. Simulation Results and Discussion

The degree of amplification of intensity of light can be measured as optical gain. Generally, the optical gain is the net amount of the stimulated emission that a photon generates as it travelled in given appropriate distance. In the semiconducting heterostructures, the optical gain is caused by photon induced transition of electrons from the conduction band to valence band. If the rate of downward transitions exceeds the rate of upward transitions, there will be a net generation of photons and optical gain can be achieved. The optical gain characteristics for strained InAlGaAs/InP type-I GRIN nanomaterialshas been simulated and shown in figure 1. This figure shows that the maximum optical gain is increased as increase in compressive strain because the quasi Fermi level separation is increased due to increase in energy space between heavy holes sub bands. The band gap is also increased as increase in compressive strain so peaks of optical gain curves are shifted towards shorter wavelength. Optical absorption and transparency lasing wavelength with compressive strain for GRIN InAlGaAs/InP type-I Nano Heterostructures are shown in Figure 3. In addition, the behaviors

of maximum optical gain and lasing wavelength with compressive strain are exhibited in Figure 3.

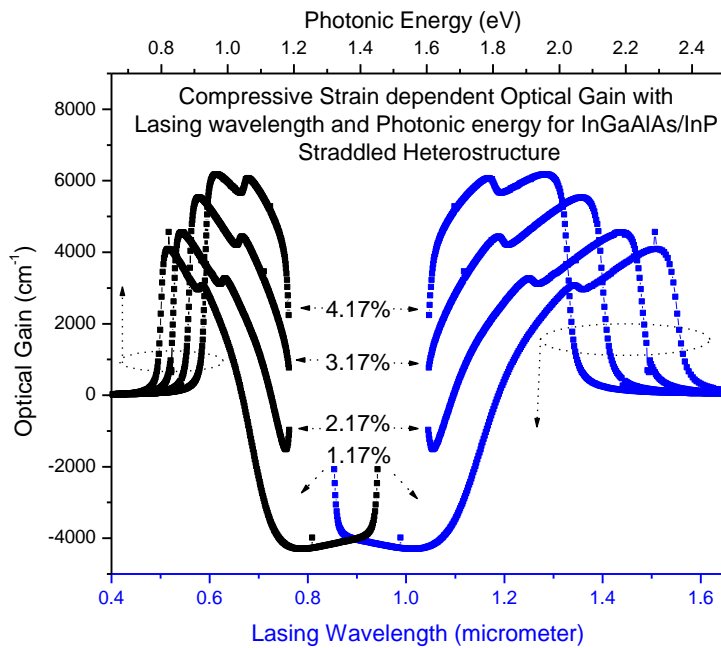


Figure 1. Optical gain with lasing wavelength and photonic energy for variable compressive strain

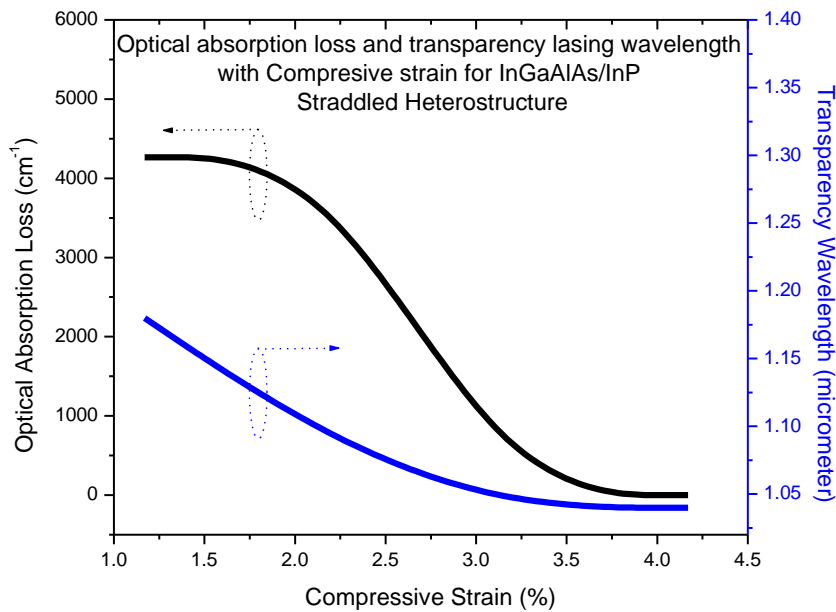


Figure 2. Optical absorption loss and transparency lasing wavelength for variable compressive strain

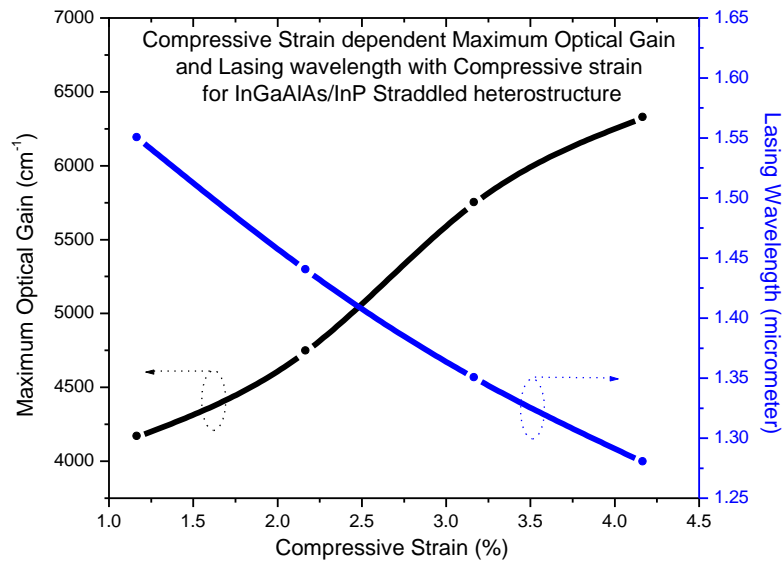


Figure 3. Effect of compressive strain on peak optical gain and lasing wavelength

4. Conclusion

A very simple quantum mechanical methodology (i. e. k.p method) has been exploited to evaluate the optical properties of type-I GRIN InAlGaAs/InPnanomaterials. In addition, strain effect on the gain characteristics has also been studied. The results achieved in this work may be of interest for the researchers working in the opto-electronic area.

Acknowledgement

Authors are very grateful to Banasthali Vidyapith for providing computational facilities.

References

- [1] P. A. Alvi, PyareLal, S. Dalela, M. J. Siddiqui, "An Extensive Study on Simple and GRIN SCH based In_{0.71}Ga_{0.21}Al_{0.08}As/InP Lasing heterostructure", *PhysicaScripta*, 85, 035402 (2012).
- [2] P. A. Alvi, PyareLal, RashmiYadav, Shobhna Dixit, S. Dalela, "Modal gain characteristics of GRIN-InGaAlAs/InP lasing nano-heterostructures" *Superlattices and Microstructures*, Vol. 61,pp. 1-12 (2013).
- [3] P. A. Alvi, "Strain-induced non-linear optical properties of straddling-type indium gallium aluminum arsenic/indium phosphide nanoscale-heterostructures", *Materials Science in Semiconductor Processing*, Vo. 31, pp. 106-115 (2015).

- [4] A. Ramam and S. J. Chua, “Features of InGaAlAs/InP heterostructures”, *Journal of Vacuum Science & Technology B: Microelectronics and Nanometer Structures Processing, Measurement, and Phenomena* **16**, 565 (1998).
- [5] D A Rybalko,, I S Polukhin et al. “Model of mode-locked quantum-well semiconductor laser based on InGaAs/InGaAlAs/InP heterostructure”, *Journal of Physics: Conference Series* 741, 012079 (2016).
- [6] S. L. Chuang, *Physics of optoelectronic devices* (Wiley, New York, 1995).

Physical and Structural Studies of Nd³⁺ doped Lead Boro-Tellurite Glasses

N B Shigihalli¹, Sushma V² and Santhosh kumar M¹

¹*Department of Physics, Soundarya Institute of Managemnt and Science, Bengaluru-560 073*

²*Deaprtmenty of Chemistry Soundarya Institute of Managemnt and Science, Bengaluru-560 073*

Corresponding Author (e-mail): *nbsphysics@gmail.com*

Abstract

Series of glasses with compositions 20PbO–20TeO₂–(60–x)B₂O₃–xNd₂O₃(in mol.%) where x= 0, 1,2,3,4 were prepared by melt quenching method. The compositional dependence of different physical parameters such as density, molar volume, polaron radius, optical basicity have been analysed and discussed. The densities and optical basicities are found to increase with increase in Nd₂O₃ concentration. Optical absorption studies reveal that the values of band gap decrease from 3.508 to 3.314 eV with increase in Nd³⁺ concentration. The slight decrease in band gap is due to increase of bonding defect and non-bridging oxygen. It is found that Urbach energy decreases with increase of Nd₂O₃ concentration which is attributed to decrease in fragility nature of the glass network. IR studies revealed that the structure of prepared glass network consists of [TeO₃] / [TeO₃₊₁], [TeO₄], [BO₃], [BO₄] and B-O-Pb linkages.

Keywords: *Boro-tellurite glasses: Neodymium-doped glasses and UV-Optical*

1. Introduction

Rare earth doped glasses have attracted a great deal of interest due to their macroscopical properties such as high mechanical resistance, chemical stability and heat- resistance [1]. Nd³⁺ doped glasses have proven to be one of the most efficient candidates for photonic devices such as fiber lasers, micro chip lasers and planar wave guides [2-4]. PbO based glasses have interesting physical properties such as high density, high linear and non-linear refractive index enabling their extensive various applications in optics and optoelectronics [5]. TeO₂ based glasses are known as good hosts for rare earth ions in possible uses for

practical laser applications [6]. B₂O₃ is one of the best and well known glass former and is present in almost all commercially important glasses. Boro-Tellurite glasses have been widely studied because of the industrial importance of tellurites in making glasses with desirable optical properties [7].

The Physical properties of glass provide an insight into the atomic arrangements in a glass network. The study of optical absorption edge is useful for understanding the optically induced transition and optical band gaps of materials. IR studies give information about structure of glass composition. These considerations motivated us to study physical properties, optical band gap and structural studies of glass compositions (in mol.%) 20PbO–20TeO₂–(60–x)B₂O₃–xNd₂O₃ (PTBN) where x= 0, 1,2,3,4.

2. Experimental

The Neodymium oxide (Nd₂O₃) doped lead–tellurite-borate glass samples were prepared by high purity analytical grade chemicals of PbO, H₃BO₃, TeO₂ and Nd₂O₃. These ingredients were thoroughly mixed and melted in a porcelain crucible in an electrical furnace at a temperature of 1150⁰C for 30 min. The melt was air quenched by pouring it on a pre-heated brass block at 250⁰C and covering it immediately with brass plate. Density of the bubble-free glass samples were measured by employing Archimedes principle using xylene as an immersion liquid. The refractive index of the samples was measured using Abbe's refractometer with mono-bromonaphthalene as the contact layer between the sample and prism of the refractometer. The light source used was sodium vapor lamp at wavelength 589.3nm. UV-Visible absorption spectra were recorded in the range 300 – 900 nm using Perkin-Elmer spectrophotometer. FT-IR transmission spectra were recorded using Thermo-Nicolet 6700 spectrometer in the range 400-1800cm⁻¹.

3. Result and Discussion

3.1. Physical properties

The formula used to calculate densities of the prepared samples is

$$\rho = \frac{W_a}{W_a - W_b} \times \rho_b \quad (1)$$

where W_a the weight in air is, W_b is the weight in xylene and ρ_b is the density of xylene.

Average molecular weight of the multi-component glass system was calculated using the relation,

$$M_{av} = X_{PbO} Z_{PbO} + X_{TeO_2} Z_{TeO_2} + X_{B_2O_3} Z_{B_2O_3} + X_{Nd_2O_3} Z_{Nd_2O_3}$$

where X_{PbO} , X_{TeO_2} , $X_{\text{B}_2\text{O}_3}$ and $X_{\text{Nd}_2\text{O}_3}$ are the mole fractions of the constituent oxides, and Z_{PbO} , Z_{TeO_2} , $Z_{\text{B}_2\text{O}_3}$ and $Z_{\text{Nd}_2\text{O}_3}$ are the molecular weights of the constituent oxides. Molar volume (V_M) was calculated using the relation:

$$V_M = \frac{M_{av}}{\rho}$$

The number density N i.e., the number of ions per cubic centimetre of the Nd^{3+} ions was calculated using the relation [8]

$$N = \frac{x \rho N_A}{M_{av}} \quad (2)$$

where x is the mole fraction of rare- earth oxide, ρ is the density of the glass, N_A is Avogadro's number and M_{av} average molecular weight of the glass.

From the known value of N , following three related physical properties were calculated [9].

$$\text{Polaron radius } r_p (\text{\AA}) = \left(\frac{1}{2}\right) \left(\frac{\pi}{6N}\right)^{1/3} \quad (3)$$

$$\text{Inter nuclear distance, } r_i (\text{\AA}) = \left(\frac{1}{N}\right)^{1/3} \quad (4)$$

$$\text{Field strength, } F (\text{cm}^2) = \left(\frac{Z}{r_p^2}\right) \quad (5)$$

where Z is the charge of the ion.

The reflection loss from the glass surface was calculated from the refractive index by using Fresnel's formula [10]

$$R \% = \left(\frac{n_d - 1}{n_d + 1}\right)^2 \times 100 \quad (6)$$

Where n_d is the refractive index of the glass at wavelength 589.3 nm.

The dielectric constant (ϵ) was calculated from the refractive index of the glass using the formula [11]

$$\epsilon = n_d^2 \quad (7)$$

The molar refractivity R_M for each glass was calculated using the relationship [12]

$$R_M = \left(\frac{n_d^2 - 1}{n_d^2 + 2}\right) \frac{M_{av}}{\rho} \quad (8)$$

The optical dielectric constant ($P \partial t / \partial P$) was calculated using the formula [13]

$$P \partial t / \partial P = (\epsilon - 1) = (n_d^2 - 1) \quad (9)$$

Variation of density and molar volume with Nd_2O_3 concentration is presented in figure 1. It can be observed that the density increases with increase in Nd_2O_3 content. This is attributed due to replacement of lower molecular weight substance B_2O_3 with higher molecular weight

of oxide ions Nd_2O_3 in the glass network. This also shows that the addition of Nd_2O_3 results in an extension of glass network. The results of various physical properties calculated are presented in Table-1.

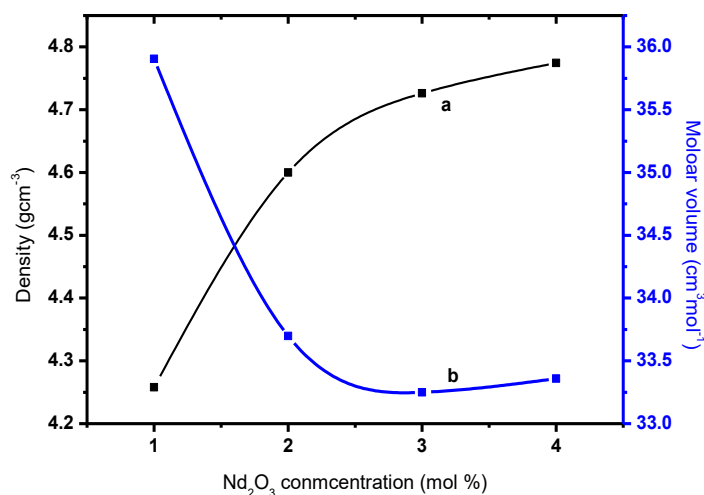


Fig.1. Variation of density and molar volume with Nd_2O_3 concentration.

The polaron radius is found to decrease with the increase in neodymium oxide content. This result agrees with literature [14]. As expected the intermolecular distance for rare earth ions shows an expected decrease on increasing Nd_2O_3 content. The molar refractivity, which depends on the refractive index, density and average molecular weight of glass, shows minimum around 2 mol% of Nd_2O_3 . This agrees with results reported in literature [15]. The data presented in Table 1 show that an increase in the average molecular weight influences significantly both the density and also other physical quantities. The variation of physical quantities with increase in Nd_2O_3 content agree with reported in literature [10].

3.2 Optical band gap

Room temperature the UV-Visible absorption spectra of Nd^{3+} doped glass system is as shown in Figure 2. The absence of sharp peaks in the absorption spectra corresponds to characteristics of amorphous nature. It is observed that the absorption intensity of the observed bands increases with increases of Nd_2O_3 concentration.

In order to study the optically induced transitions, optical band gaps have been computed from the UV-Visible absorption spectra of the glasses. The optical absorption at the fundamental edge in terms of the theory given by Davis and Mott [16] in the general form is

$$\alpha(\nu) = \frac{B}{h\nu} (h\nu - E_{\text{opt}})^n \quad (10)$$

This relation can be written as

$$(\alpha h\nu)^{\frac{1}{n}} = B (h\nu - E_{\text{opt}}) \quad (11)$$

where B is a constant called band tailing parameter, $h\nu$ is the photon energy and E_{opt} is the optical energy gap. Values of n are 1/2 and 2 for direct and indirect forbidden transitions, respectively.

Table 1 :Physical properties of Nd³⁺doped PTB glasses

Physical property	PTBN1	PTBN2	PTBN3	PTBN4
Density, ρ (g/cm ³)	4.258	4.600	4.726	4.774
Optical path length (cm)	0.165	0.193	0.181	0.180
Refractive index, (n_d) at 589.3nm	1.420	1.440	1.460	1.490
Average Molecular weight, M_{av} (g)	152.881	155.010	157.138	159.266
Molar volume, V_M (cm ³)	35.899	33.696	33.248	33.359
Nd ³⁺ -ion concentration, N ($\times 10^{20}$ ions/cm ³)	1.677	3.574	5.434	7.2303
Polaron radius, r_p (Å)	7.308	5.676	4.938	4.490
Inter nuclear distance, r_i (Å)	18.135	14.152	12.254	11.141
Field strength, F ($\times 10^{15}$ cm ⁻²)	0.561	0.931	1.230	1.668
Reflection loss, R %	3.012	3.251	3.496	3.872
Dielectric constant, ϵ	2.016	2.073	2.131	2.220
Molar refractivity, R_M (cm ³)	9.0084	8.880	9.1063	9.642
Optical dielectric constant , $P \partial t / \partial P$	1.016	1.073	1.131	1.220

The absorption coefficients $\alpha(\nu)$ were determined near the absorption edge at different photon energies ($h\nu$) for all glass samples. It is observed that for many amorphous materials, a reasonable fit of equation (10) with $n=2$ are achieved. Therefore the typical plot of $(\alpha h\nu)^{1/2}$ versus photon energy $h\nu$ (Tauc's plot) is plotted and it is as shown in figure 3 for indirect allowed transitions. The values of band gap obtained are 3.508, 3.480, 3.420, and 3.314 eV for PTBN1, PTBN2, PTBN3 and PTBN4 respectively. It can be observed that the optical band

gap slightly decreases with the increase of Nd_2O_3 concentration and results in the increase of bonding defect and non-bridging oxygen. This leads to an increase of the degree of the localization of electrons there by the increase of donor center in the glass matrix. The increase of presence of donor centre leads to the decreases of optical band gap, therefore, the shift of absorption edge toward the longer wavelength was observed.

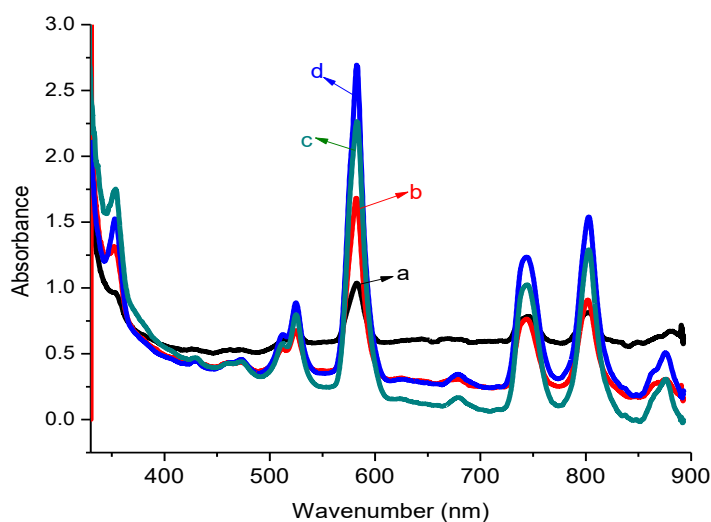


Fig.2. UV-Visible absorption spectra (a) PTBN1 (b) PTBN2 (c) PTBN3 (d) PTBN4 glasses.

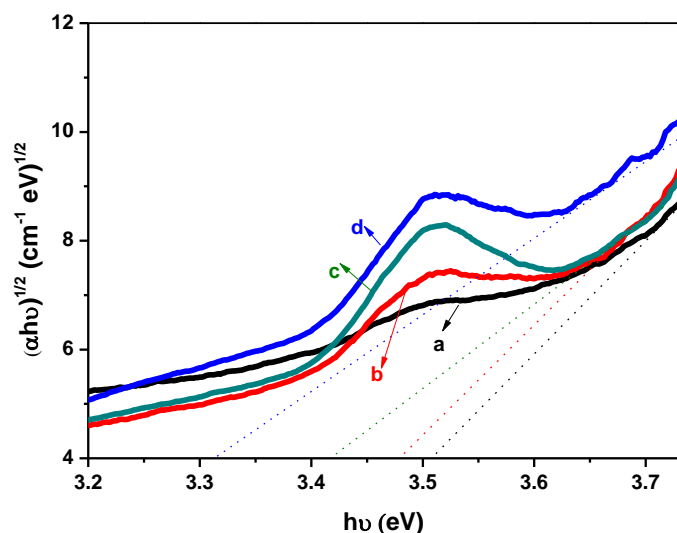


Fig.3. Tauc's plot for (a) PTBN1, (b) PTBN2, (c) PTBN3 and (d) PTBN4 glasses.

To calculate the width of energy tail, ΔE , of the density of states, the model proposed by Urbach. The following relation has been used to determine the width of the energy tail.

$$\ln\alpha = C + \frac{hv}{\Delta E} \tag{12}$$

where C is a constant. Urbach plots are the plots where natural logarithm of absorption coefficients ($\ln\alpha$) is plotted against photon energy ($h\nu$). The Urbach plot for Nd^{3+} doped PTB glasses is presented in Figure 4.

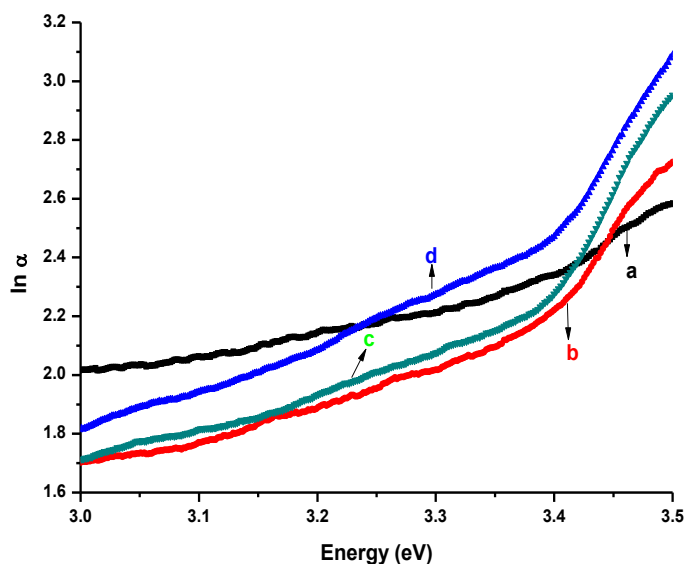


Fig. 4. Urbach plot for (a) PTBN1 (b) PTBN2 (c) PTBN3 and (d) PTBN4 glasses.

The values of Urbach energy were calculated by determining slopes of the linear regions of the curves and taking their reciprocals. The values of Urbach energies obtained are 0.352, 0.2029, 0.1347 and 0.1159 eV for (a) PTBN1 (b) PTBN2 (c) PTBN3 and (d) PTBN4 glasses respectively. It is found that Urbach energy decreases with increase of Nd_2O_3 concentration which is attributed to decrease in fragility nature of the glass network.

3.3 Optical basicity of the glasses

Theoretical optical basicity (Λ_{th}) serves in the first approximation as a measure of the ability of oxygen to donate a negative charge in the glasses. Theoretical optical basicity for the multi-component glass system has been calculated by using basicity assigned to the individual oxides on the basis of the following equation proposed by Duffy and Ingram[. For the present glass system

$$\Lambda_{th} = x_1(\text{PbO})\Lambda_1(\text{PbO}) + x_2(\text{TeO}_2)\Lambda_2(\text{TeO}_2) + x_3(\text{B}_2\text{O}_3)\Lambda_3(\text{B}_2\text{O}_3) + x_4(\text{Nd}_2\text{O}_3)\Lambda_4(\text{Nd}_2\text{O}_3) \dots\dots(13)$$

where $x_1(\text{PbO})$, $x_2(\text{TeO}_2)$, $x_3(\text{B}_2\text{O}_3)$ and $x_4(\text{Nd}_2\text{O}_3)$ are the equivalent fractions of different oxides, i.e. the proportion of the oxide atom they contribute to the glass system and $\Lambda_1(\text{PbO})$, $\Lambda_2(\text{TeO}_2)$, $\Lambda_3(\text{B}_2\text{O}_3)$ and $\Lambda_4(\text{Nd}_2\text{O}_3)$ are optical basicity values assigned to the constituent oxides taken from the literature.

The calculated values of optical basicity are 0.6822, 0.6875, 0.6928 and 0.6980 for PTBN1, PTBN2, PTBN3 and PTBN4 glasses respectively. It can be observed that optical basicity increases with an increase of Nd_2O_3 concentration. It may be due to the fact that Nd_2O_3 is having larger basicity (0.9501) than B_2O_3 (0.425). The increase of optical basicity in the present matrix shows ability of oxide ions to transfer electrons to the surrounding cations.

3.4 FTIR Spectra

The infrared transmittance spectra of the present glass system in the region $400\text{-}1800\text{cm}^{-1}$ region have large, medium, weak and broad peaks (Fig.5). A literature survey indicates that the vibrational modes of the borate network are mainly active in the three infrared spectral regions. A region around $600\text{-}700\text{cm}^{-1}$ due to the bending of the B-O-B linkage in BO_3 group, another region in $800\text{-}1200\text{cm}^{-1}$ due to the B-O bond and a region in $1200\text{-}1600$ due to stretching of the trigonal BO_3 units. The structural bands of the present glass system is characterised by IR absorption bands in the wave numbers region $400\text{-}600\text{cm}^{-1}$, $633\text{-}646\text{cm}^{-1}$, $677\text{-}688\text{cm}^{-1}$, $756\text{-}767\text{cm}^{-1}$, $910\text{-}933\text{cm}^{-1}$, $1245\text{-}1252\text{cm}^{-1}$ and $1342\text{-}1360\text{cm}^{-1}$. The IR band positions are summarised in Table 2.

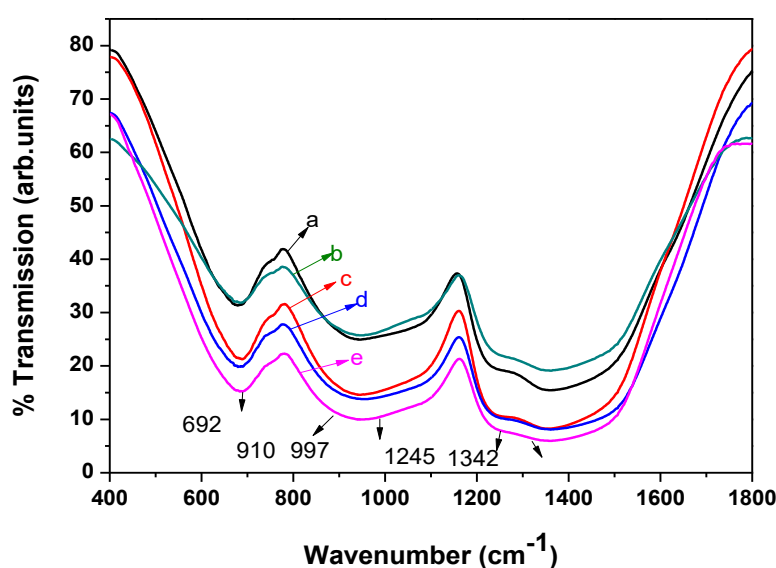


Fig. 5. IR spectra of (a) PTBNO (b) PTBN1 (c) PTBN2 (d) PTBN3 and (e) PTBN4 glasses

Intense absorption bands or weak shoulders in the region $633\text{-}767\text{cm}^{-1}$ correspond to $\text{TeO}_4\text{TeO}_3/\text{T}_3\text{O}_{3+1}$ units are preserved in all the studied glasses. In the region $600\text{-}800\text{ cm}^{-1}$, B-O-B bending vibrations manifest themselves. The peaks in the region $910\text{-}933\text{ cm}^{-1}$ are assigned to $[\text{BO}_4]$ units, those at $1245\text{-}1252\text{cm}^{-1}$ are assigned to B-O stretching vibrations in BO_3 units from Boroxol rings and peaks in the regions $1342\text{-}1360\text{cm}^{-1}$ are assigned to B-O stretching vibrations in $[\text{BO}_3]$ units from various types of borate groups [17-19]. The shoulder at 997 cm^{-1} is due to stretching vibrations of B-O-Pb linkages. IR studies revealed that the structure of prepared glass network consists of $[\text{TeO}_3] / [\text{TeO}_{3+1}]$, $[\text{TeO}_4]$, $[\text{BO}_3]$, $[\text{BO}_4]$ and B-O-Pb linkages. There is no change in the structure due to the addition of Nd_2O_3 .

Table 2 IR band assignments for the Nd^{3+} undoped and doped PTB glasses.

Characteristic IR bands in cm^{-1}	Assignment
633-646	Te-O-Te linkages
677-688	Stretching vibrations of TeO_2 trigonal by pyramidal
756-767	Stretching vibrations of TeO_3 tp
910-933	B-O-B bending vibrations in BO_4 units
~ 997	Stretching vibrations of B-O-Pb linkages
1245-1252	Asymmetric stretching vibration of B-O bonds from ortho borate groups
1342-1360	B-O bonds stretching vibrations of BO_3 units from various borate groups

4. Conclusion

Nd^{3+} doped Lead-Borate –Tellurite glasses have been successfully prepared and their physical and structural properties have been studied and analysed. Density increases with increase in Nd_2O_3 content. This is attributed due to replacement of lower molecular weight substance B_2O_3 with higher molecular weight of oxide ions Nd_2O_3 in the glass network. Optical basicity increases with increase of Nd_2O_3 concentration. It may be due to the fact that Nd_2O_3 is having larger basicity (0.9501) than B_2O_3 (0.425). Increase of Nd_2O_3 concentration results in decrease of optical band gap owing to increase in non-bridging oxygen

ions shifting the band edge to longer wavelength. Analysis of IR spectra shows that the structure of prepared glass network consists of $[\text{TeO}_3] / [\text{TeO}_{3+1}]$, $[\text{TeO}_4]$, $[\text{BO}_3]$, $[\text{BO}_4]$ and B-O-Pb linkages.

Acknowledgement

The authors wish to thank Shri Soundarya P Manjappa, Chairperson of Soundarya Educational Trust, Bengaluru and Dr. Suresh. C. Hegadi, Principal, Soundarya Institute of Management and Science, Bengaluru for their continuous encouragement to do research in pure science.

References

- [1] K. Gatterer, G. Pucker, W. Jantscher, H. P. Fitzner and S. Arafat, *J.Non-Crystalline Solids* 231 189-199 (1998).
- [2] Ki-Soo Lim, Chul-Woo Loe, Sung-Taek Kim, *J.Lumin.*,1008 87-89 (2000).
- [3] L.C.Coural, E.P.Maldonado, L. Gomes, N.D. Vieira, *Opt. Mate.*,14 81 (2000).
- [4] L.B.Shaw, R.S.F.Chang, N. Djeu, *Phys. Rev.*,B 50 6609 (1994).
- [5] D.W.Hall, H.A.NewHouse, N.F. Boreli, W.H.Dumbaugh, D.L.Weidman. *Appl. Phys. Lett.*, 54 1293 (1998).
- [6] M.J.Weber, J.D.Mayers and D.H.Blackburn, *J.Appl. Phys*, 52 2944 (1981).
- [7] M. Harish Bhat, M.Kandavel, MuniaGanguli and K J Rao, *Bull.Mater.Sci.*,27 2 189 (204).
- [8] A.S.Rao et al. *Optical Materials*, 10 245-252 (1998).
- [9] M.M. Ahmed, C.A. Hogarth, M.N. Khan, *J. Mater. Sci. Lett.*, 19 4040 (1984).
- [10] Y. Ohisti, S. Mitachi, T. Tanabe, *Phys. Chem. Glasses*, 24135 (1983).
- [11] B. Bendow, P.K. Benerjee, M.G. Drexhage, J. Lucas, *J. Am. Ceram. Soc.* 65 C92(1985).
- [12] J.E. Shelby, J. Ruller, *Phys. Chem. Glasses*28 262 (1987).
- [13] J. Schroeder, *J. Non-Cryst. Solids*, 40 549 (1980).
- [14] A.S.Budi, R. Hussain, and M.R.Sahar, *Electrical properties of neodymium phosphate glass semiconductor electronics*, proceedingsICSE, 19 247 (2002).
- [15] S.Mohan, K.S.Thind, and G.Sharma, *Brazilian Journal of Physics*, 374 (Dec. 2007).
- [16] N.F.Mott, E.A. Davis, *Electronic process in non-crystalline materials*, Carendon press
- [17] L.Bala, S. Simon, *Phys.Chem.Glasses*, 46(3),(2005) 279-283.

- [18] V.C.Veeranna Gowda, C. Narayana Reddy, K.C.Radha, R.V.Anavekar, J.Etourneau, K.J.Rao, J.Non-crystalline solids, 353 (2007) 1150-1163.

To Study AC Electrical Conductivity of PVC PMMA Polyblend Thin Films by using Pool of Mercury

S.D.Kharbade¹

¹Assistant Professor, Department of first year Engineering, Sipna College of Engineering and Technology, Amravati, Maharashtra, India.

Author email: snehakhARBade18@gmail.com

Abstract

The current work investigates the dielectric and AC conductivity constant of PVC and PMMA samples (4:1) at many constant temperatures in the frequency range (323K to 363K). The findings were presented in graph form. The dielectric constant increases with temperature increase at constant frequencies, Dielectric constant decreases with frequency increases, and AC conductivity increases with frequencies at different constant temperatures. The frequencies reach almost saturation values as the ultimate 1MHz value reaches.

Keywords: Solution cast method; percentage of amorphousness/crystallinity; 4:1 (PVC+PMMA); AC conductivity; dielectric constants

1. Introduction

When two or more polymers are mixed, poly-blends or polymer alloys are obtained. This physical mixing or blending of two polymers produces alloys with quite different properties, which can be potentially useful. Two polymers are generally incompatible as they have very low combinatorial entropy of mixing for the components. This is insufficient to overcome the positive heat of mixing of polymers to make the Gibb's free energy of mixing negative. Only when two polymers are interacted directly Mixing heat is adverse, which allows independence of mixing energy to become a negative quantity, and then random mixture (e.g., hydrogen bonding, acid-base type interaction etc). In comparison to combining small molecules, the dictum is not good for merging macromolecules like likes. However, industrially important materials are both compatible and incompatible blends. The compatible blend, that exists in one step, can form two polymers. On the other hand, the incompatible mixtures occur in two

steps. Since most blends combine immiscible materials, the resulting material includes minute particles of one polymer in the other matrix. Regulated mixing and refraction of the mix allows for the optimal concentration and sizes of particles to be formed. Blending allows the positive characteristics of many polymers to be blended. Mixing two-part polymers in the molten state is the most direct way to obtain a polymer (melt mixing). The magnitude of the mixing in this case depends on how far the molecules are spreading. Because such a combination takes high temperatures, the polymer can decompose and change chemicals.

2. Experimental Methods

2.1 Sample Preparation of PVC-PMMA undoped process of preparing the film mixes:

Preparing thin films with the Mercury pool (shown in fig (1)). Isothermal evaporation technology (Sangawar 1995, Belsare and Deogankar 1998) was used during the present work because it is ideally suited to laboratory conditions. In the traditional solvent Tetrahydrofuran, both polymers PVC PMMA were taken in the weight ratio of 4:1. The solution has been retained for 3-4 days to allow the dissolution of polymers to create a uniform solution. The solution mixture was then heated to a total uniformity for 1 hour at 60°C. A thoroughly washed glass plate (15 cm x 15 cm) with water is then used as a base with acetone. A pool of mercury was used (Figure below) in a plastic tray to achieve optimal levelling (and uniformity in the thickness of films).



Fig. 1 Pool of Mercury

The solution could be distributed evenly around the substrate and was poured on a glass tray. At room temperature, the whole device was placed in a dust-free chamber. Thus, the solvent in the solution will evaporate and dry up air entirely. The film was then removed and cut into small pieces of acceptable size on the glass surface. Through the isothermal

evaporation process, films were thus prepared. It has also been dried for three days to eliminate any solvent traces.

2.2 Thickness Measurement

Digital micro-meters (Mitutoyo Company, Japan) have been used to determine the thickness of every sample film at four different locations. The total sample thickness was four readings.



Fig 2. Digital Micrometer



Fig.3 LCR meter and sample holder for the measurement of AC conductivity

2.3 Measurement of AC Electrical Conductivity and Dielectric Constant

In conjunction with a Precision LCR (20 Hz-1MHz) of 4284 A supplied by Agilent Technology, Singapore was used to test AC electrical conductivity and dielectric constant in the form of a thermal operated electrical oven supplied by Pushpa Scientific, Hyderabad.

The film sample was loaded into the sample holder in an oven. The entire experimental set up is as shown in fig 3. The AC frequencies were applied (in the range 1 KHz -1 MHz) across the sample by using the 4284 A precision LCR meter (20 Hz -1 MHz). The corresponding dielectric constants were measured by using LCR meter. From the dielectric data, the AC conductivity of the samples was calculated by using the relation [Rao, 2000],

$$\sigma_{ac} = \frac{f \cdot \epsilon_r \cdot \tan(\delta)}{1.8 \times 10^{10}} \quad (1)$$

where, f = Frequency applied in Hz, ϵ_r = Dielectric Constant at frequency f , and $\tan(\delta)$ = Dielectric loss tangent.

3. Results and Discussion

Several investigators have researched electrical conduction / dielectric properties of different polymers composites [Shukla and Gupta 1987, Aziz and Aggour 1999, Khaled et al. 2003, Raghvendra et al. 2003, Muhammad Akram 2005.] The present work investigates a constant and reliable dielectric conductance of 4:1 PVC-PMMA blend sample at different constant temperatures (323K to 363K) and in the frequency interval (1KHz to 1MHz). The findings were shown. The following criteria have been discussed.

1) *The Dielectric Constant (ϵ_r):* *i*) Increases with temperature increases; *ii*) Decreases when the frequency is increased.

2) *The AC conductivity (σ_{ac}):* *i*) increases at different constant temperatures almost linearly with frequency over 1KH and almost constantly saturates the frequency when the maximum value is 1MH; *ii*) The changes in temp between 323K and 363K tend to be almost continuous at a constant frequency.

3.1 Effect of temperature on dielectric constant:

In the case of PVC and PMMA poly-blend samples, the value of the dielectric constant increased with the temperature rise. PVC is non-polar with two polymers used for mixing while PMMA is weakly polar. Polar polymer introduction into non-polar polymer decreases its resistance and increases both conductivity and dielectric constant (Fig.4).

3.2 Effect of frequency on dielectric constant:

In the polarisation which is or is added during preparation, the microscopic behaviour of the dielectric material is understood as being affected by the electric AC field. The polarisation effect depends on dipole nature and electrical field frequency. As previously stated, electronic polarisation, atomic polarisation and orientational polarisation contribute to the sample's net polarisation within the static electric field or the ac field of low frequency. As the frequency increases, orientation polarisation cannot obey changes in the field at higher frequencies. Consequently, dielectric constant declines with frequency increase [Muhd.Redha,(2006); Rao et al.,(2000)].

3.3 Frequency and temperature impact on AC conductivity:

AC conductivity was measured with the increased frequencies of 1KH to 1MHz for the blending method at different constant temperatures 323K, 333K, 343K, 353K and 363K. The AC conductivity increases with the increase in frequency has been observed.

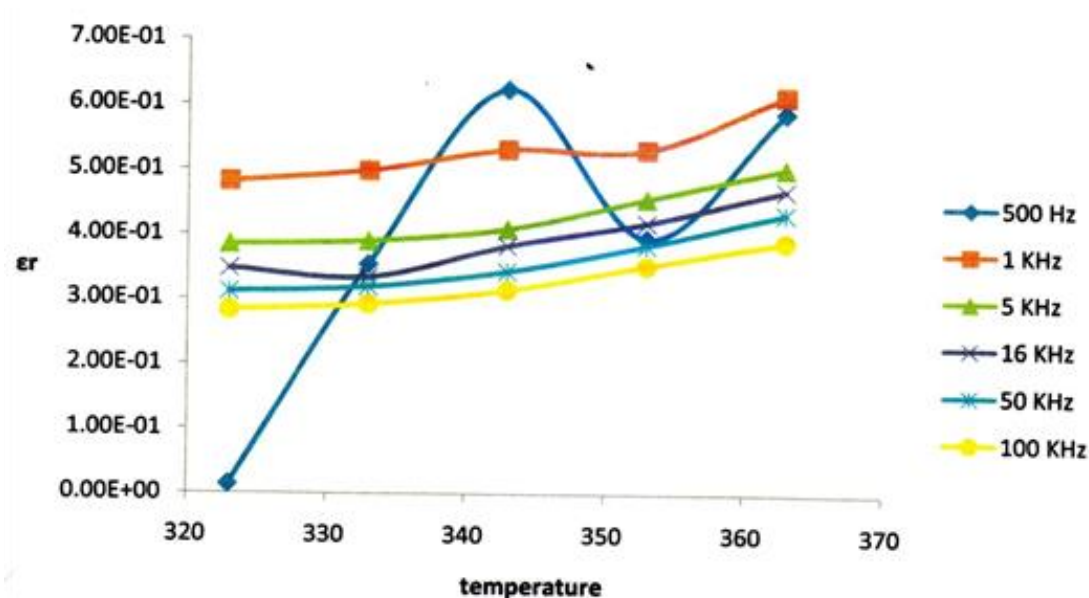


Fig. 4: Effect of temperature on dielectric constant

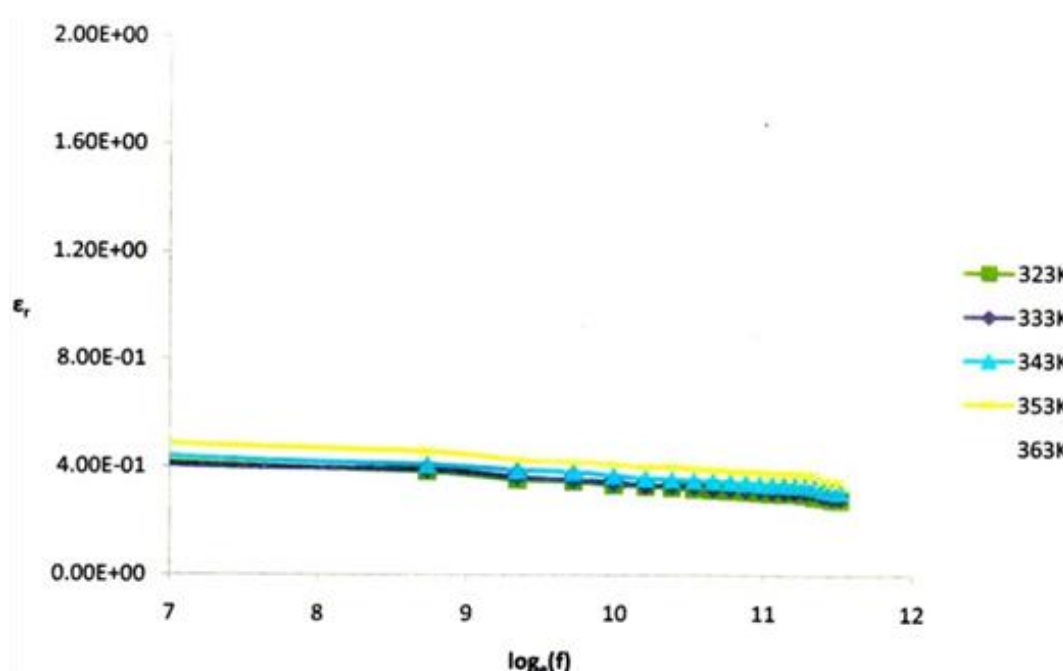


Fig. 5: Effect of frequency on dielectric constant.

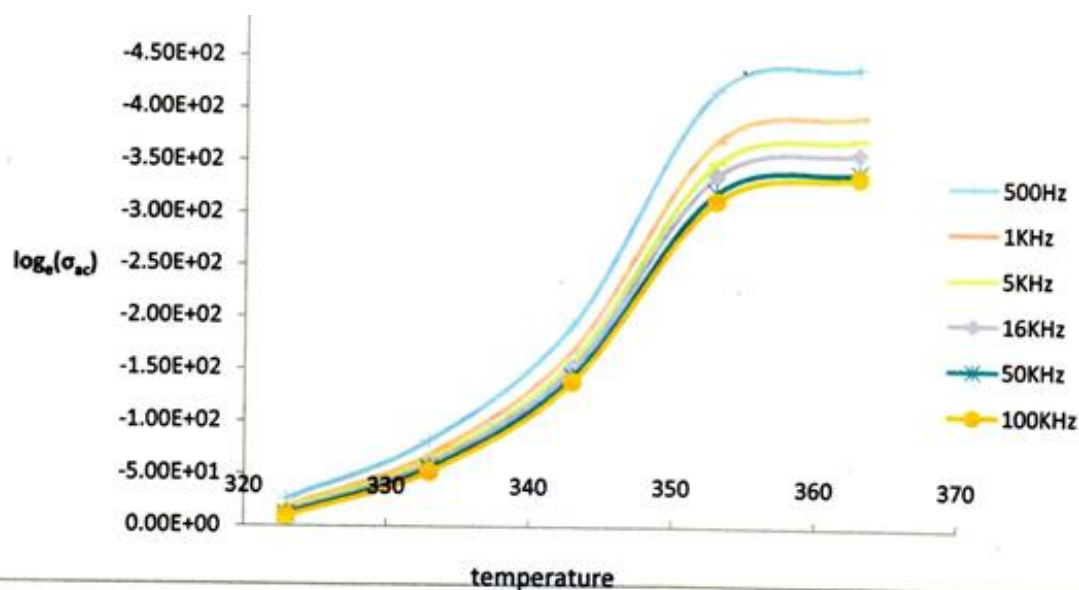


Fig .6: Frequency and temperature impact on AC conductivity

4. Conclusions

The following conclusions are drawn from the present study:

- 1) With temperature growth at constant frequencies, the dielectric constant increases
- 2) The dielectric constant decreases with constant frequency decreases in temperatures
- 3) The AC conductivity increases at different constant temperatures with frequencies
- 4) The frequency exceeds its highest value and hits almost saturation values.
- 5) The dielectric constant in the temperature range does not differ greatly.

References

- [1] Aziz M. S. and Aggour Y. A., Polymer Testing, Vol. 18, (1999) 511-521.
- [2] Belsare N. G. and Deogaonkar V. S., the Indian Pure and Applied Physics Journal, Vol. 36, (1998) 280-289.
- [3] Raghavendra S. C., Syed Khasim, Revanasiddappa M., Ambika Prasad M. V. N. and Kulkarni A. B. (2003), Bulletin of Material Science, 26 (7), 733-39.
- [4] Rao Vijayalakshmi, Ashoakan P.V. and Shridhar M. H. (2000).; Material Science and Engg. A281, 213-220.
- [5] Reda S. M., Dyes and Pigments Vol. XX. (2006), 1-7.
- [6] Shukla J. P. and Gupta M. (1987); the Indian Pure and Applied Physics Journal , Vol. 25, 242- 244.

Carbon Based Nanostructures for Energy Storage

K. Sree latha

Department of Physics, Ch. S. D. St Theresa's (A) College For Women - Eluru, W.G.Dt-534003, Andhra Pradesh

Abstract:

Materials can be made from several types of elements, either in the pure elemental form or in the form of compounds and composites. Generally, bulk materials can be classified broadly as metals, semiconductors, and insulators. And when any of these materials is produced in the nanometer scale, each displays shape-/size-dependent properties. These new properties have the potential to provide enormous opportunities for both scientists and engineers to create many novel applications that are normally not possible with conventional bulk materials. Many of the nanometer-scale properties (e.g., size, shape, surface structure, and chemical composition) have only been deciphered since the advent of advanced microscopic techniques, which has enabled researchers to precisely measure and directly visualize materials at the atomic scale in real time, something impossible just a few decades ago. And, even more impressive is the ability of these characterization techniques to give us a glimpse of materials and processes in their own localized micro-/nanoscopic environment. The nanometer-scale materials had different and remarkable properties originated with the discovery of buckminster- fullerene (C₆₀ or buckyball) in 1985. Subsequent studies ultimately led to the discovery of several other forms of exotic carbon structures, such as carbon nanotubes (CNTs; both single wall and multiwall), intercalated CNTs, carbon nanohorns, and recently graphene. These discoveries spurred researchers worldwide to actively investigate other nanometer- scale materials, especially those with inherently novel properties that could be proprietarily secured via trademarks and patents. Today, the range of elements and compounds successfully synthesized in nanometer-scale forms, characterized, and even deployed as commer- cial products include Metals, Metal oxides, Polymers, Semiconductors, Carbon compounds. The paper presents the processing and properties of different types of nanomaterials. In addition, the methods for the synthesis of different types of 1 D carbon nanotubes (CNTs) by the catalytic chemical vapour deposition (CCVD) technique by the pyrolysis of suitable hydrocarbons over selective alloy hydride catalysts and the processing of 2D

Keywords: Preparation, Processing, Properties, methods for the synthesis, Experimental techniques

1. Introduction

Carbon nano tubes (CNTs) are currently the focus of intense research world wise because of their unique properties that could impact various areas of science and technology. Recent experimental studies have shown that CNTs have mechanical strength suggesting their potential for advanced composites. The remarkable electronic properties offer them great potential for novel applications including various nano-devices. Because of their small diameter involving only a small number of carbon atoms and due to their large aspect ratio, CNTs are classified as one-dimensional (1D) carbon systems and most of the theoretical studies on CNTs emphasize their 1D properties. The most interesting of these theoretical developments was the prediction that SWNTs could be either semiconducting or metallic depending on their geometrical characteristics. Extensive effort has been taken to study the structural, electrical, mechanical and chemical properties of CNTs in order to explore the potential applications of these novel materials. The properties and applications of CNTs have been extensively reviewed by several authors. The recent developments in this field have generated great excitement in the area of nano scale science and technology.

CNTs can be used individually or as assembly for its various applications such as to build nano-electronic devices such as field effect transistors and rectifying electrodes. Bundles of nanotubes have been used for field emission based flat panel displays and other applications such as CNT based sensors and filters. Individual nanotubes have been used as tips for scanning probe microscopy. Bulk quantities of CNTs have also been used in other applications such as hydrogen storage media and composite materials with improved mechanical properties. For realizing the possible applications of CNTs, controlled and optimized growth of nanotubes is very significant. The nano-electronic applications require controlled and selective growth of CNTs on substrates.

Most of the applications demand high quality nanotubes in high yield. Even though lots of work has been carried out in recent years towards overcoming these issues, growth methods for large scale production of CNTs that are simple, efficient and inexpensive is still a major challenge. In recent years, chemical vapour deposition (CVD) method has been

shown to be promising for producing nanotubes with different morphologies in large quantities which is essential for various applications.

Graphene is a single sheet of graphitic carbon wherein the carbon atoms are tightly arranged in a 2D honeycomb like lattice. Graphene remained a theoretical construct for more than 70 years until its recent extraction in minute quantities by micromechanical cleavage. Whereas an efficient method to produce large quantities of single layer graphene still eludes the scientific community, a variety of methods for preparing (few) layered graphene sheets do exist: thermal exfoliation of graphite oxide, conversion from nanodiamond etc. Graphene sheets have excellent properties which make them suitable for a variety of applications. Intrinsic graphene is a semi-metal or a zero gap semiconductor. It has a linear energy dispersion relation resulting in zero charge carrier density (Dirac fermions). Exceptionally high electron mobility at room temperatures, with values in excess of $15000\text{cm}^2\text{V}^{-1}\text{s}^{-1}$ has been reported. However, with the increase in the number of layers these properties are expected to evolve and finally match those of bulk graphite. Interestingly, though not unexpected, few layered graphene is expected to retain many of the properties of single layer graphene and are hence suitable for a host of applications: FETs, transparent conductors, integrated circuits, ultracapacitors etc. Graphene with its extremely large surface area is also expected to be excellent materials for gas sensing applications. It is expected that with the introduction of defects and suitable dopants, graphene sheets can be engineered to detect suitable gases.

In this paper, we present the progress made in the synthesis of different types of nanomaterials and 1 D CNTs by CCVD and 2 D graphene by exfoliation of graphite oxide. Synthesis of MWNT, SWNT and metal/alloy encapsulated MWNT by pyrolysis of selective hydrocarbon over suitable alloy hydride catalysts, prepared by hydrogen decrepitation technique, will be focussed. The proposed growth mechanism of metal/alloy encapsulated MWNT produced by this technique and the various characterization methods employed are also discussed. Further, some of the applications of these CNTs with an emphasis on energy-related applications such as catalyst support material in hydrogen and alcohol based fuel cells (PEMFC, DMFC < DEFC), hydrogen sensors and hydrogen storage media are discussed in detail.

2. Synthesis of single walled carbon nanotubes, multi walled carbon nanotubes and magnetic metal-filled multi walled carbon nanotube by CCVD:

A novel, cost effective, easy and single step process for the synthesis of SWNT, MWNT and metal-filled MWNT, in large quantities using Mischmetal (Bharat Rare Earths Metals, India; composition: Ce 50%, La 35%, Pr 8%, Nd 5%, Fe 0.5% and other rare earth elements 1.5%) based AB_3 (B=Ni/Fe/Co) alloy hydride catalyst, obtained through hydrogen decrepitation technique. Catalytic chemical vapour deposition (CCVD) technique using a single-stage furnace facility has been used to grow these nanostructures in the temperature range 900⁰C to 1050⁰C. The carbon deposit obtained at 900⁰C shows the presence of MWNT. SEM image of the as grown MWNT synthesized over Mm based AB_3 alloy hydride catalyst with Ni at the B site at 900⁰C shows the presence of catalytic particles at the tips of the MWNTs. The selective EDAX pattern from the MWNT tips show the presence of Ni which is responsible for the nucleation of CNTs. These catalytic impurities can be removed by refluxing with concentrated nitric acid for approximately 24hr. SEM, TEM and HRTEM images of purified MWNT show an inner diameter of about 15 nm and outer diameter of around 60 nm.

Raman spectrum obtained from a Renishaw aRaman spectrometer using 514.5 nm excitation of the MWNT and SWNT shows typical tangential modes corresponding to the Raman allowed optical mode E_{2g} of two-dimensional graphite, centered around 1580 cm^{-1} (G-band) observed for all the samples. In addition, a peak centered at around 1350 $^{-1}$ (D-band) is mainly due to defects and carbonaceous particles present in the sample. The intensity of D-band gives the degree of disorder present along the tube.

3. Performance of PEMFC using Pt/MWNT-Pt/C composites as electrocatalysts for oxygen reduction reaction in PEMFC:

Purified MWNT were ultrasonicated in 10 ml of acetone for 1 hr and then 0.075 M H_2PtCl_6 was added slowly during stirring. After 12 hr, the mixture was reduced by adding reducing solution containing 0.1M $NaBH_4$ and 1 M NaOH. After completion of reaction, the solution was washed with de-ionized water, filtered and dried by vacuum filtration using a filter. The recovered Pt loaded MWNT were dried at 80⁰C for 3 hr. The crystallinity of the samples was obtained by X-ray powder diffraction (XRD) analysis, performed with a monochromatic $Cu-K\alpha$ radiation. Morphological characteristics of CNTs were obtained using scanning electron microscopy (SEM) and Transmission electron microscopy (TEM).

The membrane electrode assembly (MEA) was obtained by sandwiching a pre-treated Nafion 1135 (Nafion R) membrane between the anode and the cathode. Both the

anode and cathode layers consisted of a backing layer, a gas diffusion layer and a catalyst layer. To prepare the catalyst layer, the required amount of catalyst was suspended in de-ionized water and ultrasonicated by adding 5wt% Nafion solution. The suspension was spread uniformly over a carbon fabric (SGL Carbon). The electrodes were of 11.56 cm² area. The electrodes were sandwiched by hot pressing at 130⁰C and 70 bar for 2 min. The anode was a 3.4*3.4 cm² 20% Pt/C electrode, with a platinum loading of 0.25 mg cm⁻². The cathode was prepared from a suspension containing mixture of Pt/MWNT (Pt content of 20wt %) and Pt/C (Pt content of 20 wt%), with a platinum loading of 0.5 mg cm⁻². A single PEMFC was assembled using the MEA, two graphite plates with gas channels machined with a serpentine geometry, two Teflon gaskets and two aluminium end plates. The performance of the PEMFC was studied in an indigenously fabricated Fuel Cell test station, using a dc electronic load box. Since hydration of the electrolyte membrane is important for attaining maximum performance of the PEMFC, reactant gases were humidified with water.

4. SEM, TEM HRTEM images of Pt loaded MWNT:

A TEM image of Pt/MWNT shows a more or less uniform distribution of noble metal particles of size of about 3-5 nm on the CNTs. The HRTEM image of Pt/MWNT clearly indicates lattice planes of Pt particles indicating crystalline nature of catalytic Pt. The energy dispersive analysis (EDAX) shows that the amount of Pt loaded on the carbon nanotube support with reference to carbon can be evaluated qualitatively as 20%. The polarization curves were obtained from the single cell PEMFC using the same type of anode. Prior to polarization studies, the electrodes were activated between open-circuit potential and high current densities. The activation cycle is necessary to activate the catalyst for the oxygen reduction reaction. The performance of Pt/MWNT electrocatalysts, prepared using pre-treated MWNT grown over Mm based AB₃ alloy hydride catalysts, mixed with varying amounts of commercial Pt/C as cathode catalyst in PEMFC, under an operating pressure of 1 bar. In the low current density region, the voltage drop in the potential-current curve, generally known as activation polarization, reflects the sluggish kinetics intrinsic to the oxygen reduction reaction at the cathode surface. The voltage drop in the mid to high current density range, or ohmic polarization, arises from limitations in proton transport through the electrolyte membrane from anode to cathode and/or limitations in electron flow in the electrode materials. Better performance of PEMFC was observed for cathode catalyst with Pt/MWNT content compared to those containing commercial Pt/c which could be attributed

to higher catalytic activity of smaller Pt particles with uniform sizes decorated on the MWNT. The higher performance of the Pt/MWNT electrodes compared to the Pt/C electrodes could be ascribed to the networks and interiors of CNTs consisting of spaces for gas diffusion and high electric conductivity of MWNT. Pt/Ru/multiwalled carbon nanotubes are electrocatalysts for Direct methanol fuel cell.

5. Pt-Ru/multiwalled carbon nanotubes as electrocatalysts for Direct Methanol Fuel Cell:

Purified MWNT were ultrasonicated in 10 ml of acetone for 1 h and then 0.075 M H_2PtCl_6 and 0.15 M RuCl_2 solutions were added slowly during stirring. After 12 h the mixture was reduced by adding reducing solution containing 0.1 M NaBH_4 and 1M NaOH. After completion of reaction the solution was washed with de-ionised water, filtered and dried by vacuum filtration. The recovered Pt-Ru loaded MWNT were dried at 80°C for 3h. Here in DMFC, membrane electrode assembly (MEA) was obtained by sandwiching a pre-treated Nafion 1110 membrane between the anode and cathode. The anode was Pt-Ru/MWNT, with a loading of 2.5 mg cm^{-2} . The cathode was prepared from a suspension containing mixture of Pt/MWNT and 20% Pt/C, with a platinum loading of 5 mg cm^{-2} . Humidified oxygen was passed to the cathode at the flow rate of 180 sccm and 1M methanol at the anode through the serpentine channels of DMFC.

6. Conclusion

Today, the entire world faces an energy crisis such as never seen before, and many nations have to rely exclusively on costly imported fossil fuels to generate electricity to power their economy and provide energy for the population. Even in advanced economies, fossil fuels are increasingly becoming expensive and have a polluting cost associated with their continued use. Nanotechnology has shown many glimpses of instances for manipulating nanomaterial to create new avenues for sustainable clean energy and potential solutions for the future.

The nanocarbons created in Laboratory can be used to coat a simple Cu metal foil and the temperature profile plotted versus time when this carbon-coated foil is placed in direct sunlight. The levels of coatings and nature of the nanocarbons contributing to the profile can be investigated. Carbon bucky paper can be readily made from either a commercial source of carbon nanotubes (CNTs) or using graphene-based materials. These can then be characterized with the nanotools described previously and made into electrode

substrates for the microbes (either on its own or also doped with metallic NPs). Then, the efficiency of these cells can be evaluated. Fuel cells can be an alternative source of power, and one active area of research and development is in microbial fuel cells (MFCs). In this type of cell, microbes are utilized to generate hydrogen that can be used as a source of fuel. Carbon buckypaper can be readily made from either a commercial source of carbon nanotubes (CNTs) or using graphene-based materials. These can then be characterized with the nano tools described previously and made into electrode substrates for the microbes (either on its own or also doped with metallic NPs). Then, the efficiency of these cells can be evaluated.

References

- [1] Peigey, A.(2003) Tougher ceramics with carbon nanotubes. *Nature Mater.*,2 15-16.
- [2] Dresselhaus, M.S., G. Dresshaus, and R. Saito(1992) Carbon fibers based on C₆₀ and their symmetry. *Phys. Rev. B*,45,6234-6242.
- [3] Dai,H(2002) carbon nanotubes: opportunities and challenges.*Surface science*,500,218-241.
- [4] De Heer, W.A., A. Chatelain, and Dugarte (1995) A carbon nanotube field emission electron source, *science*,270,1179-1180.
- [5] Modi, N. Koratkar, E.Lass, B.Q.Wei, and P.M. Ajayan(2003) Miniaturized gas ionization sensors using carbon nanotubes. *Science*,424,171-174.
- [6] Srivastava,A., O.N.Srivastava, as. Atalapatra, ar.avajtai, P.M.Ajayan, Carbon nanotube filters, *Nature Materials*, 3, 610-614.
- [7] Hafner, J.H., C,L.Cheung, T.H.Oosterkamp, High yield assembly of individual single-walled carbon nanotube tips for scanning probe microscopies. *J.Phys.Chem.B*, 105(4) 743-746.
- [8] Tibbetts, G.G., G.P.Meisner and C.H.Olk Hydrogen storage capacity of carbon nanotubes, filaments and vapour-grown fibers, *carbon*, 39, 2291-2301.

Reduced graphene oxide Nano sheet Decorated Nb₂O₅ composite for Advanced Energy Storage Material

R. Sandhya¹, M. Mylarappa^{*2}, S. Kantharaju², Rajaiah B¹, Deepushree S.R¹

¹Department of Chemistry, KLE Society's S.Nijalingappa College, Bengaluru-560010,

²Department of chemistry, Sri Jagadguru Renukacharya College of Science, Arts and Commerce, Bengaluru-560009.

*Corresponding author: E-mail address: mylu4mkalihatti@gmail.com

Abstract

Facile synthesis of rGO-Nb₂O₅ composite for energy storage studies has been reported. Graphene oxide (rGO) was prepared by the modified Hummer's method. The metal oxide (Nb₂O₅) was introduced to the rGO to form the composite by the hydrothermal method. The prepared samples were characterized by X-ray diffraction, scanning electron microscopy, Fourier transform infrared spectroscopy and UV-Visible spectroscopy. The CV measurements reveal a significant enhancement in electrochemical reversibility and the specific capacitance of rGO and Nb₂O₅/rGO were found to be 45 Fg⁻¹ and 110 Fg⁻¹ respectively. These results indicates that capacitive behaviour and electron transfer of Nb₂O₅/rGO nano composite was predominantly more compared to rGO. The charge-discharge curves display well-symmetry and linear deviations with change of the time indicating superior capacitance. This is mainly because of the electrode reversible reaction and also revealed that as a kind of super capacitor electrode materials. The obtained electrode materials showing the highest specific capacitance with excellent rate capability.

Keywords: rGO, Nb₂O₅/rGO composite, characterization, energy storage studies.

1. Introduction

Industry and research centres around the globe are coping to address the world-wide energy demand and are competing with all available alternative technologies. Super capacitors signify an attractive alternative for portable electronics and automotive applications due to their high specific power and extended life. In fact, the growing demand of portable systems and hybrid electric vehicles, memory protection in complementary metal-oxide-semiconductor (CMOs), logic circuit, vapour-compression refrigeration system (VCRs), CD players, PCs and UPS in security alarm systems, remote sensing, smoke detectors etc. require high power in short-term pulses [1].

Reduced graphene oxide (rGO) - metal oxide nanocomposite is the trending field, with applications in batteries, supercapacitors, tracing and absorption of heavy and toxic elements, photocatalytic dye degradation, fire fighting coatings, biosensors and electrocatalysts in oxide fuel cells [2-9]. Many studies have observed rGO nano composite materials decorated with metal and reported that the resulting materials have enhanced properties that are absent in their individual components [10].

The functionalization of metal oxide nanocomposite on the graphene matrix improves the performance of metal oxide nanocomposite, which exhibit properties like agglomeration and Ostwald ripening. The composite of graphene with metal oxides like SnO₂, MnO₂, Co₃O₄, Nb₂O₅, V₂O₅, Fe₂O₃ and RuO₂ have proved the enhancement of electrochemical and pseudocapacitance behaviour by overcoming the limitations such as reduced electrical conductivity, poor electrochemical cycling ability and low specific capacitance. A hybrid system consisting of graphite cathode and Nb₂O₅ anode has been tested for suitability as a hybrid supercapacitor [11-16].

Synthesis of reduced graphene oxide-Nb₂O₅ nanocomposite and its structural, optical and electrochemical properties have been reported. Shishun Qi et al. studied the photocatalytic applications of graphene nanocluster decorated niobium oxide nanofibers [17]. T-Nb₂O₅/graphene based pseudo capacitive electrode for asymmetric supercapacitor has been reported by Kong et al. with a specific capacitance value of 80 Fg⁻¹ at 0.2 Ag⁻¹ [18]. Wang et al. reported the fabrication of hybrid electrochemical capacitor with binder-free Nb₂O₅/graphene and studied the electrochemical characteristics with the discharge specific capacity of 58 Fg⁻¹ at 0.1 Ag⁻¹ [19]. Nb₂O₅ anchored graphene nanocomposite has been

synthesized with low amount of graphene content with the capacitance value of 34 Fg^{-1} at 0.05 Ag^{-1} [20].

In the present investigation, the synthesis of rGO-Nb₂O₅ nanocomposites by hydrothermal method has been presented. This method resulted in the formation of homogeneous composite with uniform distribution of Nb₂O₅ on the graphene surface. The structural, optical and electrochemical properties of the rGO-Nb₂O₅ nanocomposites were systematically studied and the results were compared with pure graphene and Nb₂O₅ nanoparticles.

2.1 Materials and Method

2.1.1 Materials

The materials used for the entire work with all the specifications, purity, grades, structural and chemical formulas with supplier names are mentioned in the Table 1.

Table 1. Details about the chemicals used

Materials	Formula	Specifications	Suppliers
Sodium Nitrate	NaNO ₃	Molar mass: 84.9g/mol	Merck, Bangalore
Sulphuric acid	H ₂ SO ₄	Molar mass: 39.9 g/mol	Sigma Aldrich
Hydrogen peroxide	H ₂ O ₂	Molar mass: 34.01 g/mol	Merck, Bangalore
Potassium permanganate	KMnO ₄	Molar mass: 158.0 g/mol	Merck, Bangalore
Niobium chloride	NbCl ₅	Molar mass: 270.17g/mol	Sigma Aldrich
tri-Sodium citrate	Na ₃ C ₆ H ₅ O ₇	molar mass:294.10 g/mol	Merck
Sodium Sulphite	Na ₂ SO ₃	molar mass: 126.0 g/mol	Merck, Mumbai

2.2 Experimental

2.2.1 Synthesis of Graphene Oxide (GO)

Graphene oxide (GO) was prepared by 1g NaNO₃ and 2g of graphite powder was added to 1000ml beaker which was placed in ice bath and temperature was maintained from 0-6°C.

Then 98% H₂SO₄ was added to it slowly .The reaction mixture with ice bath was kept on magnetic stirrer with constant stirring. Accurately 6g of KMnO₄ was added very slowly in instalments with duration of 3 hours. While adding KMnO₄, the mixture starts to spill and effervescence is observed therefore caution must be taken to avoid explosion. After 2 hours the beaker was removed from ice bath and was placed on a hot plate with magnetic stirrer and temperature was maintained at 30°C. The colour slowly changes to brownish black and the temperature was increased every half an hour. After 2 hours add 100 ml of H₂O with constant stirring and by turning off heat .Then 80 ml H₂O₂ was added to terminate the reaction and to remove excess KMnO₄ .When ppt. settles down yellow colour solution is obtained. The obtained solution was filtered using Buckner funnel and then placed in hot air oven at less than 90°c overnight.

2.2.2 Preparation of Nb₂O₅/rGO nanocomposites

In a typical synthesis process, 0.3 g of the reduced graphene oxide was dispersed in distilled water and sonicated for 3 h. Then 0.1 g of NbCl₅ was added and stirred using a magnetic stirrer. After 1 h, 1% sodium citrate was boiled for 55 minutes and 100 mg of sodium sulphite in 5 ml of distilled water were added to the solution and stirred for 3 hours, cooled to the room temperature.The solution was filtered using a Wattman filter paper and the product washed with distilled water and ethanol for several times. The prepared composite solution was dried in vacuum at 333K for 24 h to obtain the rGO-Nb₂O₅ nanocomposite.

3. Result and Discussion

3.1. X-Ray Diffraction Studies

The phase composition and the crystallinity of the powder was detected by X-ray diffractometer using the Shimadzu-7000 X-ray diffract meter with monochromatized Cu Ka radiation. The XRD of rGO, Nb₂O₅ and Nb₂O₅/rGO were shown in Fig. 4.1 a) to Fig. 4.3 c). The average crystallite sizes of particles were assessed in agreement with Scherer's equation using full width at half maximum (FWHM) evidence.

$$D = \frac{0.9 \lambda}{\beta \cos \theta} \dots \dots (1)$$

where k ; constant depends on the grain shape (about 0.90), λ ; the X- ray wavelength (0.15418 nm), β ; the full width at half maximum (FWHM) of the diffraction line and θ ; the diffraction angle.

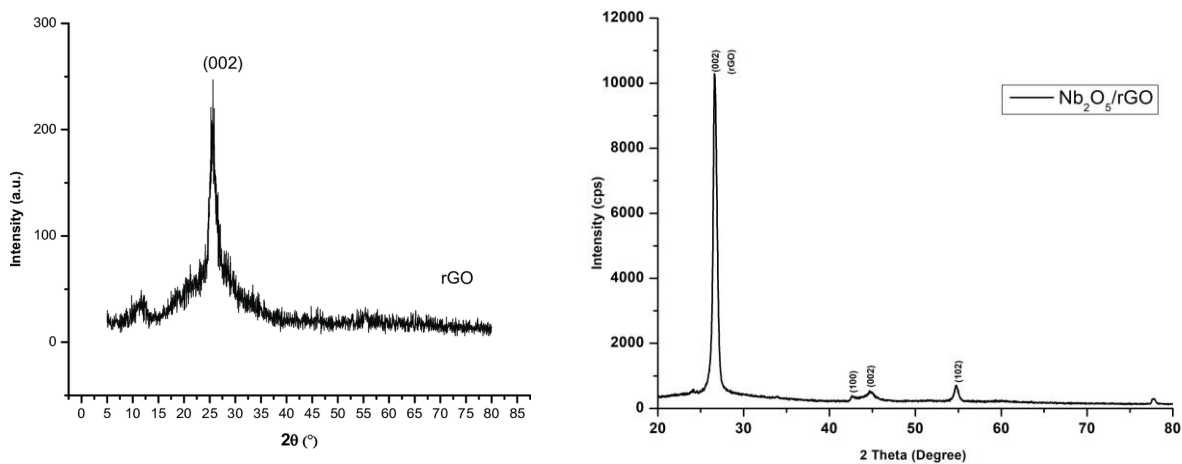


Fig.1 XRD spectrum of a) graphene oxide b) Nb₂O₅/rGO.

The calculated mean crystallite size of the rGO, Nb₂O₅ and Nb₂O₅/rGO were found to be 14, 20 and 9.8 nm. The peaks shown in the XRD pattern of Nb₂O₅/rGO are intense and sharp, representing good crystallinity of the prepared sample. No evidence of impurity peaks was detected, which indicated that high pureness. The strong and narrow peak signifies that the product has well crystalline nature of particles. The Scherer’s equation and Williamson and Hall (W-H) method were used to calculate the total crystalline sizes of rGO, Nb₂O₅ and Nb₂O₅/rGO. The W-H method recommended that when the domain effect and lattice micro strain effect were together concurrently working, their mutual effects gives the final line broadening FWHM which was the sum of grain size and lattice distortion.

$$\cos\theta = \varepsilon(4\sin\theta) + \frac{\lambda}{D} \tag{2}$$

The equation (2) indicates a straight line between $4\sin\theta$ and $\beta\cos\theta$ where ε ; the strain associated with the nano composites. The intercept $(0.90\lambda/D)$ of the line gives crystallite size (D) and slope of line gives the strain (ε). The values obtained from above equation were analogous with the crystallite size calculated from Scherer’s equation. The other structural

parameters such as dislocation density (δ), strain (ϵ) and stacking fault (SF) were controlled by the accompanying connection. The dislocation density and stacking fault were estimated by using the following relations.

$$\delta = \frac{1}{D^2} \tag{3}$$

$$\epsilon = \frac{\beta \cos\theta}{4} \tag{4}$$

$$SF = \frac{2\pi^2}{45\sqrt{3} \tan\theta} \tag{5}$$

3.2 Field Emission Scanning Electron Microscopy and EDS Studies

The energy-dispersive X-ray (EDX) analyses were obtained for as prepared materials to confirm the existence of Niobium, Oxygen and Carbon as the elementary components in the morphology of the prepared composites was studied by Field emission scanning electron microscope (FE-SEM) and the images are shown in Fig.2. The morphology of Nb₂O₅/rGO composite contains graphene sheets and it is observed that Nb₂O₅ is intercalated between the graphene sheets as shown in Fig.2. Higher magnification image confirms the paper like structure of graphene with Nb₂O₅ attached on the surface. The increase in the graphene weight percent causes the aggregation of Nb₂O₅ with graphene and hence graphene structure becomes irregular flake-like morphology as shown in the magnified image.

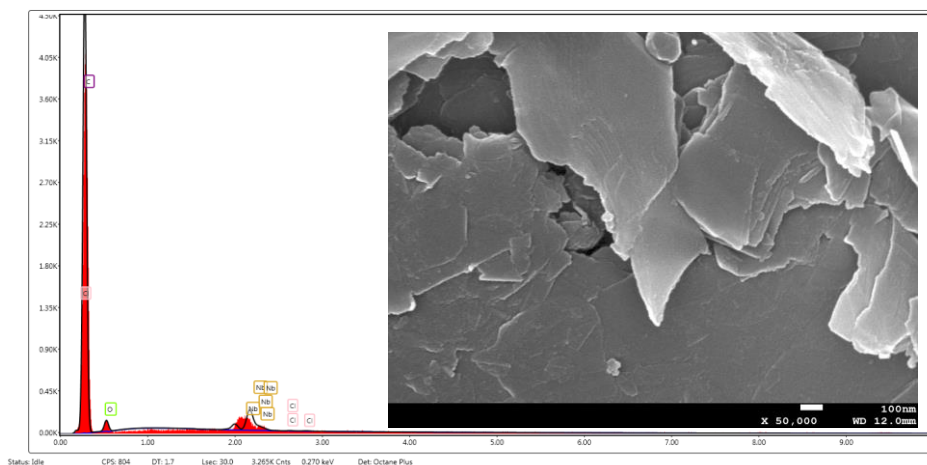


Fig.2 EDAX/FESEM micrographs of Nb₂O₅/rGO nano composite

3.3 Fourier transforms infrared spectrometer studies

FT-IR measurements was carried out to obtain further insights on Nb₂O₅/rGO nanocomposites as shown in Fig.3. The broad band observed at ~3430 cm⁻¹ for the as-synthesized samples corresponds to the O–H stretching vibration of physically adsorbed water and/or intercalated water molecules in the GO and rGO nanocomposites. Other FT-IR peaks at 1724 cm⁻¹ (C=O stretching vibration of –COOH group), 1624 cm⁻¹ (C=C stretching vibration), 1231 cm⁻¹ (C–O stretching vibrations in epoxide), 1084 cm⁻¹ (C–OH stretching vibration in alkoxy group). The FT-IR spectrum of Nb₂O₅ shows a band at 510 cm⁻¹ attributed to the Nb–O vibration of the Nb₂O₅ crystal.

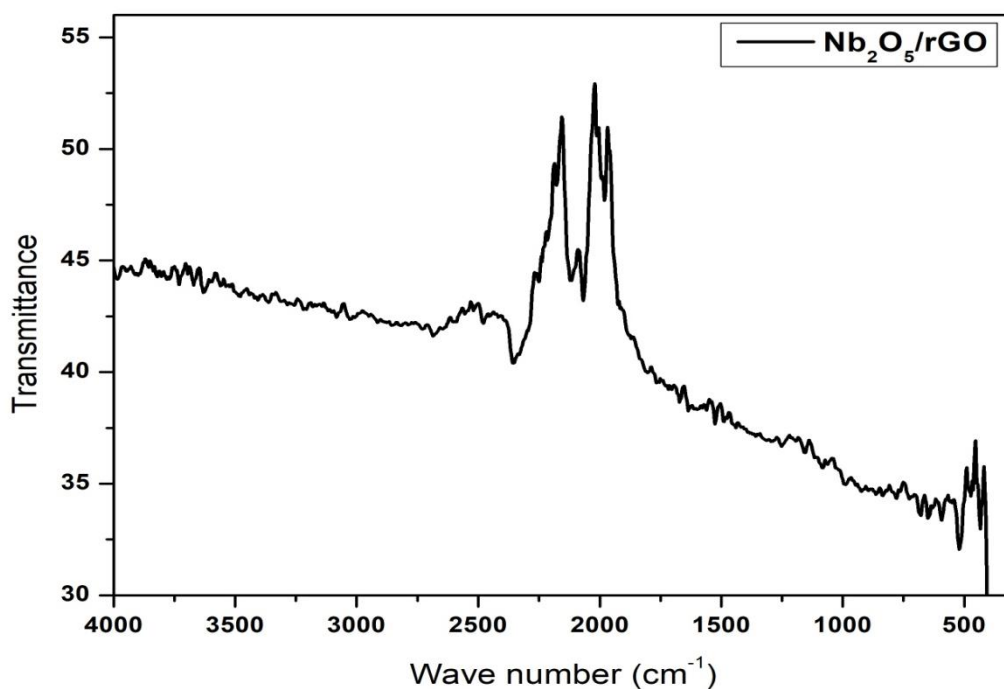


Fig.3 EDAX/FESEM micrographs of Nb₂O₅/rGO nano composite

3.4 Band gap analysis

In the present case optical studies of the unirradiated and electron irradiated films were carried out in the wavelength range 190-700 nm. Here for any set of measurements, first the wavelength scan is performed without the sample as reference in the beam path and then the samples are placed within the sample holder having a hole of 2 mm diameter and kept in the

beam path. The samples are scanned and the absorbance's were calculated with the aid of the stored reference data and accumulated in computer memory. The optical band gap (E_g) is determined from the observed UV-Visible spectral dependence of the absorption near the absorption edge. Based on Urbach rule the absorption coefficient (α) is calculated from the optical absorption spectrum. It is known that the absorption coefficient for non-crystalline materials varies with frequency and the relationship between the absorption coefficient (α) and the optical band gap E_g obeys the classical Tauc's expression. Hence the observed absorption spectrum is translated in to Tauc's plot using the equation. For all samples a plot of the product of absorption coefficient (α) and photon energy ($\alpha h\nu$)^{1/2} versus the photon energy $h\nu$ at room temperature shows a linear behaviour, which can be considered as an evidence for the indirect allowed transition. Extrapolation of the linear portion of this curve to a point ($\alpha h\nu$)^{1/2} = 0 gives the optical band gap E_g . In Fig 4, the energy band gap of Nb_2O_5/rGO nanocomposites was found to be 5.6 eV respectively.

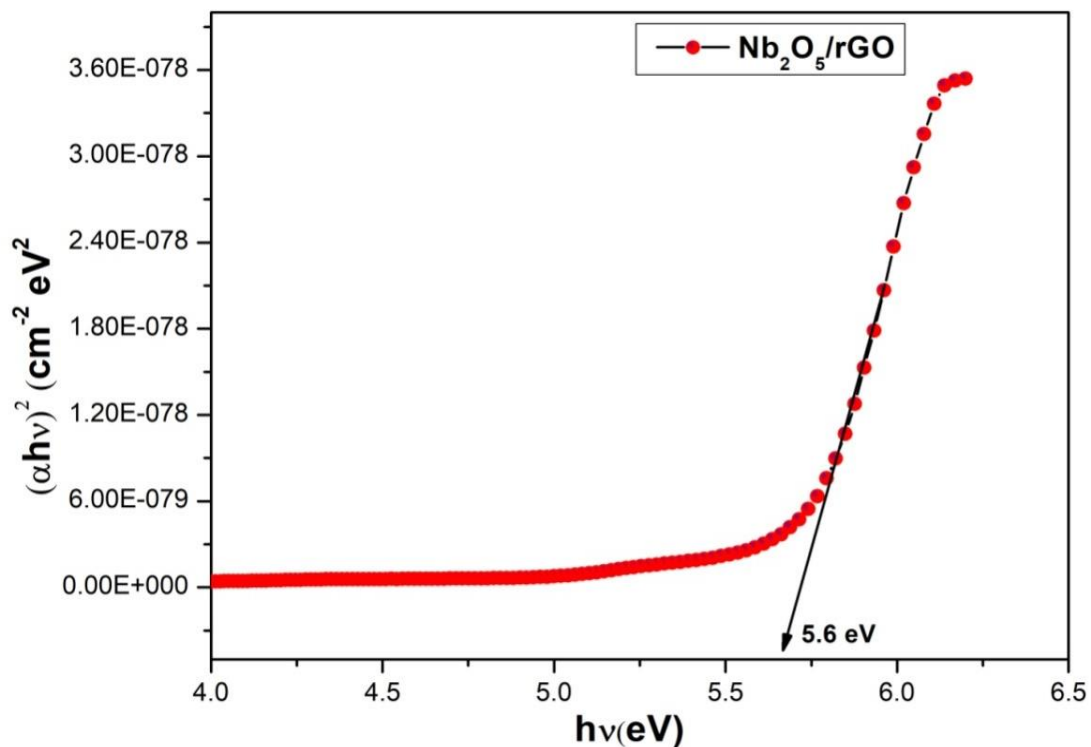


Fig.4 Energy gap of Nb_2O_5/rGO nano composite.

4. Electrochemical Studies

4.1. Cyclic Voltammetry studies

In the CV analysis, the working electrode ($\text{Nb}_2\text{O}_5/\text{rGO}$) was prepared by mixing 0.025 g of active material + 0.475 g of graphite +3-5 drops of polytetrafluoroethylene (PTFE) solution which was added as a binder and blended by hand mixing with a mortar and pestle for about 30 minutes until a uniform thin sheet achieved. The obtained thin sheet was pressed on nickel mesh (area about 1 cm^2) to create a good conductivity with the Ni mesh and active material. The obtained electrode was dried at 50°C for 48 hours and the prepared electrodes were kept for 20 days electrode setting because for stability of the electrode as shown in Fig.5.

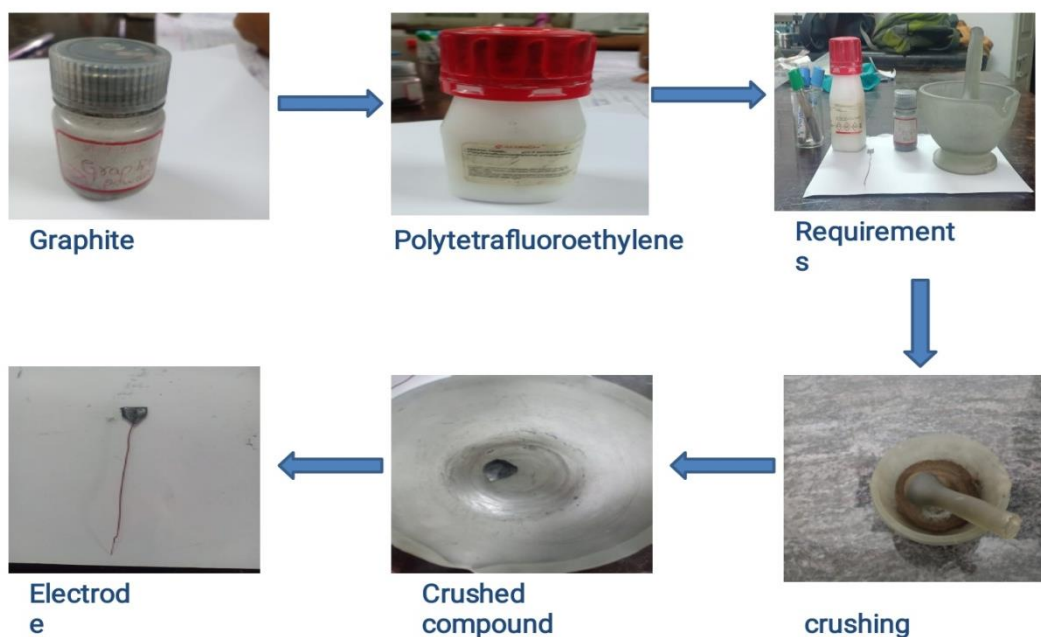


Fig.5 Method of Preparation of working electrode using graphite and binder.

An electrochemical measurement comprises three electrode system having active material, Ag/AgCl electrode and a platinum as counter electrode. CV measurements were applied in the potential range -0.6 to 0.02 V using 3M KOH as shown in the Fig.6 a) and Fig.6 b). In Fig.6 a) and Fig.6 b). the electrochemical reversibility was calculated by seeing of the difference between the E_{O} and E_{R} at 0.01 V/s scan rate. The results revealed that the electrode

reversibility reaction of Nb₂O₅/rGO (Table 2) was decreased as compared to that of rGO and CV curves displays a quasi-reversible electron transfer process representing that capacitive behaviour was predominantly based on the redox mechanism. According to the Randles-Sevcik equation for reversible process, the height current is denoted by the equation.

$$I_p = 2.69 \times 10^5 \times n^{3/2} \times A \times D^{1/2} \times C_0 \times v^{1/2}$$

where *n* is the number of electron transferred in the reaction, the active surface area (*A*), diffusion co-efficient (*D*), scanning rate (*v*) and initial concentration of the chemical (*C*₀) respectively. The greater linear association involving in peak current (*i*_p) and number of electron transferred (*n*^{1/2}) confirm that the electrode reaction of rGO and Nb₂O₅/rGO was measured by hydrogen diffusion co-efficient (*D*). The increased *D* values of Nb₂O₅/rGO revealed that electrochemical activity are more effective compared to that of rGO respectively.

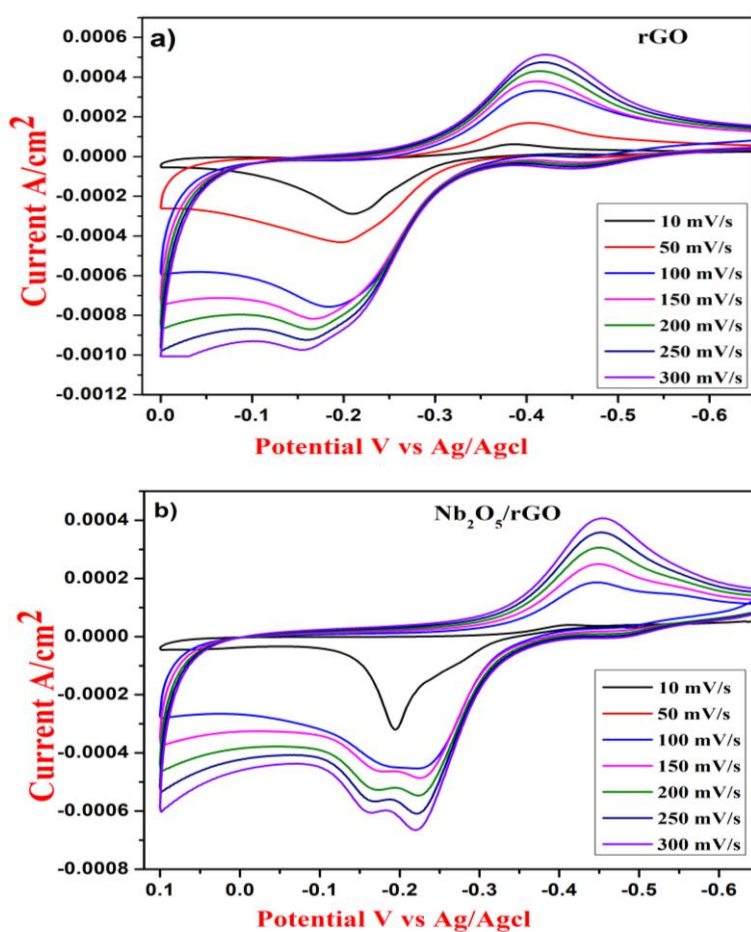


Fig.6. CV curves of a) rGO b) Nb₂O₅/rGO

Table 2. Specific capacitance calculated from CV curve.

Electrode	Csp from CV method	Energy density (E)	Power density (P)
rGO	45 Fg ⁻¹	5.18 whK/g	7.73 Kw/Kg
Nb ₂ O ₅ /rGO	110 Fg ⁻¹	21.4 whK/g	10.23 Kw/Kg

The electrode surface area and specific capacitance of rGO and Nb₂O₅/rGO from CV method were calculated by using the relation.

Specific capacitance $C_p = \frac{Q}{mV}$

Where, Q - charge stored in coulombs, m - is the mass of active material in gram, V - is the potential and Cp is the specific capacitance.

We know that, $I = \frac{Q}{t}$, $Q = I \times t$

Substitute, $C_p = \frac{I \times t}{mV}$

Divide the neumarator and denominator by 't'

$$C_p = \frac{I \times \frac{t}{t}}{\frac{mV}{t}}$$

$C_p = \frac{I}{\frac{mV}{t}}$ in the above equation $\frac{V}{t}$ is the scan rate of CV and I represent current k

$$C_p = \frac{I}{m \times k}$$

$I = C_p \times m \times k$

In CV curve the current changes by change in potential from V₁ to V₂

∴ in the equation (3) can be written as

$$\int_{V_1}^{V_2} I(V)dV = \int_{V_1}^{V_2} (Cp \times m \times k)dV$$

If we look above equation integrate the left side

$$\int_{V_1}^{V_2} I(V)dV = \text{Area represents the area of the CV at the centre}$$

$$I(V) \times dV = Y \times X = \text{Area}$$

∴ the equation (4) becomes

$$\text{Area} = \int_{V_1}^{V_2} (Cp \times m \times k)dV - (5) \text{ for specific material the } Cp, m, k \text{ constant}$$

∴ the integral equation (5) becomes solved as

$$\text{Area} = (V_2 - V_1) Cp \times m \times k$$

During the charging of capacitor then the Area = A and the equation becomes

$$A_1 = (V_2 - V_1) Cp \times m \times k$$

Similarly, during discharging capacitor the area A and the equation becomes

$$A_2 = (V_2 - V_1) Cp \times m \times k$$

From the calculations of area A inside the CV curve we have to substitute equation (3.9) from equation (3.10)

$$A = A_1 - A_2 = [(V_2 - V_1) Cp \times m \times k] - [(V_1 - V_2) Cp \times m \times k]$$

$$A = 2 (V_2 - V_1) Cp \times m \times k]$$

$$\frac{A}{2} = (V_2 - V_1) Cp \times m \times k$$

$$\frac{A}{2 (V_2 - V_1) m \times k} = Cp \text{ Or } Cp = \frac{A}{2 m k (V_2 - V_1)}$$

where Cp = Specific capacitance F/g , A = Area inside the CV curve unit AV

m = mass of active, k = scan rate of material CV (total range) is the potential difference window of CV (total voltage range) we will have equation can be used. In Fig.6 a)-b), the specific capacitance values of rGO and Nb₂O₅/rGO were calculated and found to be 45 Fg⁻¹ and 110 Fg⁻¹ respectively.

5. Conclusion

rGO-Nb₂O₅ nanocomposite was successfully prepared by hydrothermal method. The morphology and structure of the composite were studied by XRD, FESEM EDS and UV analyses. From electrochemical studies, the specific capacitance values of rGO and Nb₂O₅/rGO was found to be 45 Fg⁻¹ and 110 Fg⁻¹ respectively.

Acknowledgment

The authors' thanks to the Sri Jagadguru Renukacharya Education Society (SJRES) and Principal of SJRC for their encouragement in extending the lab facilities for completion of the research work.

References

- [1] Humberto Gómeza, Manoj K. Ramb, Farah. Alvia, P. Villalba, Elias (Lee) Stefanakosc, Ashok Kumara, J. Power Sources. 196 (2011) 4108.
- [2] X. Zhu, Y. Zhu, M. Shanthi, M.D. Stoller, S. Rodney J. Ruoff, Power Sources. 196 (2011) 6473. .
- [3] I.T. Kim, A. Magasinski, K. Jacob, G. Yushin, R. Tannenbaum, Carbon. 52 (2013) 56.
- [4] H. Yang, J. Jiang, W. Zhou, L. Lai, L. Xi, Y. M. Lam, Z. Shen, B. Khezri, T. Yu, Nanoscale Res. Let. 6 (2011) 1.
- [5] A.K. Mishra, S. Ramaprabhu, J. App. Phy.112 (2012) 104315.
- [6] B.P. Sahoo, S. Sahoo, A.K. Satpati, D. Li, D. Bahadur, Biosensors and Bioelectronics. 43 (2013) 293.
- [7] S. Guo, G. Zhang, Y. Guo, J.C. Yu, Carbon. 60 (2013) 437.
- [8] C. Bao, L. Song, C.A. Wilkie, B. Yuan, Y. Guo, Y. Hu, and X. Gong, J. Mat. Chem. 22 (2012) 16399.
- [9] W. Hong, H. Bai, Y. Xu, Z. Yao, Z. Gu, G. Shi, J. Phys. Chem. C. 114 (2010) 1822.
- [10] V. Goyal, A.A. Balandin, Appl. Phys. Lett. 100 (2012) 073113-1.
- [11] F. Li, J. Song, H. Yang, S. Gan, Q. Zhang, D. Han, A. Ivaska, L. Niu, Nanotech. 20 (2009) 455602. [21] S. Chen, J. Zhu, X. Wu, Q. Han, X. Wang, ACS. Nano. 5 (2010) 2822.
- [12] K. SengáTan, C. MingáLi, Phy. Chem. Phy.13 (2011) 14462.

- [13] R. Thangappan, S. Kalaiselvam, A. Elayaperumal, R. Jayavel, *Solid State Ionics*. 5 (2014) 15321.
- [14] K.K. Lee, S. Deng, H.M. Fan, S. Mhaisalkar, H.R. Tan, E.S. Tok, K.P. Loh, W.S. Chin, C.H. Sow, *Nanoscale*. 4 (2012) 2958.
- [15] Minoh Lee¹, Suresh Kannan Balasingam, Hu Young Jeong, Won G. Hong, Han-Bo-Ram Lee, Byung Hoon Kim & Yongseok Jun. 5 (2015) 8151.
- [16] Gum-Jae Park, D. Kalpana, AK. Thapa, H. Nakamura, Y.S Lee, M.Yoshio, *Bull. Korean Chem. Soc.* 30 (2009) 817.
- [17] S. Qi, L. Fei, R. Zuo, Y. Wang, Y. Wua., *J. Mater. Chem. A*, 2 (2014) 8190.
- [18] L. Kong, C. Zhang, S. Zhang, J. Wang, R. Cai, C. Lv, W. Qiao, L. Linga D. Long, *J. Mater. Chem. A*. 2 (2014) 17962.
- [19] L.P. Wang, L. Yu, R. Satish, J. Zhu, Q. Yan, M. Srinivasan, Z. Xu, *RSC Adv*. 4 (2014) 37394.
- [20] P. Arunkumar, A.G. Ashish, B. Babu, S. Sarang, A.Suresh, C.H. Sharma, M. Thalukulama, M. M. Shaijumon, *RSC Advances*. 5 (2014) 59997.

Prospective Nanomaterial Applications for Various Fields

D.Rama Rao ^{1*}, M.V.K.Mehar ², N.Srinivas ³, K. Ashok ⁴,

¹*Department of Chemistry, P.R. Govt College (A) Kakinada, AP, India*

²*Department of Physics, P.R. Govt College (A) Kakinada, AP, India*

³*Department of Zoology, P.R. Govt College (A) Kakinada East Godavari*

⁴*Department of Statistics, P.R. Govt College (A) Kakinada East Godavari*

**Corresponding author (Email):* drraoprga@gmail.com

Abstract

Nanotechnology is a Scientific Technology, to manufacture the tools, materials and devices at single atomic and molecular compositions, with the production of very microscopic sized particles called nanomaterial. They are the nano-crystalline particles which due the grain size with very little ranges of very small about 10-9m. Nano materials have noticeable smart and valued characteristics which can be implied for greatest of sciences and technologies present days. The use of nanotechnology in various applications of therapeutics has developed the field of medicine and used for diagnostics, therapeutics and as biomedical tools for research. Newer and better-quality methods of cancer discovery based on nanoparticles are being developed. Current modalities of diagnosis and conduct of various diseases, specifically cancer have major limitations such as very low sensitivity or specificity and drug toxicities respectively. They are used as different agents, fluorescent materials, molecular research tools and drugs with targeting antibodies. Use of nanotechnology in medical therapeutics essential passable assessment of its risk and safety factors. This review discusses the various platforms of nanotechnology being used in different aspects of medicine like diagnostics and therapeutics. The safety of Nano medicine is not yet fully defined. However, it is possible that Nano medicine in future would play a crucial role in the treatment of human diseases and also in enhancement of normal human physiology. With contemporary application of nanotechnology in different areas, its utility is likely to extend further into diagnostics, molecular investigation techniques.

Keywords: Diagnosis, Human, Nanomedicine, Toxicities, Investigation

1. Introduction

Nanoparticles (NPs) are replicated by different properties and various applications, topic on their size and characteristic active form. Abundant surface capacity ratio gives altered properties matched to the similar materials on macroscopic ranges, creation unique applications projected¹. The changes are owing to significant effects: transformation in the electronic structure, and high number of artificial atoms, rise in unsaturated bonds². This powerfully controls their applications. The products of the chemical industry are used to produce objects that vary enormously in their size from say the iron girders for bridge building to silicon chips in microprocessors³. However, techniques are now available which make it possible to manipulate materials arranged the atomic or molecular level toward produce objects which no more than limited nanometres in diameter. Nanometre is more than a 1000 times smaller than a silicon chip. The Nanoparticles can be fit for various applications. Nano medicine⁴, sensors^{5,6}, drug delivery^{7,8}. The practices used to make then manipulate such materials are renowned as nanotechnology and the materials or entities are stand nanomaterials⁹. The Nanoparticles size gained by exact synthesis in order to obtain nanomaterial in definite applications¹⁰. Nanotechnology develops the manufacturing for tools and nano-devices by monitoring the matter at the atomic level¹¹. It also said that Nanotechnology is a Scientific Technology, dominated by advances in Elementary science, Chemistry, Physics and medical Researches¹², where the occurrences on very small levels are implied to offer the materials or tools and structures that achieve the tasks which are impossible to perform using the tools in their Typical Macroscopic System¹³. In this framework, scientific research is constantly evolving, making it possible to synthesize new materials and find novel applications¹⁴. NPs allow one to find nanostructures with specific morphologies, controlled structures for useful properties. The exclusive physical and chemical properties of noble metal NPs offer them high multifunctionality¹⁵.

Nanotechnology focuses on material at sizes in the nanometer scale length (0.1-100 nm), and thus can be useful for a inclusive range of uses and applications, and the formation of several types of nanomaterial and nanodevices¹⁶. Materials or objects (Fig-1) that need to be measured in nanometers have always existed but the techniques for manipulating materials on this scale have only been developed during the last twenty years or so¹⁷ (Rehman, 2018)

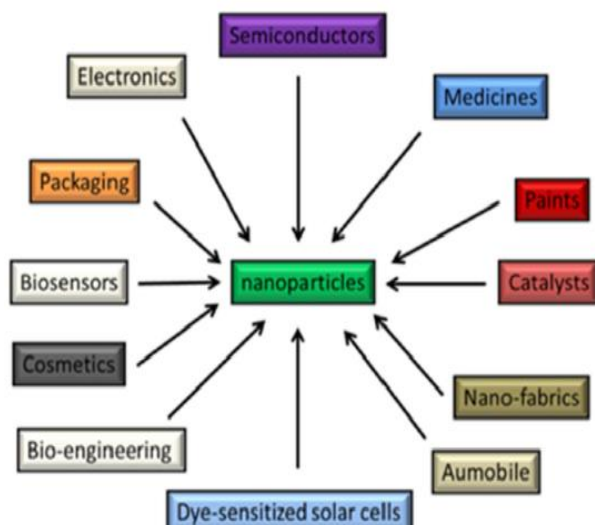


Fig.1: Applications of Nano materials

Nanomaterials are the nano-crystalline particles which owing the grain size with very minute ranges of about 10^{-9} m. Nanomaterials have noticeable fascinating and valuable characteristics¹⁸ which can be implied for most of sciences and technologies today.

2. Medicinal use of Nano Materials:

Nano medicine is a comparatively novel field of science and technology. By interrelating with biotic particles at nano scale, nanotechnology advances the possibility of research and applications¹⁹.

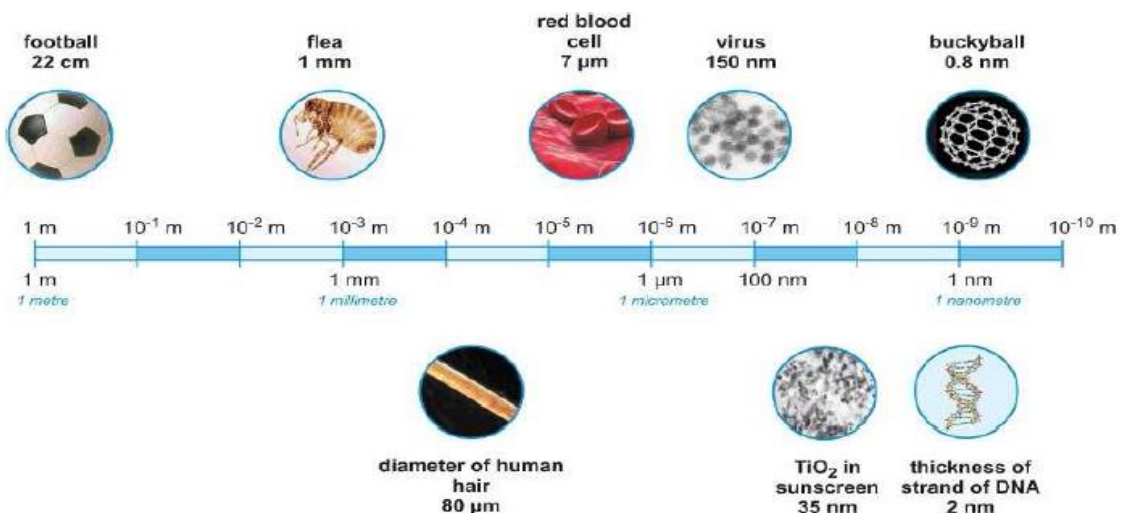


Fig.2: A scale to show the relative dimensions of various objects drug delivery

In nanotechnology nanomaterials are used for site specific drug delivery. In this technique the required drug dose is used and side-effects are lowered significantly as the active agent is deposited in the morbid region only. This highly selective approach can reduce costs and pain to the patients. Thus variety of nanomaterials such as dendrimers, and nano porous materials find application. Iron nanomaterials or gold shells are finding important application in the cancer treatment. (*J. Basic. Appl. Sci. Res.*, 8(4)1-1, 2018)

The applications of nanomaterials in drug delivery

Nano technology and drug delivery is based upon three facts: 1) effective encapsulation of the drugs, 2) positive delivery of said drugs to the directed area of the body

Improved Properties

Metal matrix composites such as continuous carbon or boron fiber reinforced aluminum and magnesium, and silicon carbide reinforced aluminum have been used for aerospace applications due to their lightweight and tailor able properties. There is much interest in producing metal matrix Nano composites that incorporate nanoparticles and nanotubes for structural applications, as these materials exhibit even greater improvements in their physical, mechanical and biological properties as compared to composites with micron-sized reinforcements.²⁰⁻²¹

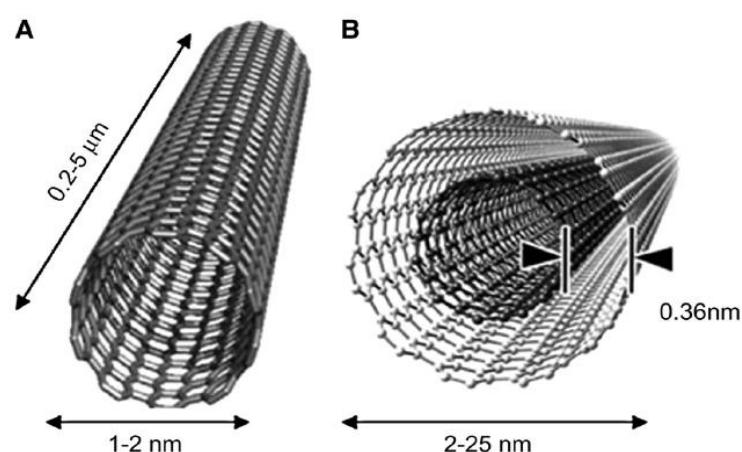


Fig: 3. Carbon Nanotube

3. Carbon Nanotubes

These are small and macromolecules that stay one of a kind for their size (Fig.3), shape, and have excellent physical characteristics. Nano tubes have some exceptional favorable circumstances²² over other medication conveyance and symptomatic frameworks because of their physical properties (*J. Basic. Appl. Sci. Res.*, 8(4)1-1, 2018)

4. Metallic nano particles

Metallic nano particles have used in drug delivery, especially in treatment of cancer and also in biosensors. Amongst various metals, silver and gold nano particles are of prime importance for biomedical use.

5. Cancer Treatment

These nano shells are focused to attach to carcinogenic cells by conjugating antibodies or peptides to the nano shell surface. Range of the tumor²⁷ is illuminated with an infrared laser, which warms the gold adequately and murders the disease cells. The applications of various nano systems in cancer therapy are summarized as:

- **Dendrimers**, less than 10 nm in size are useful for controlled release drug delivery, and as image contrast agents.
- **Nano crystals**, of 2-9.5 nm size source improved construction for poorly-soluble drugs, labeling of breast cancer marker Her2 surface of cancer cells.
- **Nano particles** are of 10-1000 nm size and are used in MRI and ultrasound image contrast agents and for targeted drug delivery, as permeation

6. Conclusion

Nano materials have extended surface area on a nano scale impacts, successively utilized as a promising instrument for the headway of medication and quality conveyance, biomedical imaging and symptomatic biosensors. The demand for nanotechnology engineered materials is increasing globally and their impact is being felt in a wide variety of biomedical sciences, agriculture and food industry, and physical disciplines, including military applications. Due to their specificity and site targeting properties, the nanomaterial may be a real boon for the diagnosis and treatment of diseases. For instance, nano particles can be exploited to create excellent pictures of tumor destinations; single walled carbon nanotubes, have been utilized as high-productivity conveyance transporters for biomolecules into cells. There is a brilliant future of nano innovation, by its converging with different developments, inventive

advances. Science based improvements are interlaced with nanotechnology. As nanoparticles are known to increase the solubility and permeability of the drugs, the imbibitions of drugs on nanoparticles or the stents will not only improve the bioavailability of the therapeutic agents but will also affect their predetermined release profiles. Regarding the long-term environmental influence of Nano scale particles, toxicity assessment of NPs, cellular and nontoxicity of Nano medicines. Nanotechnology is now used to control hereditary material. Improvements in nanotechnology security to renovate the medication blend, sedate supply, and curative diagnostics. In spite of the fact that quite a bit of this work is still in its leading times, investigators, analysts are creation of novel devices and rising new strategies for urgent research zones of medication planning sedate bearers, focusing on advances, lethality diminishment, and materials streamlining. Capability of nanotechnology to enterprise matter at the smallest scale is upsetting territories, for example, data innovation experienced science and technology and innovative, interlinking these and different fields. In more over inquire about in nanotechnology it can be appreciated for each part of human life.

References

- [1] Fratoddi, I.; Matassa, R.; Fontana, L.; Venditti, I.; Familiari, G.; Battocchio, C.; Magnano, E.; Nappini, S.; Leahu, G.; Belardini, A.; et al. Electronic Properties of a Functionalized Noble Metal Nanoparticles Covalent Network. *J. Phys. Chem. C* 2017, 121, 18110–18119.
- [2] Rapa, M.; Vinci, G. Nanotechnology nel settore alimentare: Regolamento CE 2283/2015 e la sua applicazione. *Ind. Alim.* 2018, 587, 11–17.
- [3] Roco MC, Williams RS, Alivisatos P, editors. Nanotechnology research directions: IWGN workshop report: vision for nanotechnology in the next decade. Springer Science & Business Media; 2000 Mar 31.
- [4] Venditti, I.; Fontana, L.; Fratoddi, I.; Battocchio, C.; Cametti, C.; Sennato, S.; Mura, F.; Sciubba, F.; Delfini, M.; Russo, M.V. Direct interaction of hydrophilic gold nanoparticles with dexamethasone drug: loading and release study. *J. Colloid Interface Sci.* 2014, 15, 52–60.
- [5] Fontana, L.; Fratoddi, I.; Venditti, I.; Matassa, R.; Familiari, G.; Battocchio, C.; Magnano, E.; Nappini, S.; Leahu, G.; Belardini, A.; et al. Hydrophilic Metal Nanoparticles Functionalized by 2-Diethylaminoethanethiol: A Close Look at

- theMetal–Ligand Interaction and Interface Chemical Structure. *J. Phys. Chem. C* 2017, 127, 18110–18119.
- [6] Farid, S.; Kuljic, R.; Poduri, S.; Dutta, M.; Darling, S.B. Tailoring uniform gold nanoparticle arrays and nanoporous films for next-generation optoelectronic devices. *SuperlatticesMicrostruct.* 2018, 118, 1–6.
- [7] Bearzotti, A.; Fontana, L.; Fratoddi, I.; Venditti, I.; Testa, G.; Rasi, S.; Gatta, V.; Russo, M.V.; Zampetti, E.;Papa, P.; et al. Hydrophobic Noble Metal Nanoparticles: Synthesis, Characterization and Perspectives as GasSensing Materials. *Procedia Eng.* 2015, 120, 781–786.
- [8] Proposito, P.; Mochi, F.; Ciotta, E.; Casalboni, M.; De Matteis, F.; Venditti, I.; Fontana, L.; Testa, G.; Fratoddi, I. Hydrophilic silver nanoparticles with tunable optical properties: application for the detection of heavymetals in water. *Beilstein J. Nanotechnol.* 2016, 7, 1654–1661. *Bioengineering* 2019, 6, 109 of 12.
- [9] Chong KP. Nanoscience and engineering in mechanics and materials. *Journal of Physics and Chemistry of Solids.* 2004 Sep 30;65(8):1501-6.
- [10] Venditti, I.; Testa, G.; Sciubba, F.; Carlini, L.; Porcaro, F.; Meneghini, C.; Fratoddi, I. Hydrophilic MetalNanoparticles Functionalized by fr²- DiethylaminoethaneThiol: A Close Look on the Metal- ligandInteraction and Interface Chemical Structure. *J. Phys. Chem. C* 2017, 121, 8002–8013.
- [11] Chong KP. Nanoscience and engineering in mechanics and materials. *Journal of Physics and Chemistry of Solids.* 2004 Sep 30;65(8):1501-6.
- [12] Pankhurst QA, Thanh NT, Jones SK, Dobson J. Progress in applications of magnetic nanoparticles in biomedicine. *Journal of Physics D: Applied Physics.* 2009 Nov 6;42(22):224001.
- [13] Huang X, Neretina S, El-Sayed MA. Gold nanorods: from synthesis and properties to biological and biomedical applications. *Advanced Materials.* 2009 Dec 28;21(48):4880-910.
- [14] Yang, C.; Bromma, K.; Di Ciano-Oliveira, C.; Zafarana, G.; Van Prooijen, M.; Chithrani, D.B. Effects of GoldNanoparticles in Cells in a Combined Treatment with Cisplatin and Radiation at Therapeutic MegavoltageEnergies. *Cancers* 2018, 10, 150.
- [15] Fratoddi, I.; Cartoni, A.; Venditti, I.; Catone, D.; O’Keeffe, P.; Paladini, A.; Toschi, F.; Turchini, S.; Sciubba, F.;Testa, G.; et al. Gold nanoparticles functionalized by

- Rhodamine B Isothiocyanate: a new tool to control Plasmonic Effects. *J. Colloid Surf. Sci.* 2018, 513, 10–19.
- [16] Hakomori S. Glycosylation defining cancer malignancy: new wine in an old bottle. *Proceedings of the National Academy of Sciences.* 2002 Aug 6; 99(16):10231-3.
- [17] Dwek RA. Glycobiology: toward understanding the function of sugars. *Chemical reviews.* 1996 Mar 28;96(2):683-720.
- [18] Garcia I, Marradi M, Penades S. Glyconanoparticles: multifunctional nanomaterials for biomedical applications. *Nanomedicine.* 2010 Jul;5(5):777-92.
- [19] Qiao R, Yang C, Gao M. Superparamagnetic iron oxide nanoparticles: from preparations to in vivo MRI applications. *Journal of Materials Chemistry.* 2009; 19(35):6274-93.
- [20] Takagi, M., et al. *Scripta Mater.* 2001, 44, 2145.
- [21] Dong, S.R. et al. *Mater. Sci. Eng., A* 2001, A313, 83.
- [22] Nourmohammadi N. New Study Shows Promise in Using RNA Nanotechnology to Treat Cancers and Viral Infections. *Nano medicine: Notes, Fierce Drug Delivery.* 2012.
- [23] Laurance J. Scientists develop nanoparticle method to help tackle major diseases. *The Independent.* 2012.

Polarizability And Diamagnetic Susceptibility Of Cyanobiphenyl Alkyl Aniline Benzylidene Liquid Crystalline Compound

Syed habeebullahassain¹, K. Nagi Reddy², C.M. Subhan³ and K. Fakruddin^{4*}

1. Department of Physics, MES Degree College, Malleswaram, Bangalore

2. Department of Physics, KLE Society's S. Nijalingappa College, Rajajinagar, Bengaluru

3. Department of physics, SV Degree & PG College, Anantapur, India

4. Department of physics GCE Ramanagara. Karnataka, India

* Corresponding author: drfakruddin2008@gmail.com

Abstract:

The mean molecular polarizability of the 4-cyanobiphenyl alkylanilinebenzylidene liquid crystal with spacer $n=5$ and terminal group $m=10$ are estimated by using vibrational frequencies by Molecular vibration method. From the mean molecular polarizabilities, the diamagnetic susceptibilities are also estimated. These diamagnetic susceptibility values are compared with Pascal method calculation by using atomic susceptibilities. In both the methods the values of mean diamagnetic susceptibilities are almost same.

Keywords: Polarizabilities, Susceptibilities; Liquid crystal; Molecular vibration.

1. Introduction

The technological applications of liquid crystals are growing steadily. Apart from their well known uses in display technology and thermography. These unique properties of the liquid crystalline phases are now being utilized in the production of electronic related devices. Knowledge of the molecular organization in different liquid crystalline materials is evidently necessary for the deeper understanding of these and other possible applications. Molecular spectroscopic studies have been much interest in recent years to study the structural and physical properties of liquid crystals [1-8]. These studies are quite helpful in getting the better understanding of the molecular and structural characteristics of the material. The polarizability is one of the most important material parameters of the nematic phase. It

determines all the anisotropic properties and the relation between macroscopic and microscopic properties. There are different methods for the evaluation of mean molecular polarizabilities. In present investigation, the refractivity method is used for experimental studies. In molecular vibration method any small deviation in intermolecular forces due to changes in chemical environment will be truly registered in their force constants and vibrational frequencies. The changes in vibrational frequencies in *cis* and *trans* configurations, *ortho*, *para* and *meta* substitutions are examples. The molecular polarizabilities evaluated by vibrational approach are compared with experimental values. The diamagnetic susceptibilities were also estimated and compared the values with Pascal's method.

2. Estimation of mean polarizability from Molecular vibration method

The mean molecular polarizability α_M is calculated by the expression

$$\alpha_M = \sum_i n_i \frac{(b_L + 2b_T)_i}{3} \quad (1)$$

Where n_i is the number of bonds of type i , b_L and b_T are the longitudinal and transverse polarizabilities of the bonds.

Rao and Murthy [9] have developed the following relations between bond polarizabilities and bond force constants of various chemical bonds. These relations completely empirical one and

The proposed equations are connected to the above parameters reads as

$$b_L - b_T = A \left[(x_1 x_2)^{S/2} \left(\frac{a_N}{k-b} \right)^{2S/3} \right] \quad (2)$$

$$b_L + 2b_T = [C p^j (j)^n \nu \sigma^{1/2}] \quad (3)$$

Various terms in the above equations and the detailed method are explained in reference [10].

Utilizing the expressions (1),(2) & (3) the bond polarizability coefficients b_L and b_T and mean molecular polarizability α_M are evaluated. In order to facilitate the evaluation of b_L and b_T individually, b_L values are taken from the estimation of bond polarizabilities of Denbigh [11] and Le Fevre [12].

3. Estimation of mean diamagnetic susceptibility

3.1 Polarizability method

Diamagnetic susceptibilities and mean molecular polarizabilities depend upon the effective number of free electrons which will be free to take part in magnetic and optical interactions. In view of these considerations a semi empirical relation between the diamagnetic susceptibility and mean polarizability of liquid crystals is given by [13-14].

$$-\chi = (\gamma m \sigma') \alpha \quad (4)$$

$\gamma = (0.9)^n$ represents saturation state of the molecule with n denoting the number of unsaturation rings and bonds present in the molecule. σ' is the degree of the covalency of the characteristic group and is given as

$$\sigma' = (\sigma_1^{1/n_1} \sigma_2^{1/n_2} \dots \sigma_p^{1/n_p})^{1/2} \quad (5)$$

Where $\sigma_1, \sigma_2, \dots, \sigma_p$ are the Pauling's percentage of covalence characters of the bonds present in the characteristic group; n_1, n_2, \dots, n_p are the bond orders of the various bonds in the characteristic group, m is a constant which is equal to 0.72×10^{19} . The values of $\sigma_1, \sigma_2, \dots, \sigma_p$ are taken from Pauling [15].

3.2 Pascal's method

Pascal's method [16] is based on the atomic increment systems of various atoms along with a particular constitutive correction factor for each specific class of molecules. According to this system, the diamagnetic susceptibility χ of a molecule given as

$$\chi_M = \sum_i n_i \chi_{ai} + \sum_i \lambda_i \quad (6)$$

where n_i is the number of times an atom i of susceptibility χ_i is repeated in the molecule and λ_i is the constitution correlation factor.

4. Results and Discussion

In our present investigation we estimated the mean molecular polarizability by utilizing the vibrational frequencies of different bonds obtained from IR data. By using the polarizability values obtained by molecular vibration method are used to evaluate diamagnetic susceptibilities. The mean diamagnetic susceptibility obtained from Rao's method agrees with the results obtained from Pascal's Method. As the applicability of Pascal's method is already established by Bahadur et al. [17] and de Jeu et al. [18] the agreement with this

method indicates the general applicability in evaluating the diamagnetic susceptibilities of liquid crystals.

Table 1. Vibrational frequencies of different bonds in a molecule measured by IR spectrometer

Sl.No.	Bond	Vibrational frequency
1	C-H	2849
2	C-C	1196
3	C=C	1626
4	C-N	1496
5	C=N	1626
6	C≡N	2237
7	C-O	1196
8	O-H	2917

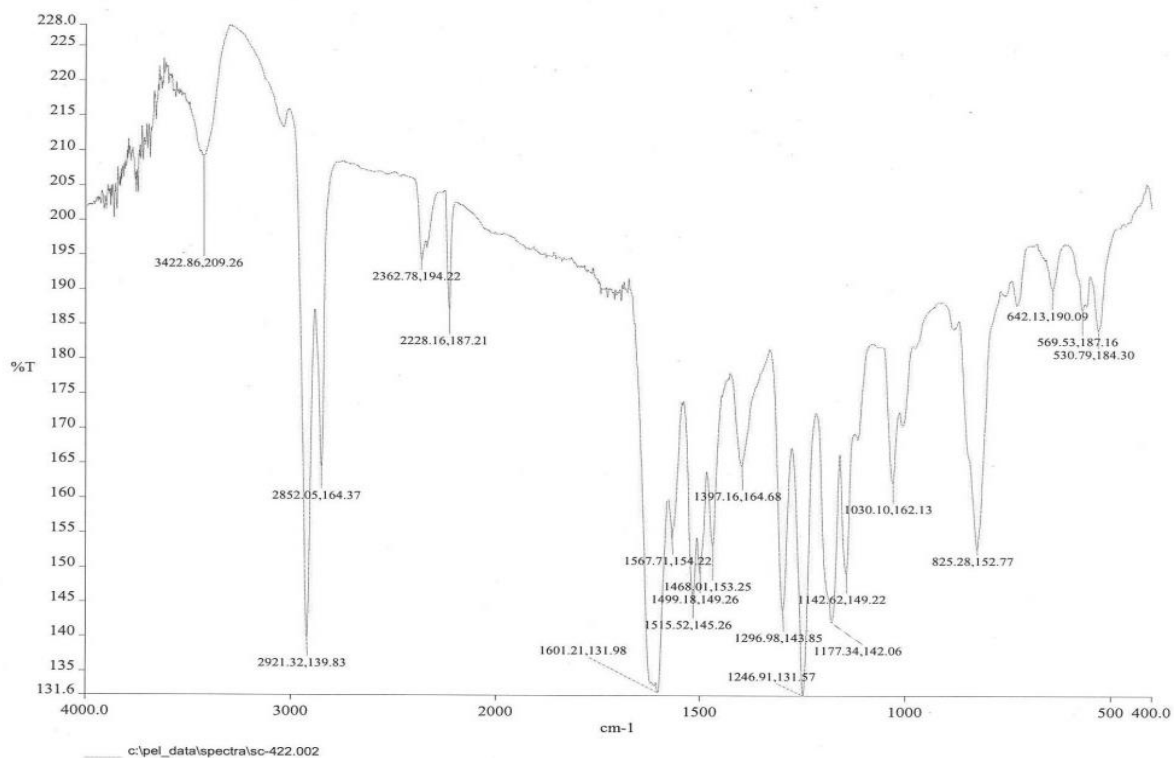


Figure 1. IR data of C1 compound

Sl.No.	Compound	Molecular Polarizabilities α_M [10^{-24}cm^3]	Pascal Method $\chi_M(\text{cm}^3 \text{mol}^{-1})$	Polarizability Method $\chi_M(\text{cm}^3 \text{mol}^{-1})$
1	C1	81.09	45.04	43.61

Acknowledgment

Authors express their thanks to the Department of Physics, Ghousia College of Engineering, Ramanagaram for providing laboratory facilities. The authors are thankful to Dr.C.M.Yellamagad and Dr. D.S.Shankar Rao for providing liquid crystalline compounds to carry out the present studies.

References

- [1] Stephen JP, Theo JD, Louis AM, Oriano F, Edward TS. Uniaxial to biaxial nematic phase transition in a bent-core thermotropic liquid crystal by polarising microscopy. *Liq. Cryst.* **2012**;39: 19–23.
- [2] Mallikharjuna RD, Soney V. Synthesis and characterisation of azomethine class thermotropic liquid crystals and their application in nonlinear optics. *Liq. Cryst.* **2012**; 39 : 63–70.
- [3] K. Fakruddin, R.JeevanKumar, P.V.DattaPrasad, V.G.K.M.Pisipati, *Mol. Cryst. Liq. Cryst.* **511**, 146 (2009).
- [4] S. Chandrasekhar, N. V. Madhusudana, (1969) *J. Physique.*, 30:. 24.
- [5] H. S. Subrahmanyam, D. Krishnamurthi, (1973) Polarization Field and Molecular Order in Nematic Liquid Crystals, *Mol. Cryst. Liquid Cryst.*, 22: 239-248.
- [6] W. H. De Jeu, P. Bordewijk, (1978) Physical studies of Nematicazoxybenzenes I. Magnetic susceptibilities and the order parameters, *J. Chem. Phys.*, 68: 109.
- [7] .I. H. Ibrahim, W. Haase, (1981) On the Molecular Polarizability of Nematic Liquid Crystals, *Mol. Cryst. Liquid Cryst.*, 66: 189-198
- [8] P. PalfyMuhoray, D. A. Balzarini, (1981) The Clausis-Mossotti relation for anisotropic molecular fluids, *Can. J. Phys.*, 59: 375-377.

- [9] B.P. Rao and V.R. Murthy, *Ind. Chem.J.XIII*. 17(1979).
- [10] Y.N. Murthy, V.R. Murthy, R.N.V. Ranga Reddy, *Acta Physica PolonicaA*.**6**, 91 (1997).
- [11] K.G. Denbigh, *Trans.Faraday Soc.***36**, 936(1940).
- [12] R.J.W. Le Fevre, *Rev. pure and Appl. Chem.* **20**, 67 (1970).
- [13] B. P. Rao, V. R. Murthy, D. V. Subbaiah and S. V. Naidu, *ActaCienciaIndica*, 5, 118 (1974).
- [14] R. N. V. Ranga Reddy, D. V. Subbaiah, V. R. Murthy, T. V. S. Arun Murthy, *Ind. J. Phys.*, 65, 535 (1991).
- [15] L. Pauling, *The Nature of chemical bond*, Oxford and IBH Pub., New Delhi 1969.
- [16] Pascal, P., *Ann. Chim. et Phys.*, **29**, 218 (1913).
- [17] B. Bahadur, (1977) Magnetic Susceptibilities studies of the liquid crystal N(p-hexyloxybenzylidene0-ptoluidine(HBT), *J. Chem. Phys.* 67: 3272-3273
- [18] W. H. De Jeu, W. A. P. Classen, (1978) Physical studies of Nematic azoxybenzenes II. Refractive indices and the internal field, *J. Chem. Phys.* 68: 102-108.

Fluorescence Quenching Studies of Nitroaromatics Employing sulphonic acids Doped polymers

Dr. ParvathiPatil^{1*}. Dr.Jaishree Badiger²

1. Department of Chemistry, Assistnat Professor Smt V.G Women's Degree College, Kalaburagi-585106, India.

2 Department of Chemistry, AssistnatProfessor, HKES SreeVeerendraPatil Degree College, Bengaluru-80, India.

Corresponding author (Email): parvathipatil03@gmail.com

Abstract

Polymers was synthesized by chemical oxidation method. Polymers was synthesized in the presence of ammonium persulfate as oxidant and para toluene sulfonic acid benzne, camphorsuphonic acids, deoxybenznesuphonic acids as dopant. In this study, fluorescence characteristics of polyaniline doped with suphonicacids in Dimethyl sulfoxide, nitro methyl pyrrolide solvent is undertaken. . The detection of quencher Nitroaromatics is studied through the observed intense quenching of fluorescence signals in the emission spectra of the sulphoorganic acids – polymer solution. The preparation of polymer solution is found to be ppm solution of organic acids -Polymer solution.

Keywords: Polymer, Fluorescence quenching; sulfonic acid, Nitroarmatics

1. Introduction

Polymer is one of the most hopeful conjugated conducting polymers for technological applications owing to its good electrical properties, ecological stability, low invention cost, and ease of synthesis, low ionization potential, high electron affinity and the ability to be oxidized or reduced more reversibly than predictable polymer. Nitro aromatics are controlling

explosives and also deadly pollutants and their finding is great concern due to national security, industrial and ecological protection. Among various nitro aromatics Trinitro phenols, Picric Acid, trinitrotoluene, Meta dinitroBenzene are important ingredients of industrial explosives. Nitro aromatics is widely used as explosive and slenderly for various medical preparations. In addition, picric acid it's a serious pollutant generated from leather, pharmaceuticals, chemicals and peroxide industries⁴. Pyrene functionalized Fluor fragments for the recognition of nitro aromatics has been reported by Zhang et al.. Dr. Timothy Swager has patented Fido as an explosive sensor at MIT using a conjugated fluorescent polymer and has used it to detect femtogram levels of Para Nitro Toluene. Very recently fluorescence quenching based finding has attracted much attention due to their high sensitivity and selectivity and its ability to be employed both in solution and solid phase. Detection limit in parts per billion and parts per trillion are realized through photo induced electron assignment mechanism (Fluorescence). Yolanda et al. have conveyed an innovative sensing mechanism of nitro aromatic explosives using silica gated mesoporous hybrid materials. Numerous p-electron-rich fluorescent conjugated polymers have been synthesized and are used in the detection of trace of nitroaromatics.

In this paper, we have studied the effect of the concentration of quencher on the fluorescence intensity of sulphonic acid- polymer employing DMSO as solvent. The study was carried out at room temperature. The fluorescence of sulphonic acid- polymer has been quenched and quenching in accordance with S-V relation. The S-V constant is noted. Fluorescence quenching experiments were carried out with 100 ppm sulphonic acid- polymer solution in a quartz cell using DMSO as solvent. The fluorescence emission is measured by exciting the polymer at λ_{max} derived. The fluorescence quenching of sulphonic acid- polymer has been exciting at and the fluorescence intensity of the polymer is effectively quenched upon addition of nitroaromatics and its corresponding Stern - Volmer plot is noted.

2. Fluorescence quenching studies

The polymer shows fluorescence emission due to $\pi - \pi^*$ transition of the benzenoid ring. Quinoid groups in example of polymer PANI are short-lived excited states with no fluorescence and act as deceptions and quench the fluorescence from together benzenoid groups. The benzenoid and quinoid groups are emission stability. Addition of Picric Acid $9I_0/I$

versus the concentration of quencher is called Stern-Volmer(SV) plot is shown in the. The efficiency of the quencher is given by the slope of the Stern-Volmer (S-V) plot. the lower concentration of quencher required. Higher the value of K_{sv} to quench the fluorescence and vice versa. Stern-Volmer constants are assessed from the linear part of the quenching curve for low quencher concentration which indicates quenching efficiency detection of trace amounts of a quencher.

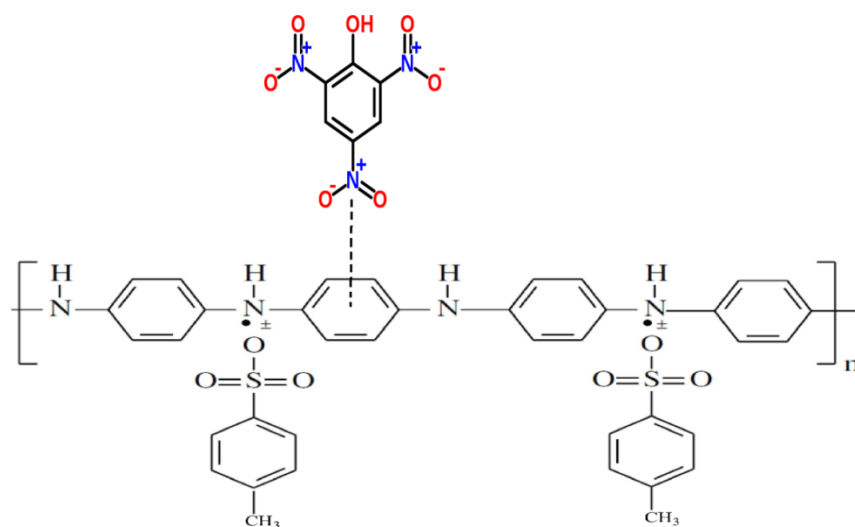


Fig. 1. Schematic Representation of electron transfer from sulphonic acid-polymer nitroaromatics(Polyaniline).

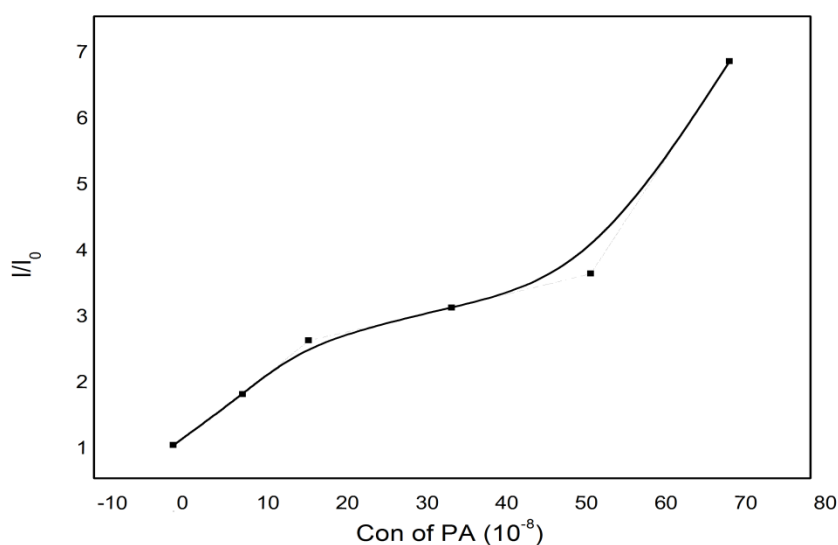


Fig.2. S-V plot between sulphonic acid polymer with varying concentration of nitroaromatics. (Polyaniline)

From S-V plot it is clear that at the lower concentration the plot is linear. At higher concentration, it departs from linearity and exponentially indicating the amplified quenching process. To explore the selectivity of sulphonic acid polymer Nitro aromatics, we carried out similar fluorescence quenching titrations, under identical conditions, with electron deficient nonphenolic compound like P-Nitro toluene with nitroaromatics. Fluorescence quenching is also measured with the help of S-V plots and quenching constants. The quenching constant is higher for it and it is a better quencher due to its more electron deficient nature because of the strong electron-withdrawing effect of Nitro(NO_2) groups whereas Para Nitro Toluene exhibits only moderate quenching due to the presence of (+I) inductive effect of the methyl group in Para Nitrotoluene.

3. Sensing Mechanism:

The example of polymer the repeating units are electronically coupled to form prolonged pi-conjugation, the interaction between the orbitals creates a semiconductor band structure having valence and conduction band. On photoexcitation, the electrons from the valence band (LUMO) are excited to the conduction band (HOMO) and leave a hole in the valence band. The hole-electron pair is called exciton which drifts along the polymer's backbone freely over several repeat units and creates molecular wire effect which is an important feature essential for enlarged quenching and the exciton travels over many different receptor sites and comes back to the ground state with the emission of radiation as fluorescence. But in the presence of quenchers like nitroaromatics in solution, the quencher, and the polymer form a weak excimer complex. This static suggestion prevents the transfer of electron on the conjugated chain, and electrons are transferred to LUMO of quencher which is less energetic than the ground state of polymer and lies in between HOMO and LUMO of polymer. The electrons come back to the ground state with the non-radiative process resulting in marked decrease fluorescent intensity of conjugated polymer indicating a possibility of energy transfer from the energy donor polymer host to the energy acceptor Picric acid. With the increase in

the number of electron deficient nitro (NO_2) groups, electron transfer from the polymer to the analyte becomes thermodynamically more achievable.

The fluorescence quenching mechanism was explained using semiconductor band theory proposed by Chen et al. In general, the fluorescence quenching of any device upon binding with analyte can follow two dissimilar mechanisms such as static and dynamic quenching. Quenching via static mechanism is expected not to distress the excited-state lifetime of fluorophore and in contrast, dynamic quenching does affect the life-time of fluorophore.

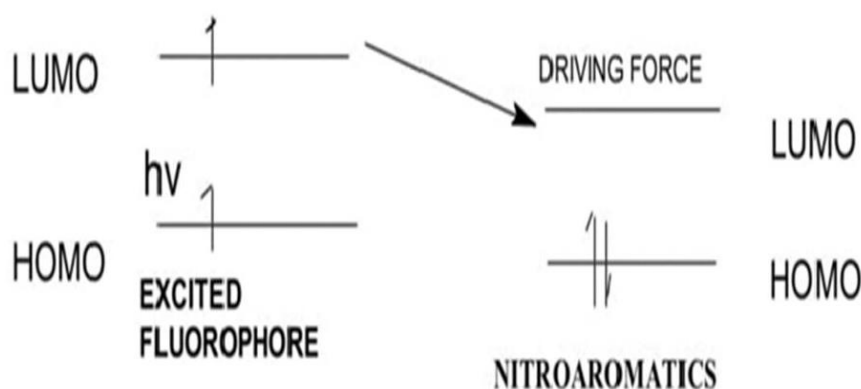


Fig. 4. Band diagram showing electron transmission from conjugated polymer to electron lacking Nitro Aromatics during fluorescence quenching

In static quenching, complexation occurs between the excited fluorophore and the ground state of the quenching types. In this mechanism, quenching of the excited fluorophore by the complex quencher transpires upon contamination. Due to the little lifetimes they only display static quenching. General mechanism of fluorescence quenching-based discovery basically involves the formation of a donor–acceptor charge-transfer complex between quencher and fluorophore have electron deficient acceptors via π – π interactions and the π -electron rich donors. Fluorescence passion changes acutely in fluorescent conjugated polymers, because of their magnification effect. When Nitro aromatics explosives contact with the conjugated polymers, charge assignment will occur between the electron-poor nitro aromatics quenchers and electron-rich polymers. After the binding sites in conjugated polymers are occupied by nitro aromatics quick-tempered molecules, the electrons do not transfer anymore, so the fluorescence intensity of the system decreases sharply.

4. Conclusion

The S-V plot has clearly given the theplotting graph about the static quenching of sulphonic acids doped polymer with Picric acid. The applicability of example of sulphonic acid polymer is producing electronic movements may be given a peek in devising devices to detect High Energy Materials with nitro efficient groups. The attention of the study herein was to produce processable conjugated polymers with probable for use in sensing. Polymerdoped with functionalized dopants like sulfonic acid is synthesized by chemical oxidation method to increase the process ability. The synthesized PANI was soluble in polar solvents like, N-Methyl pyrrolidine (NMP). Dimethyl sulfoxide (DMSO) Dimethyl formamide (DMF).

References

- [1] M.Mangusuon T.H. and S.M. Butorin A, Agui, C. Sathe, J.Nordgren, A.P. MonmkmanJournal of Chemical physics 1999,111
- [2] 4756-4761 [11] Y.Salinas R.M Manez, M.D. marcos, F.Sancemon, A.M costeroM.Parra and S.GilChem Soc. Rev. 2012, 41
- [3] Raghu M and Heager A-J Physical Review B 47(4):1758 (1993).
- [4] Yese J Wang Z.H CromackK.R. Epstein A.J: MacDiarmid A.G. J.Am chem. Soc. 19
- [5] N.L.Sheela, S.M. Umesh. L.B. Swaminath V.A Prashant. R.P Shivajiroa and B.K. Govind Bull Chem. Soc. Ethip. 2009, 23(2) 231-238. 91,113, 2665-2671.
- [6] Sinha.S.BhadraS.Khastgir, D.J. Appl. Polym. Sci.2009. 112,3135-3140.
- [7] B.D.Gokcen, D.Bihter and B.Mehmet Chemical Communications 2013, 49, 6140-6142.
- [8] Gilat,S.L; Adronov, A ;Frechet,J. M.J. Angew. Chem.Ed. 1999, 38, 1422-1427
- [9] Cheng-Ho Chen. Thermal and morphological studies of chemically prepared emeraldine- base- form polyaniline powder. Journal of Applied Polymer science.,
- [10] Gupta K K, Jasnal M, Agarwal K. Sol-gel derived titanium dioxide finishing of cotton fabric for self-cleaning. Indian Journal of fiber and Textile research., 2008, 33:443- 450.
- [11] Sariciftci N S, Kuzmany H, Neugebauer H, Neckel A. Structural and electronic transitions in Polyaniline: A Fourier transforms infrared spectroscopic study. J. Chem. Phys., 1990, 92:4530-45

Electrical Conductivity Study of Lithium-Borate Glasses containing Gd³⁺ ions

Hanumantharaju. N¹, Sardar Pasha, K.R², Sriprakash. G¹ and Veeranna Gowda*

¹Maharani's Science College for Women, Palace Road, Bangalore-560 001.

²Government First Grade College, Yelahanka, Bangalore-560 064.

*Corresponding E-mail: vcvgowda@gmail.com

Abstract

Lithium borate containing gadolinium oxide glasses were prepared by melt quenching method. The electrical conductivity measurements were carried out in the temperature and frequency range of 393 K-573 K and 100 Hz-5 MHz respectively. DC electrical conductivity (σ_{dc}) values were obtained by fitting the conductivity data to a Jonscher Power law equation. The obtained σ_{dc} values were very much consistent with the values determined from Nyquist Plot. The Arrhenius plots were used to calculate the dc activation energy. The frequency dependence of the ac conductivity was found to obey Johscher power law relation. The non-linear variation in conductivity with gadolinium concentration could be due to structural changes occurring in the lithium-borate glass network. The results were discussed in view of the structure of borate glass network.

Keywords: AC conductivity; Borate glass; Nyquist plot; Structure-property.

1. Introduction

Oxide glasses doped with rare earth ions are of considerable interest due to their outstanding applications in a device such as solid state laser, optical amplifiers and battery materials [1-2]. Borate glasses is considered to be good host matrices for the rare earth oxides due to their wide glass forming region compared to other conventional glass formers [3-4]. It has been also suggested that the addition of rare earth ions in glasses possess two possibilities, firstly, the dopant oxide by giving its oxide ions to glass former and can occupy an individual site where it enters into the network as glass modifier. Secondly, the dopant ion can modify the geometry of the glass network to meet the requirement for the bonding arrangements of

gadolinium ion. It is therefore considered that during this process the rare earth ion promote the formation of non-bridging oxygen atoms.

Lithium atoms are light weight and highly electropositive character and have high energy density. When it is introduced into borate glass, it acts as a network modifier. It modifies the glass by loosening the network structure borate upon the addition. Therefore, lithium based borate glasses possess high electrical conductivity. In the present work AC and DC electrical conductivity have been studied for $\text{Li}_2\text{O}-\text{B}_2\text{O}_3-\text{Gd}_2\text{O}_3$ glasses over a wide range of composition.

2. Experimental

The rare earth ion doped glasses with the composition $(100-x) (33.35\text{Li}_2\text{O} - 66.65\text{B}_2\text{O}_3) - x\text{Gd}_2\text{O}_3$, where $(x = 0, 0.5, 1, 1.5 \text{ and } 2 \text{ mol}\%)$ were prepared by melt quenching method. The appropriate weight of the mixtures was taken in porcelain crucible and melted in an electric muffle furnace at temperature in the range $1050^\circ\text{C} - 1150^\circ\text{C}$. The homogeneous melts were quenched between aluminium blocks. The glass samples were annealed at 180°C for 2 hours to remove the thermal strain which generally forms during quenching.

AC Electrical conductivity measurements were carried out by Wayne Kerr precision impedance LCR analyser 6500B, in the frequency range of 100Hz to 5MHz in the temperature range of 303 K – 573 K. The prepared samples were well polished so as to get a uniform thickness. The annealed circular glass pieces coated with silver paint on both side were used for the measurement. The sample temperature was measured using Pt – Cr thermocouples. The temperature was controlled by using temperature controller and temperature constancy of $\pm 2 \text{ K}$ was achieved in the entire range of measurements.

3. Results and Discussion

3.1 Nyquist impedance analysis

The real and imaginary parts of complex impedance for the investigated glasses were calculated using the relation [5];

$$Z^* = Z' + Z'' = \frac{1}{G + j\omega C_p} \quad (1)$$

$$Z' = \frac{G}{(G^2 + \omega^2 C_p^2)} \quad (2)$$

$$Z'' = \frac{\omega C_p}{(G^2 + \omega^2 C_p^2)} \quad (3)$$

where C_p , G and ω are the capacitance, conductance and angular frequency respectively. The Nyquist plots have been used to analyse the ac conductivity data by the method of complex impedance. The semicircle at the higher frequency region in the Nyquist plot represents bulk contribution, in the intermediate region and in the lowest frequency side it represents the grain boundary and silver electrode contribution respectively.

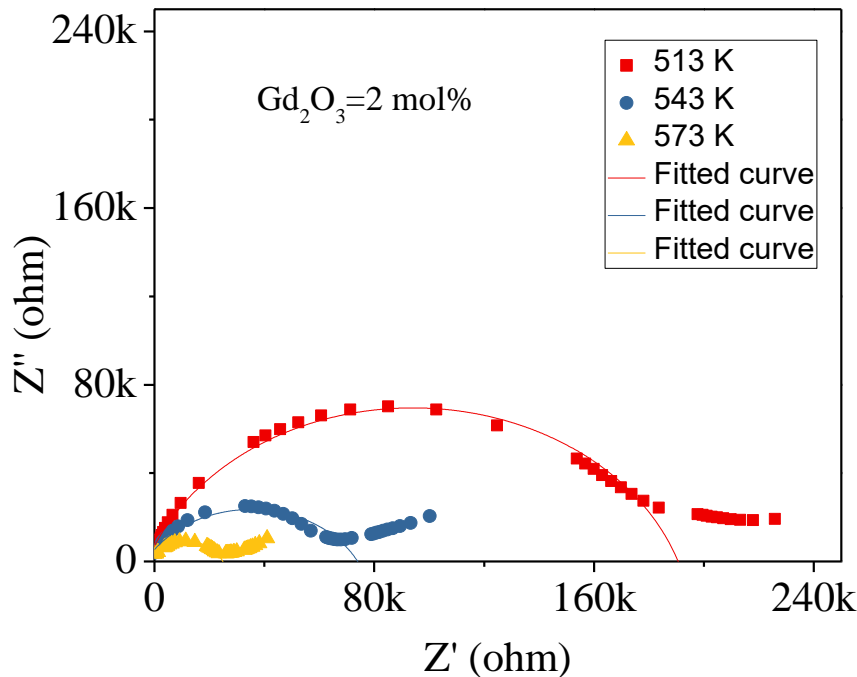


Figure 1: Variation of Z'' versus Z' for 2 mol% of Gd_2O_3

The variation of Z'' against Z' at different temperatures for the lithium borate glass containing 2 mol% of Gd_2O_3 is shown in Figure 1. It can be seen from Figure 1 that Z'' values reach a maximum (Z''_{max}) at a particular frequency and then decrease with frequency and finally it reaches the same value near zero at higher frequencies. The Z''_{max} shifts to higher frequencies with temperature and the peak height decreases as temperature is increased. This decrease in peak value indicates that there is a reduction in bulk resistance of the sample with increase in temperature.

The bulk conductivities of the samples were calculated by taking the resistance value of intersection of low frequency end of the semicircle using the relation:

$$\sigma = \frac{d}{RA} \tag{4}$$

where d and A are the thickness and area of the sample and R is the bulk resistance. The bulk conductivities plotted against reciprocal of temperature reveals linear relationship.

3. 2. AC conductivity

The variation of electrical conductivity with frequency for lithium-borate glasses is shown in Figure 2. The nature of the conductivity behaviour remains the same for all the glasses studied. The conductivity plot exhibits two regions, a frequency independent conductivity at lower frequency shows plateau region referred as dc conductivity (σ_{dc}) which is attributed to the long-range migrations of ions. The region beyond plateau corresponds to frequency dispersion referred as ac conductivity which becomes more pronounced at higher temperature. Besides, the frequency dispersion, ac conductivity is also found to be significant.

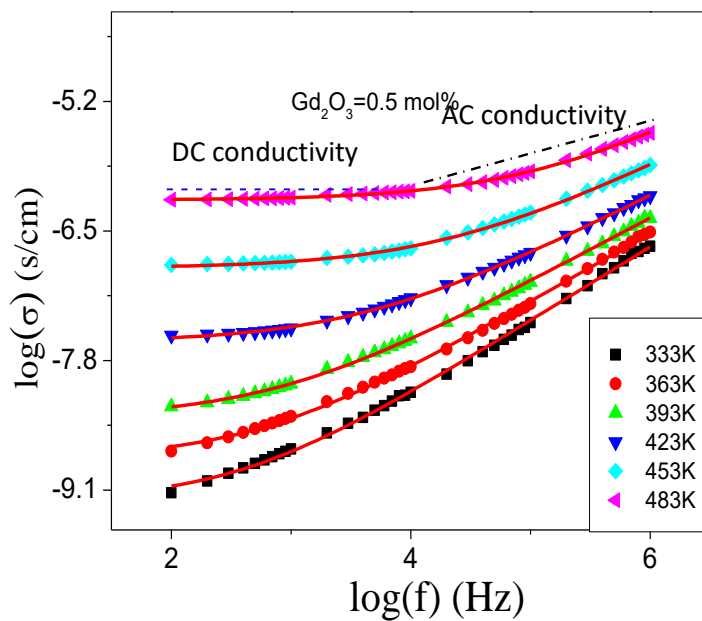


Figure 2: Variation of $\log(\sigma)$ with $\log(f)$ for 0.5 mol% Gd_2O_3 .

The frequency dependence of conductivity behaviour is analysed by fitting the conductivity data to Jonhscher’s Power law equation [6].

$$\sigma_\omega = \sigma_{dc} + A\omega^s \tag{5}$$

where σ_{dc} is frequency independent term, A is pre-exponential constant and s is power law exponent.

The variation of AC conductivity with temperature can be attributed to the thermal activation of charge carriers. At low temperature and high frequency there is a sharp increase in its conductivity. This change of conductivity from frequency independence to frequency dependence shows the establishment of conductivity relaxation phenomenon. It is well known that the hopping of charge carriers from one site to the nearest neighbouring site is mainly responsible for the AC conductivity in alkali oxide glasses. In this process the charge carriers possess arbitrary potential energy and the conductivity follows the equation:

$$\sigma(\omega) = A\omega^s \tag{6}$$

where A is a constant, ω and s are frequency and power law exponent respectively. The power law exponent is explicitly expressed as a function of temperature. The temperature and composition dependence of power law exponent gives a clear insight into the degree of interaction with local environment of the glass structure.

3.3. DC conductivity and activation energy

The variation of dc conductivity of gadolinium doped lithium-borate glasses with inverse temperature is shown in Figure 3.

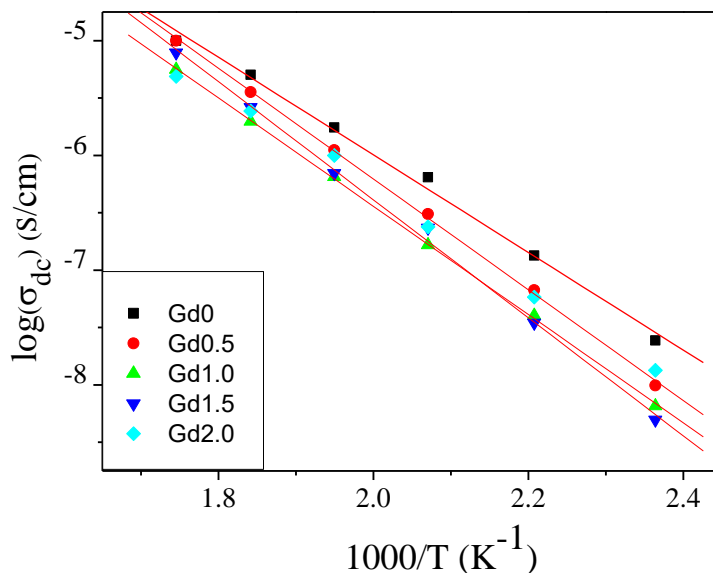


Figure 3: Variation of dc conductivity with inverse temperature

The dc conductivity found to decrease with increase of Gd₂O₃ content up to 1.5 mol% and further addition of Gd₂O₃ enhances the conductivity. The slope values obtained from least square fitting of Arrhenius plot is used to calculate the activation energy (E_a). It can be seen

from figure 3 that the Arrhenius plot reveals the existence of lone activation barrier in the present glasses. The dc conductivity and activation energy has opposite behaviour. The activation energy found to increase with Gd_2O_3 up to 1.5 mol% and then it decreases for further addition of Gd_2O_3 content. The non-linear variation of conductivity and activation energy is explained by considering two factors; in the first region the decrease in conductivity (when Gd_2O_3 content is increased up to 1.5 mol%) could be due to increase in cross link density, which impedes the motion of mobile lithium ions and in the second region (when Gd_2O_3 content is above 1.5 mol%), the increase in conductivity could be due to the creation of excess volume, leads to the formation of more number of non-bridging oxygen atoms which facilitate the motion of mobile cations.

4. Conclusion

The AC and DC electrical conductivities for gadolinium doped lithium borate glasses ($0 \leq x \leq 2$), were studied over a wide range of frequency (100Hz-6MHz) and temperature (393 K-573 K). It was found that the increase in Gd_2O_3 content up to 1.5 mol% increases the formation of bridging oxygen atoms. This would strengthen the structure of borate glass network and conductivity found to decrease. Further addition of Gd_2O_3 , weakens the stability of the glass. This would lead to the formation of more number of non-bridging oxygen atoms. This causes to decrease the rigidity of the glass, which in turn increases the mobility of charge carriers. Hence the conductivity found to increase when Gd_2O_3 content exceeds 1.5 mol%. DC conductivity values determined using Jonscher power law fit were consistent with the values determined using Nyquist plot. The activation energy values were found to increase up to 1.5 mol% of Gd_2O_3 and then it decreases.

References

- [1] C.K. Jayasankar, V. Venkatramu, S. SurendraBabu, P. Babu, J. Alloys. Compds 374 (2004) 22.
- [2] G. Lakshminarayana, S. Buddhudu, Physica B, 373 (2006) 100.
- [3] N.J. Kreidl in: D.R. Uhlmann,, N.J. Kreidl (Eds). Glass Science and Technology, Vol.1 Academic, New York. 1983.
- [4] R. Ihara, T. Honma, Y. Benino, T. Fujiwara, T. Komastu, Opt. Mater. 27 (2004) 403.

- [5] J.R. Macdonald, W.B. Johnson, Fundamentals of Impedance Spectroscopy in: Basoukov, J.R. Macdonald (Eds.) Impedance Spectroscopy Theory, Experiment, and Applications, second ed., John Wiley & Sons, United States of America, 2005.
- [6] A.K. Jonscher, Nature, 267 (1977) 673.
- [7] I.G. Austin and N.F. Mott Adv. Phys. 18 (1969) 657.

Synthesis and Characterization of Zn Substituted Li–Ni Nano Ferrites

R. G. Kharabe¹ and B. K. Chougule²

¹ Department of Physics, KLE's GIB College, Nippani 591237, Karnataka, India

² Department of Physics Shivaji University, Kolhapur 416004, Maharashtra, India

Abstract

Nanosized Li–Ni–Zn ferrites with general chemical formula $\text{Li}_{0.5} \text{Ni}_{0.75-x/2} \text{Zn}_{x/2} \text{Fe}_2\text{O}_4$ ($0 < x < 1$) were synthesized from a simple polymer matrix based precursor solution. The solution was composed of metal nitrates, polymer (PVA) and disaccharide (sucrose). Thermolysis/flame pyrolysis of the precursor mass in an external temperature resulted in the oxide phase formation. X-ray diffraction studies confirm the formation of single phase ferrites. The micro structural analysis has been carried out by SEM. The crystallite size calculated by Debye-Scherrer method and lattice diameter is found to vary from 16 nm to 33 nm.

Keywords: Nano Ferrites; XRD; Microstructure

1. Introduction

Ferrites have long been considered as highly important electronics materials. They are mainly composed of iron oxide and other divalent metal oxides. The ferrites have high resistivity, low eddy current losses and have remarkable magnetic properties and applications in radio frequency region. The properties of spinel ferrites are enhanced when the size of particle reaches the nanometer range.¹ In recent years, fabrication and characterization of a nanophase and nanostructure materials have attracting a great deal of attention because of their potential applications in areas such as electronics, optics, catalysis, ceramics and magnetic storage. A central aspect of nanoscience is the development of nanomaterials below 100 nm range. Nanoparticles have large surface area and it has been shown that overall physical properties are determined by the surface environment and bonding of the surface cations. They increase saturation magnetization M_s and lower coercivity H_c at room temperature.²

Lithium ferrite is a unique member of spinel class of ferrimagnets. These ferrite materials are dominating the field of microwave applications because of their rectangular and

square hysteresis loop characteristics, high Curie temperature and large saturation magnetization. The synthesis of nanocrystalline Ni-Zn ferrites has been investigated intensively in recent years due to their potential applications, in non-resonant devices, radio frequency circuits, high-quality filters, rod antenna's, transformer cores, read / write heads for electronic devices etc.³ Now a day these materials are largely synthesized in nanometric scale for new improvised properties.⁴

They exhibit interesting electrical and magnetic properties. Many researchers have studied Li-Ni-Cd, Li-Mg-Zn, Li-Ni ferrite systems prepared by conventional ceramic method.^{5,6} In this communication we report on the synthesis and characterization of nanosized Zn substituted Li-Ni nano ferrites prepared by wet chemical method.

2. Experimental

Ferrites with the general chemical formula $\text{Li}_{0.5} - \text{Ni}_{0.75-x/2} \text{Zn}_{x/2} \text{Fe}_2\text{O}_4$ ($0 < x < 1$) were prepared by the chemical route by using Metal nitrates, sucrose and PVA. The powders were presintered at 600 °C for 6 hours in air medium. The powders were pressed into pellets by applying a pressure of about 5 tone/sq. inch for 5 minutes by putting a powder of about 1gr in a die of 1cm diameter. The pellets were subjected to final sintering at 800 °C for 8 hours and furnace cooled in air.

The single phase formation of the samples was confirmed by X-ray diffraction studies using Philips PW-1710 X-ray diffractometer with Cu K α radiation ($\lambda = 1.5418 \text{ \AA}$). The SEM micrographs of the samples were obtained using SEM Model JEOL-JSM. The average grain diameter for each composition was calculated using the Scherrer formula

$$D = 0.9\lambda / \beta \text{ Cos}\theta$$

where λ is wavelength of radiation, β is full width at half maximum (FWHM) and θ is the angle of diffraction.

3. Results and Discussion

The single phase spinel formation of the samples was confirmed by XRD patterns as shown in Fig.1. The variation of lattice parameter 'a' with Zn content is shown Fig.2. It can be seen that the lattice parameter increases linearly with Zinc content obeying Vegard's law. The Zn^{2+} ion have large ionic radius (0.88 Å) than Fe^{3+} (0.65 Å) Ni^{2+} (0.74 Å) and Li^{1+} (0.71 Å) ions. The Zn^{2+} ions successively replace the Fe^{3+} ions on A site. This results in increase of

lattice parameter with content of zinc. A similar type of variation is also observed in Ni-Zn nanoferrites.⁷From the x-ray diffraction data the values of bond lengths R_A and R_B and ionic site radii r_A and r_B were calculated and are listed in Table I. It can be seen that the bond lengths R_A and R_B increase linearly with the contents of Zn which can be attributed to the increase in lattice parameter with Zn content. Jadhav also observed similar results in Li-Cu-Zn ferrite.⁷It is also observed that site radii r_A and r_B increase linearly with Zn. content.

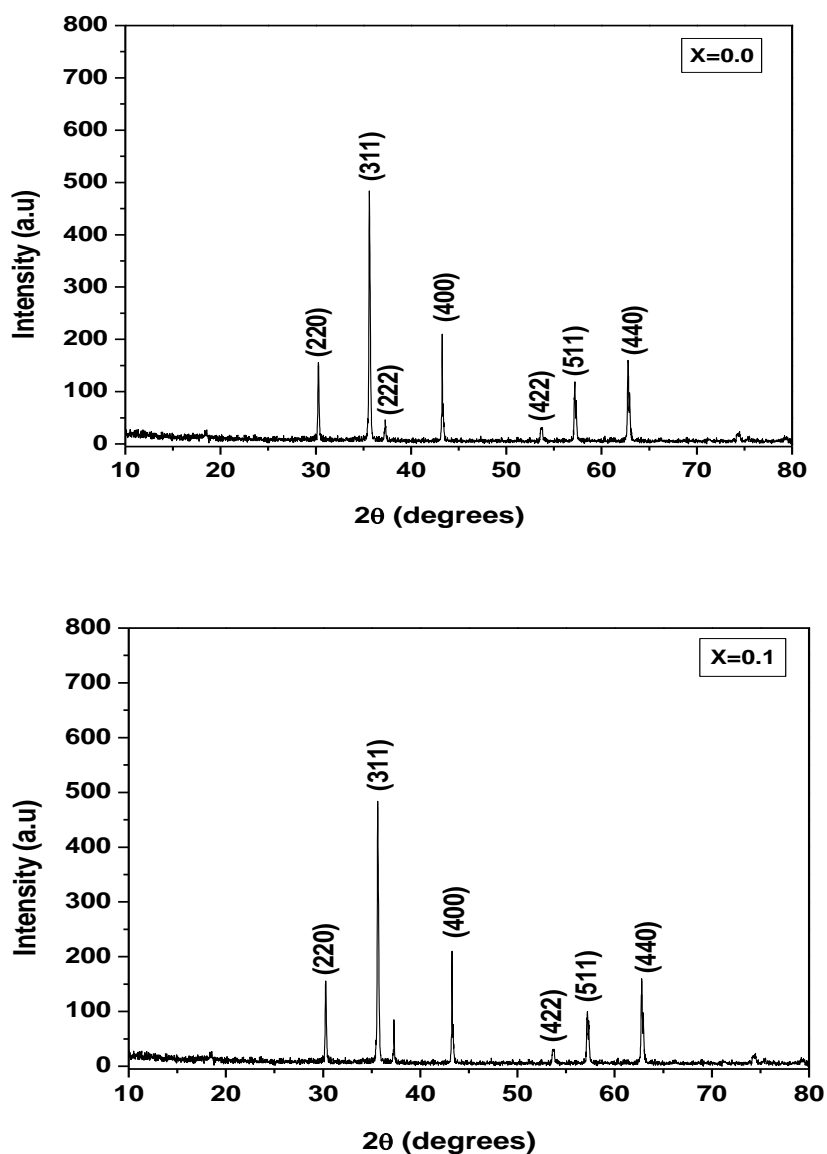


Fig. 1 X-ray diffraction pattern of $\text{Li}_{0.5}\text{Ni}_{0.75-x/2}\text{Zn}_{x/2}\text{Fe}_2\text{O}_4$ ferrite samples

The SEM micrographs of the samples are shown in the Fig.3. The micrographs reveals that all the samples show fine grains, segregation of impurity phases is not found and

the porosity of the samples varies from sample to sample. The compositional variation of average grain diameter along with porosity is given in Table II. The average grain diameter increases with Zn content up to 0.15 and then decreases beyond this limit. Similar variation has been reported in the case of (Zn²⁺, Cd²⁺ Ti⁴⁺) substituted lithium ferrite.⁸ An increase in grain diameter with Zn content can be attributed to the diffusion phenomenon involving Zn/oxygen vacancies and pores without its deposition on grain boundaries that hampers the grain growth. The increase in grain diameter with Zn content is attributed to the low solid solubility of nickel in the samples.

Table I. Data of Lattice parameter, bond lengths and site radii of Li_{0.5} Ni_{0.75-x/2} Zn_{x/2} Fe₂O₄ ferrite samples

Composition(x)	Lattice Parameter (Å)	R_A Å	R_B Å	r_A Å	r_B Å
0.0	8.337	1.920	2.019	0.568	0.667
0.1	8.356	1.925	2.024	0.572	0.672
0.3	8.360	1.926	2.025	0.574	0.674
0.5	8.371	1.928	2.027	0.576	0.675
0.7	8.372	1.929	2.028	0.578	0.677
0.9	8.397	1.934	2.034	0.582	0.682

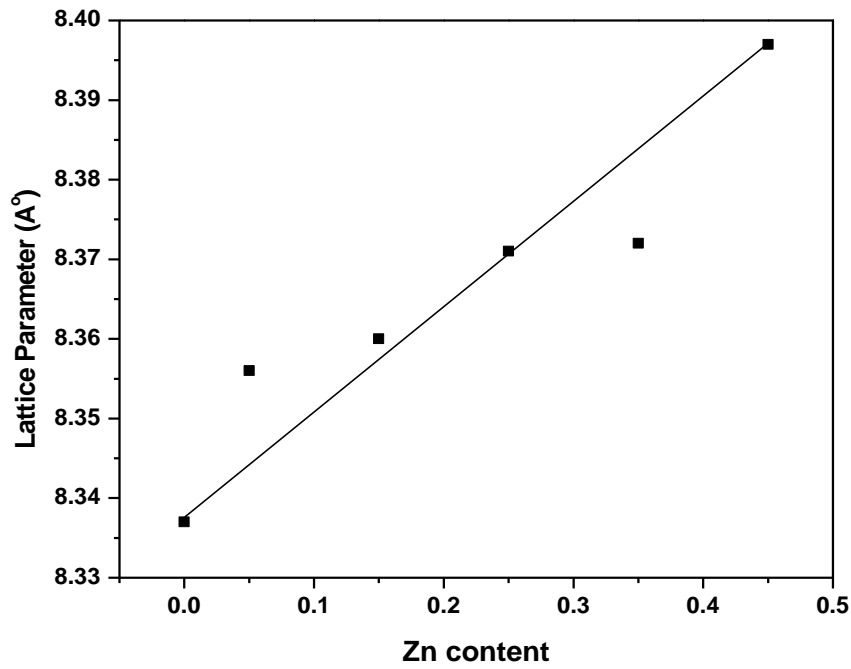


Fig. 2 Variation of lattice parameter with Zn content

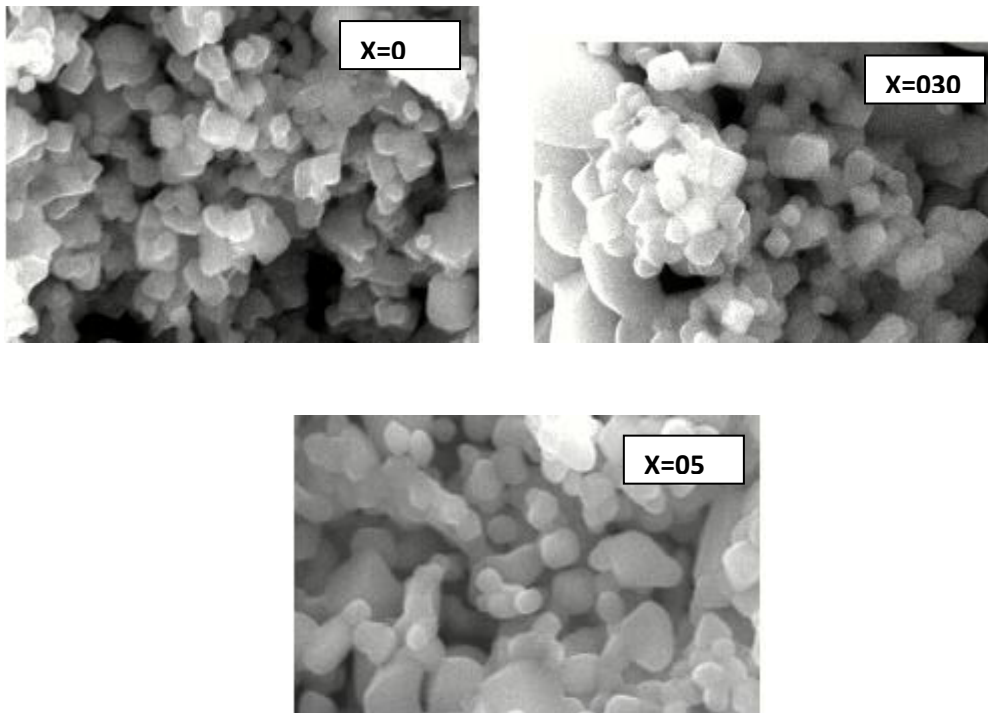


Fig.3. Scanning electron micrographs for $Li_{0.5} Ni_{0.75-x/2} Zn_{x/2} Fe_2O_4$ ferrites

Table II. Data on average grain diameter and porosity of $Li_{0.5} Ni_{0.75-x/2} Zn_{x/2} Fe_2O_4$ ferrite samples

Zn content	Average grain diameter(nm)	Porosity (%)
0.00	16.0	14.3
0.05	31.1	30.0
0.15	33.56	13.7
0.25	30.37	30.8
0.35	28.72	18.02
0.45	26.2	35

4. Conclusions

Ferrites with the general chemical formula $\text{Li}_{0.5} - \text{Ni}_{0.75-x/2} \text{Zn}_{x/2} \text{Fe}_2\text{O}_4$ ($0 < x < 1$) were prepared by chemical route. The single phase spinel formation of the samples was confirmed by XRD patterns. From the SEM studies it is seen that all the samples show fine grains, segregation of impurity phases is not found and the porosity of the samples varies from sample to sample.

Acknowledgements

The author (RGK) is thankful to University Grants Commission, New Delhi, India for sanctioning the Minor Research Project under Xth -Plan.

References

- [1] J. Ding, X. Y. Liu, J. Wang Y. Shi, *Mater. Lett.* 44, 19 (2000).
- [2] P. Poddar, H. Shrikant, S. A. Morrisson, E. E. Caspenter, *J. Magn.*
- [3] *Magn. Mater.* 288, 443 (2005).
- [4] S. Bid, S. K. Padhan, *Mater. Chem. Phys.* 84, 291 (2004).
- [5] C. S. Kim, Y. S. Yi., K. T. Park, H. Namgung, J. G. Lee, *J. Appl. Phys.* 85, 5223 (1999).
- [6] R. G. Kharabe, R. S. Devan, C. M. Kanamadi, B. K. Chougule, *Smart. Mater. Struct.* 15, 36 (2006).

- [7] A. M. Shaikh, S. A. Jadhav, S. C. Watave and B. K. Chougule, *Mater. Letts.* 44, 192 (2000).
- [8] A. E. Verdin, K. O. Grady, *J. Magn, Magn. Mater.* 290, 868 (2005).
- [9] C. M. Kanmadi, R. G. Kharabe, R. B. Pujar, B.K.Chougule, *Indian. J. Phys.* 79, 257(2005).

Effects of different radiation on the growth of strontium doped copper tartrate single crystals

Pradeep kumar K V*, Jagannatha N*, Rohith P S, Delma D'Souza and Susheela K L.

*Department of physics, F M K M C College, Madikeri-571201

Corresponding Author: jagannathnettar@yahoo.co.in

Abstract

Strontium doped copper tartrate crystals were grown in controlled diffusion silica gel by exposing different radiation. The optimum conditions were obtained by varying parameters such as pH of gel, concentration of gel, gel setting time, concentration of reactance. Crystals having different morphologies were obtained such as greenish semi-transparent crystals. The metallic compositions in the crystals were estimated by Energy-dispersive X-ray analysis (EDAX). Thermo gravimetric analysis (TGA) of pure and doped strontium copper tartrate crystals suggest the possibility of the presence of co-ordinated water molecule in the crystalline structure. The functional groups present in the crystals were identified using Fourier transform infrared (FTIR) analysis. UV-VIS-NIR transmission spectrum was recorded to study the optical transparency of the grown crystals.

Keywords: Gel growth, Strontium copper tartrate, EDAX, TGA, FTIR, UV-VIS-NIR.

1. Introduction

Crystals are the pillars of modern technology. Crystal growth in silica gel medium was become more popular in many researchers scientifically and technologically. The modern single crystals technological suitable for develop availability of single crystals. The many number of crystals is used in electronics, superconductors and optical industries. Hence today's demand is to grown large single crystals. The most of tartrate compounds were insoluble in water. Hence tartrate compounds cannot grow by slow evaporation method and melt technique. In this circumstance gel method is one of the method for grown tartrate compounds. The several tartrate compounds interesting physical and non-linear optical

properties. The tartrate compounds are several applications in science and technology such as optics, medicine, ferroelectric, piezoelectric, dielectric etc^(2,5)...

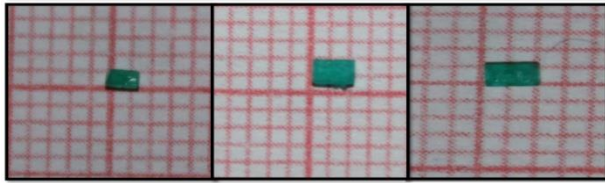
In the present investigation, Strontium doped copper tartrate were grown in silica gel method at exposes different light radiation. The grown strontium doped copper tartrate crystals in silica gel method at different light radiation and same environmental condition, which contains major two elements Copper chloride and strontium chloride. These crystals are identified and characterized by EDAX, FTIR, Thermogravimetry analysis (TGA) and UV visible spectroscopy⁽¹⁾.

2. Materials and Methods

Strontium doped copper tartrate (SCT) crystals were grown in silica gel by employing the test tube diffusion method. Silica gel was prepared by adding sodium meta silicate solution of specific gravity 1.05 gm/cc to tartaric acid (1 M) drop by drop with continuous stirring with a view to avoid excessive local ion concentration which may cause premature local gelling and make the final solution inhomogeneous and turbid. The pH of the gel was adjusted to attain the value of 3.5 to 6. This gelling mixture was allowed to set in glass tubes of 20×2.5 cm. The gel was found to set in about 4 days. After ensuring firm gel setting, a mixture of aqueous solutions of strontium chloride (0.5 M) and copper chloride (1 M) was poured above the set gel with the help of a pipette, so as to allow the solution to fall steadily along the wall of the tube to prevent the gelled surface from cracking. The supernatant solution diffuses into the gel column and reacts with the inner reactant, giving rise to the formation of strontium doped copper tartrate crystals. The crystals were harvested after a month. All the chemicals used were of AR grade^(1,3,4).



Fig.1. Growth of SCT crystals various radiation



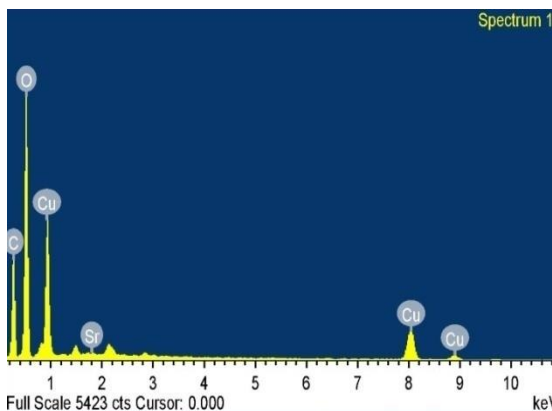
Table(1).Optimum condition for growth of SCT

Conditions	SCT
Density of sodium meta silicate	1.05 gm/cm ³
Concentration of <u>Tarttric acid</u>	1 M
pH of the mixture	4.5
Concentration of CuCl ₂	1 M
Concentration of SrCl ₂	0.5 M
Room temperature	28 C
Period of growth	4 weeks

3. Result and Discussions

3.1 Energy Dispersive X-ray analysis

In order to confirm the presence of the elements in the grown SCT crystals, the sample of grown crystals were subjected to Energy Dispersive X-ray analysis. The obtained spectrum confirms the presence of strontium and copper. The elemental analysis of strontium doped copper tartrate crystals were shown in figure 3a, 3b and 3c. Table gives the observed and calculated atomic/weight% of strontium doped copper tartrate crystals^(2,3,4).



Crystals	Elements	Atomic	Weight%
Without	Cu	10.81	19.52
	Sr	0.04	0.09
CFL	Cu	11.37	33.64
	Sr	0.02	0.10
LASER	Cu	11.35	26.05
	Sr	0.04	0.11

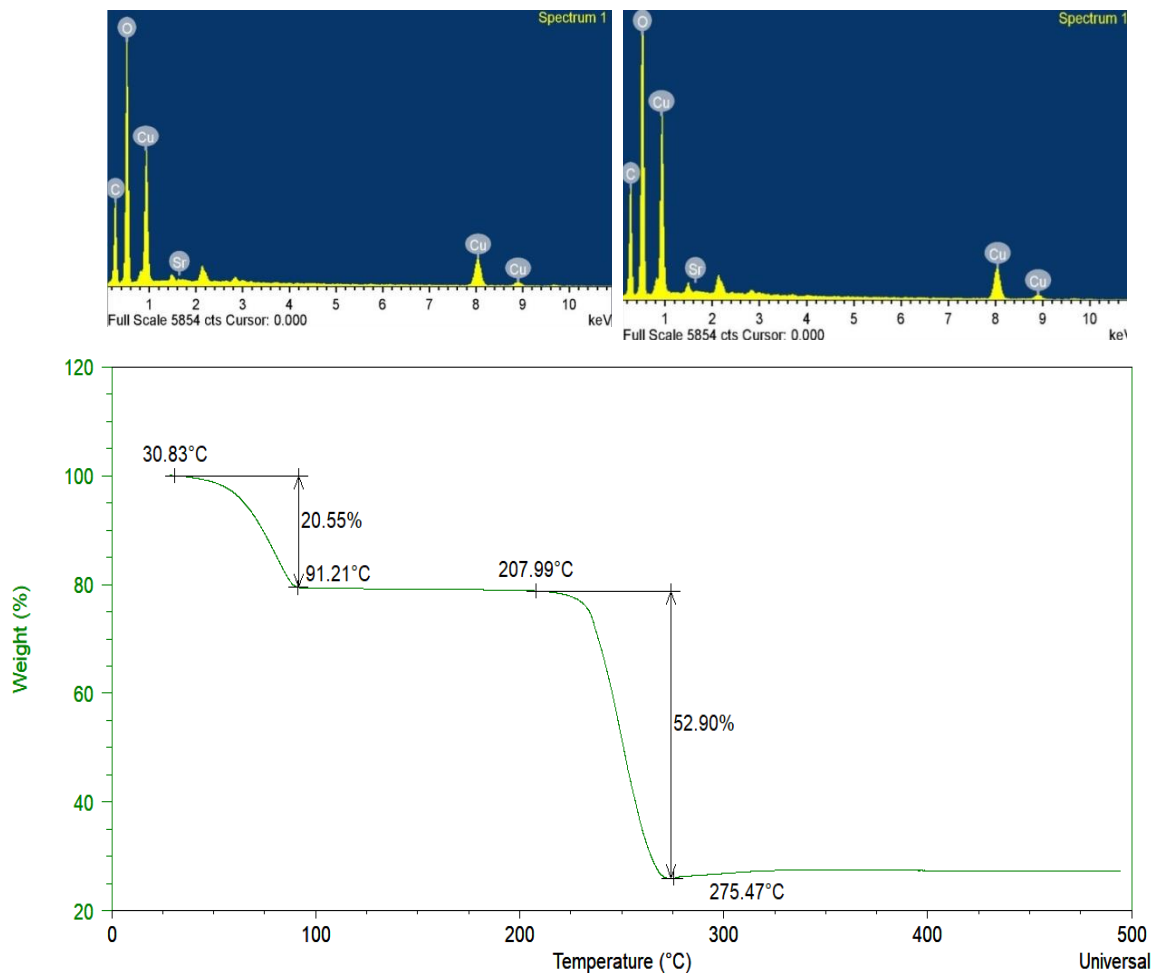


Fig.3b . CFL

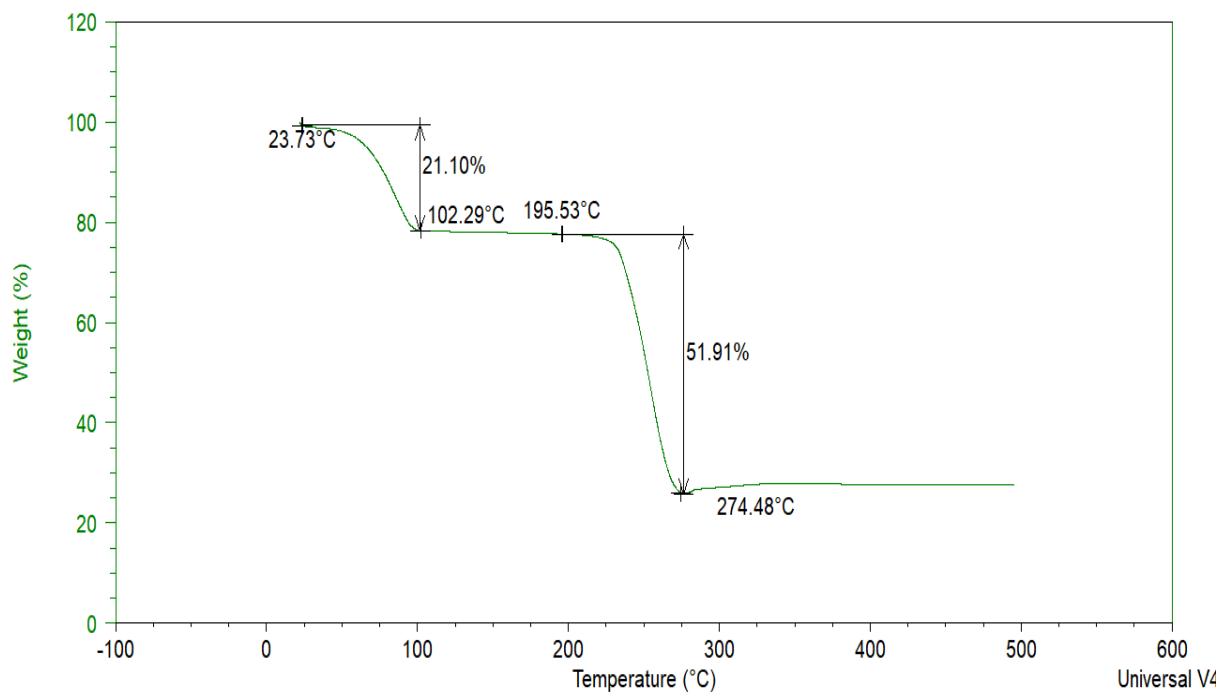
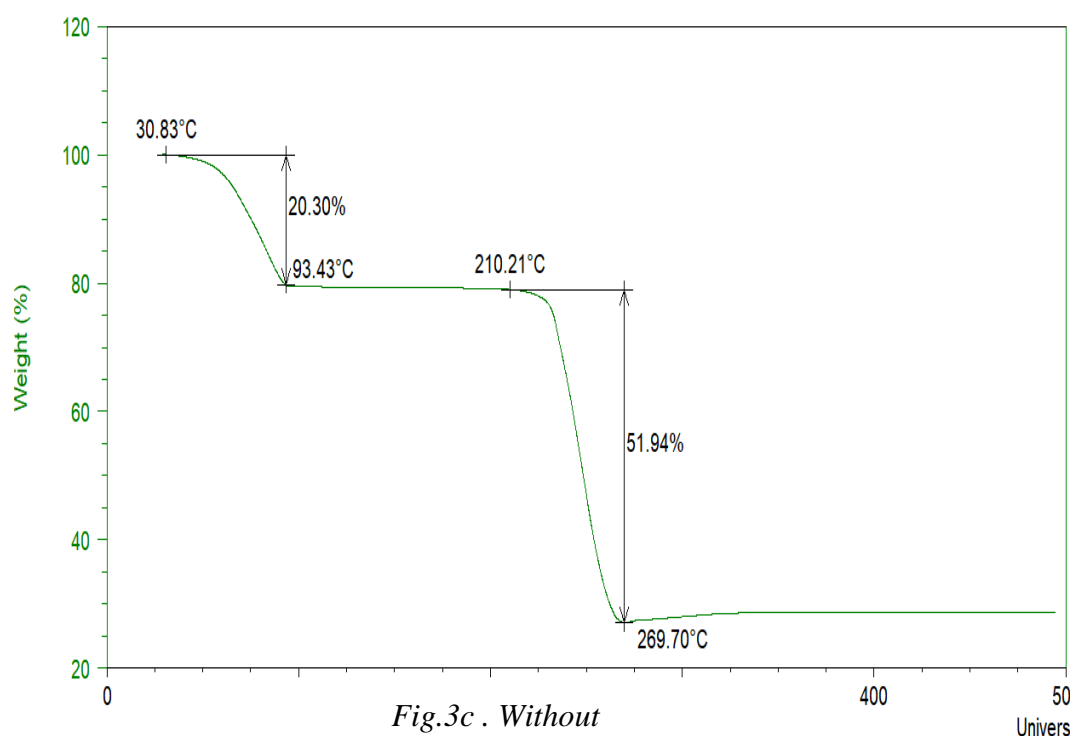


Fig.3b . CFL



The thermal decomposition of the crystals occurs in two stages between of 23-495°C. Decomposition of the sample at 23°C and terminates at 276°C. There are two stages of decompositions. At first stage the crystal loss water and become anhydrous in the temperature range of 23 to 103°C. Then it decompose into carbonate at the temperature range of 195 - 276°C^(1,4,7). The weight losses of strontium doped copper tartrate with various radiations were tabulated below.

Table 2: The weight loss of strontium doped copper tartrate with various radiations

Sl. No	LASER RADIATION		CFL LIGHT RADIATION		WITHOUT RADIATION	
	Temperature Range °C	Weight loss %	Temperature Range °C	Weight loss %	Temperature Range °C	Weight loss %
1	30.83-91.21	20.55	23.73-102.29	21.10	30.83-93.43	20.30
2	207.99-275.47	52.90	195.53-274.48	51.51	210.21-269.70	51.94

3.2 FTIR

The FTIR spectra recorded for the grown crystals are shown in Figure.5. Due to the small dopant concentration, there is no significant difference observed for the doped crystals. The functional groups identified from the FTIR spectra confirm the material of the grown crystals as strontium doped copper tartrate. The O-H stretching frequency due to free water symmetry appears at around 3356 cm^{-1} and 2925 cm^{-1} indicating the presence of water in all the crystals considered. The strong C=O stretch is found at around 1399 cm^{-1} . The bending mode of water was observed at around 425 cm^{-1} . C-C asymmetric strong stretching was observed in the range 1451 cm^{-1} . The asymmetric stretch of water has been observed at around 1310 cm^{-1} (4,6,8).

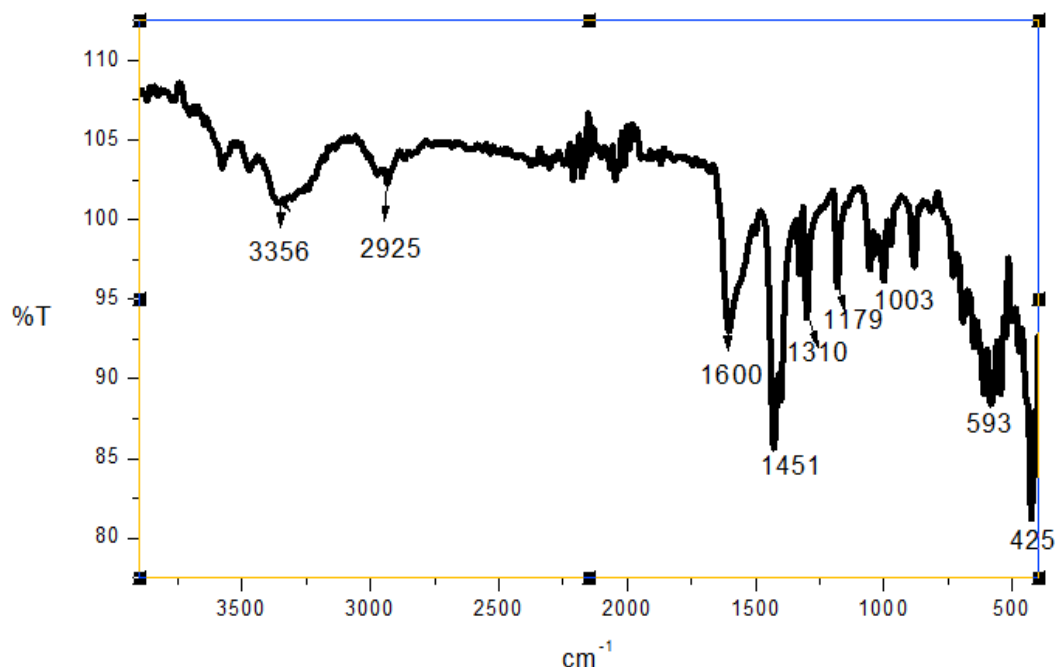


Fig.5. FTIR spectrum of SCT crystal

Table 2: Wavenumbers and corresponding peak assignments

Wave numbers (cm^{-1})	Peak assignments
3356-2925	O-H stretching
1600	C=O stretching
1310	O-H
1451	C-C stretching

3.3 UV-VIS-NIR

UV-VIS spectrum of SCT crystals were found to be active in the Visible and UV region having a significant absorption in the lowest cut off wavelength of 445 nm were shown in figure 6. In the high photon energy region, the energy dependence of absorption coefficient

$$\alpha = \frac{2.303}{t} \log \frac{I}{I_0}$$

where ‘t’ is the thickness of the crystal sample. Absorption coefficient ‘α’ suggests the occurrence of direct band gap of the crystal obeying the following equation for high photon energies (hv),

$$(\alpha h\nu)^2 = A(E_g - h\nu)$$

where ‘α’ is the absorption coefficient, ‘h’ is the Plank’s constant, ‘A’ is a constant ‘ν’ is the frequency of the incident photon and ‘E_g’ is the optical band gap. The Tauc’s graph plot between $(\alpha h\nu)^2$ and the photon energy ($h\nu$) is shown in figure 6b. The extrapolation of the linear part of the graph gives the optical band gap energy value to be 6.2074 eV, this wide band gap of SCT crystals confirms the transparency in the visible range^(5,6,7,8).

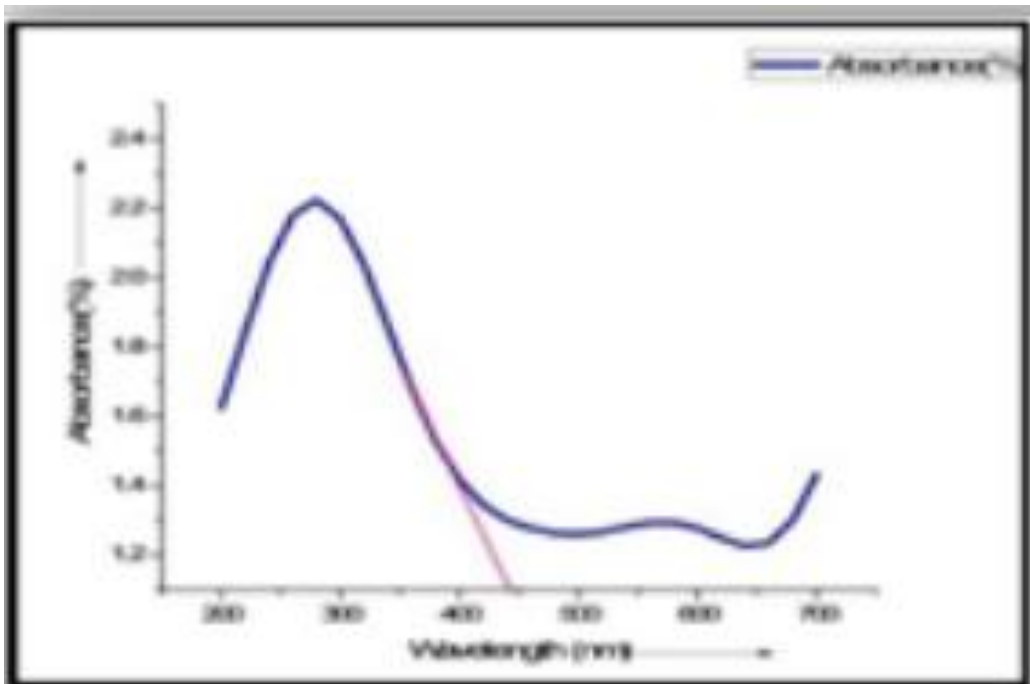
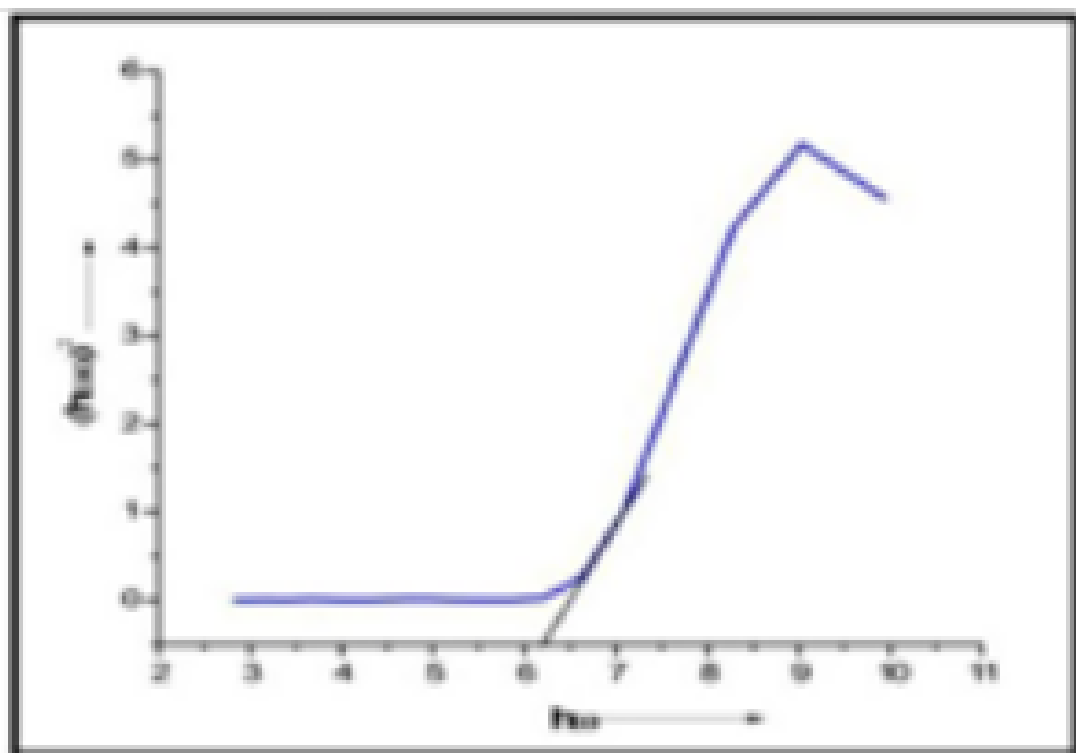


Fig.6a UV-Vis-NIR Absorption spectrum.



6b. $h\nu$ vs $(ah\nu)^2$ of SCT crystal.

4. Conclusion

Strontium doped Copper tartrate single crystals were grown by the silica gel method. The optimum conditions were identified by varying different parameters. FTIR and EDAX spectral studies confirm the presence of expected functional and metal-oxygen bonded groups of as grown crystal. The band gap energy, wide transparent nature indicates that the SCT crystals were insulators and suitable for the fabrication of materials for opto-electronic devices. The thermal stability was studied by the TGA supporting its application in the electronic industries.

Acknowledgements

The authors are thankful to the scientific officer DST-PURSE laboratory Mangalore University, Chairman Department of studies in Physics Mangalore University, Director USIC Mangalore University for providing facilities for the characterization and technical support to carry out the work.

References

- [1] G. Kanchana, P.sundaramoorthi and G P Jeyanthi *Journal of Minerals & Materials Characterization & Engineering*, VOL.8, No.1(2009) pp 37-45.
- [2] M. Mary Freeda, T H Freeda and Mary Delphine *Asian Journal of Chemistry* Vol 25, No.4(2013),1863-1865.
- [3] Quasim,A.Firdous, B.want, S.K.KhosaD.N.Kotru *.Journal of crystal growth* 310(2008)5357-5363.
- [4] P. Sudaramoorthi, et al., *Asian J. Chem.* 19 (2007) 2783–2791.
- [5] H.K. Hnisch, J.M. Garcia-Ruiz, *J. Cryst. Growth* 75 (1986) 195.
- [6] K. P. Nagaraja , K. J. Pampa, N. K. Lokanath, *Studies on Growth, Optical, Electrical and Dielectric Properties of Strontium and Calcium Mixed Cadmium Oxalate Crystals*, *J. Applicable Chem.*, 7(2)(2018)457-466.
- [7] Delma D'Souza, N. Jagannatha, K. P. Nagaraja, P. S. Rohith, and K. V. Pradeepkumar,*Growth and characterization of divalent transition metal ions doped zinc hydrogen phosphate single crystals*. *American Institute of Physics*1953(2018) 070023.
- [8] P.S. Rohith, N. Jagannatha and K.V. Pradeep Kumar, *Studies on Thermal and Spectroscopic Properties of Magnesium Doped Single Crystal*.*J. Applicable Chem.*, 7 (4) (2018)1033-1039.

Effect of Barium Incorporation on Thermal and Optical Properties of Copper Mixed Cadmium Oxalate Single Crystals

P. S. Rohith¹, N.Jagannatha², K.V. Pradeep Kumar³, Delma D'Souza⁴, K B Reema⁵

¹Post Graduate Department of Physics, FMKMC College, Madikeri, Mangalore University
Constituent College, Karnataka, India

Corresponding author (N.Jagannatha): jagannathnettar@yahoo.co.in

Abstract

Single crystals of Barium doped copper cadmium oxalate (BCCO) were grown in silica hydro gel media. Specific gravity of Sodium Meta Silicate (SMS), gel setting time, pH of the gel, concentrations of Oxalic acid and concentration of supernatant solutions were varied to establish the optimum conditions for growth. Powder X-ray diffraction (P-XRD) studies showed that BCCO crystals belong to triclinic system. Energy Dispersive X-ray (EDX) measurements predicted the matrix of Ba²⁺ ions with parental CCO crystal. FTIR spectral studies confirmed the presence of Oxalate group, water molecules and metal oxygen link in BCCO crystals. Thermo Gravimetric Analysis (TGA) showed the thermal stability of the crystals in their anhydrous state. From UV visible Spectrophotometric studies, band gap energy measured was 6.09eV for BCCO crystal.

Keywords: Gel Grown Crystal, CCO, BCCO, XRD, TGA, EDX

1. Introduction

The more ordered form of solids are crystals and these crystals are appropriate in understanding physical, chemical and optical properties of solids[1]. In the field of semiconductor laser diodes and various optoelectronic devices the doped crystals are having great importance and they have vast application in it. The thermal stability and band gap energy found applications in optoelectronic industries can be explained by the Thermo gravimetric analysis (TGA) and optical characteristics of oxalates. One of the main property of oxalate is that they are insoluble in water and which is useful in separating the transition elements from the mineral as oxalates precipitate. Quality and perfectness of the grown single crystals is the main advantage in growing oxalate crystals by single diffusion gel method. In

semiconductor industries importance is given to doping and mixing of impurities to intrinsic crystals by various crystallization processes. Nano crystals of Barium doped oxalate crystals show semiconducting properties find their applications in high temperature electronics [2]. More importance has been given to alkaline earth ion doped crystals since the dopants enhances their physical properties. Ultimately, the present study mainly focused to study the growth of **barium** doped copper cadmium oxalate (BCCO) crystals, their Thermal and Optical properties.

2. Experimental

2.1 Crystal growth

The crystal growth of BCCO were done using single diffusion silica hydro gel method. Na_2SiO_3 (SMS) solution with different specific gravity were prepared and acidified by 0.5 N oxalic acid to set the silica gel. After setting the gel, upper reactants (barium chloride, copper chloride and cadmium chloride) of desired molarities were poured over the gel surface without disturbing the gel. Nucleation starts within a minute and cations from the supernatant solution diffused into the gel through fine pores in the gel. A thick blue precipitate was formed, below which small crystals appeared and slowly starts to move down in the gel. The crystals become rectangular and gain maximum size in about 3 weeks.

Table 1. Optimum condition for growth of CCO and BCCO crystal Figure. 1. Growth of CCO and BCCO single Crystals: (a) formation in silica gel CCO, BCCO (b) Photograph of as-grown CCO crystal c) Photograph of as-grown BCCO crystal

Various Parameters	Optimum Condition
	BCCO
Density of sodium meta silicate	1.04
pH of gel	4.5
Concentration of CdCl_2 and CuCl_2	1M
Concentration of BaCl_2	0.5M
Gel setting period	8 days
Gel aging	48 hours
Period of growth	15 days
Quality	Transparent

The experiment was repeated by varying the growth parameters. The specific gravity of the gel were varied between 1.02 to 1.06 and specific gravity of 1.03,1.04 yields good single crystals of maximum size. pH of the gel were varied from 4 to 8 . pH values below 5 yields good quality single crystals. Thickness of the blue precipitate increase, size of the crystals reduced with increase of pH above 5. Concentration of oxalic acid were varied from 0.2N to 0.8N, low molarities of oxalic acid reduces the number of crystals. Concentration of barium chloride, copper chloride and cadmium chloride were varied from 0.2N to 1.5N to observe the changes in crystallization. The number of crystals and size of the crystals were very less at higher concentration of the reactants.

The optimum conditions for obtaining good quality crystals are recorded in Table 1. The growth set up and grown crystals of CCO and BCCO are given in Figs. 1

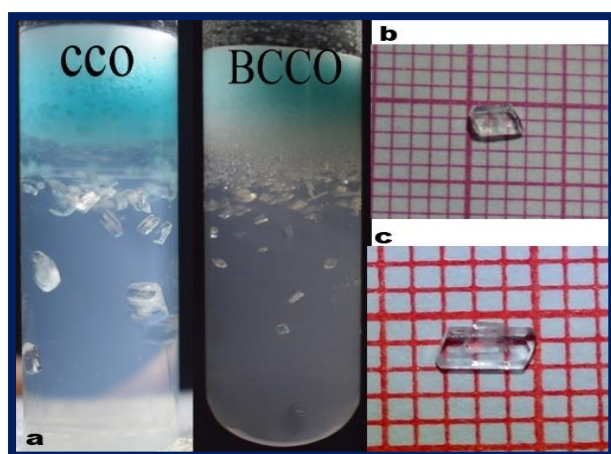


Fig. 1. growth set up and grown crystals of CCO and BCCO

2.2 Characterization

Elemental composition of the grown crystals was determined using CARL ZIESSFESEM attached with EDS system (Oxford instruments). EDX analysis is used for chemical characterization of materials to detect chemical elements present in nanometers depth from the surface of crystal. Functional groups of crystals are identified using Bruker (Alpha). FTIR analysis (using FTIR spectrophotometer within the wave number range $400\text{-}4500\text{ cm}^{-1}$) is the spectroscopic technique used for analyzing the structural units of samples from their vibrational modes. Thermal properties of NZP and

CNZP crystals are studied by TGA using DSC-TGA TA (SDT-Q600) instrument. TGA finds the percentage weight loss of a sample for the increase in temperature. Powder XRD studies of the crystals are carried out with the aid of powder XRD analyzing instrument Minflex 600 Rigaku having X-ray Cu-K alpha of wavelength 1.54 \AA at a scan speed of 10 min^{-1} . Optical absorption studies are carried out using UV-Visible Spectrophotometer (UV-1800 SCHIMADZU) in the spectral range 190-1000 nm. Electrical conductivities of the crystals are measured using Roy instruments (IR-503, Sl. No.CDM-17076) operating in the range of $0\text{-}1000 \text{ mMho cm}^{-1}$.

3. Results and Discussion

3.1 X-ray diffraction analysis

Powder XRD patterns of BCCO crystals show well defined peak at specific 2θ values, exhibit high crystalline nature of the grown crystals (Figure 2). Observed XRD pattern of the crystals were indexed using N-TREOR09 program. Obtained d -spacing and the Miller indices are in agreement with the standard values (JCPDS data).

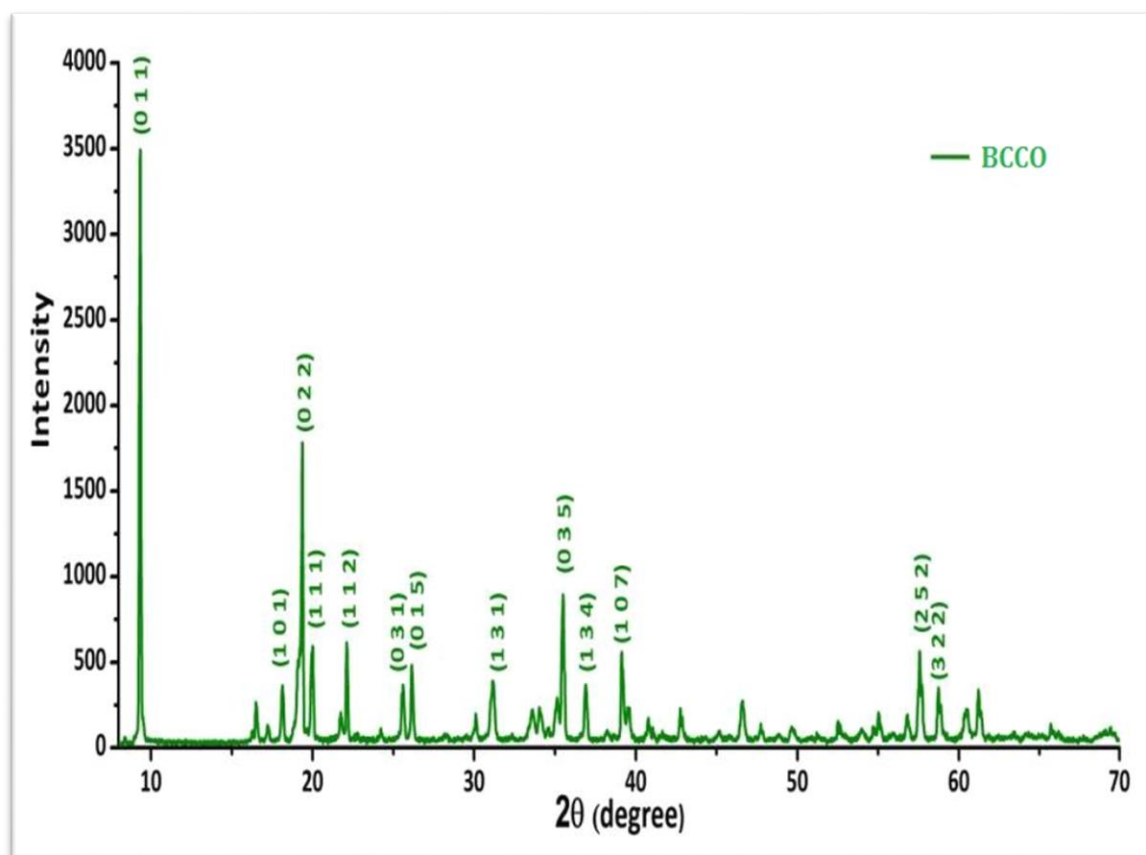


Figure 2. Powder XRD patterns of BCCO crystals.

3.2 FTIR analysis

FT-IR vibrational spectra of CCO and BCCO (Fig. 3) crystals grown in silica gel exhibits strong absorption peaks in between 3400 and 3500 cm^{-1} , which is due to OH stretching vibrations of water [3-4]. On adding Barium as dopant, the shift in the band from its usual position to the lower wave number side was observed, which may be due to the OH bond weakness caused by the interaction of the additionally added metal ion Ba^{2+} in the crystal lattice. The bands at approximately 1600 cm^{-1} were attributed to the C=O stretch of the carbonyl group and the peaks at around 1300 cm^{-1} was assigned to C=O symmetric and O=C=O modes[5]. The bands below 800 cm^{-1} were due to metal–oxygen bonds [6]. As seen, Barium -doped CCO has more number of absorption bands in the lower wave number region ($<800 \text{ cm}^{-1}$), which reveals the incorporation of barium ions in the crystal lattice forming additional metal–oxygen (Ba–O) bonding [7-8].

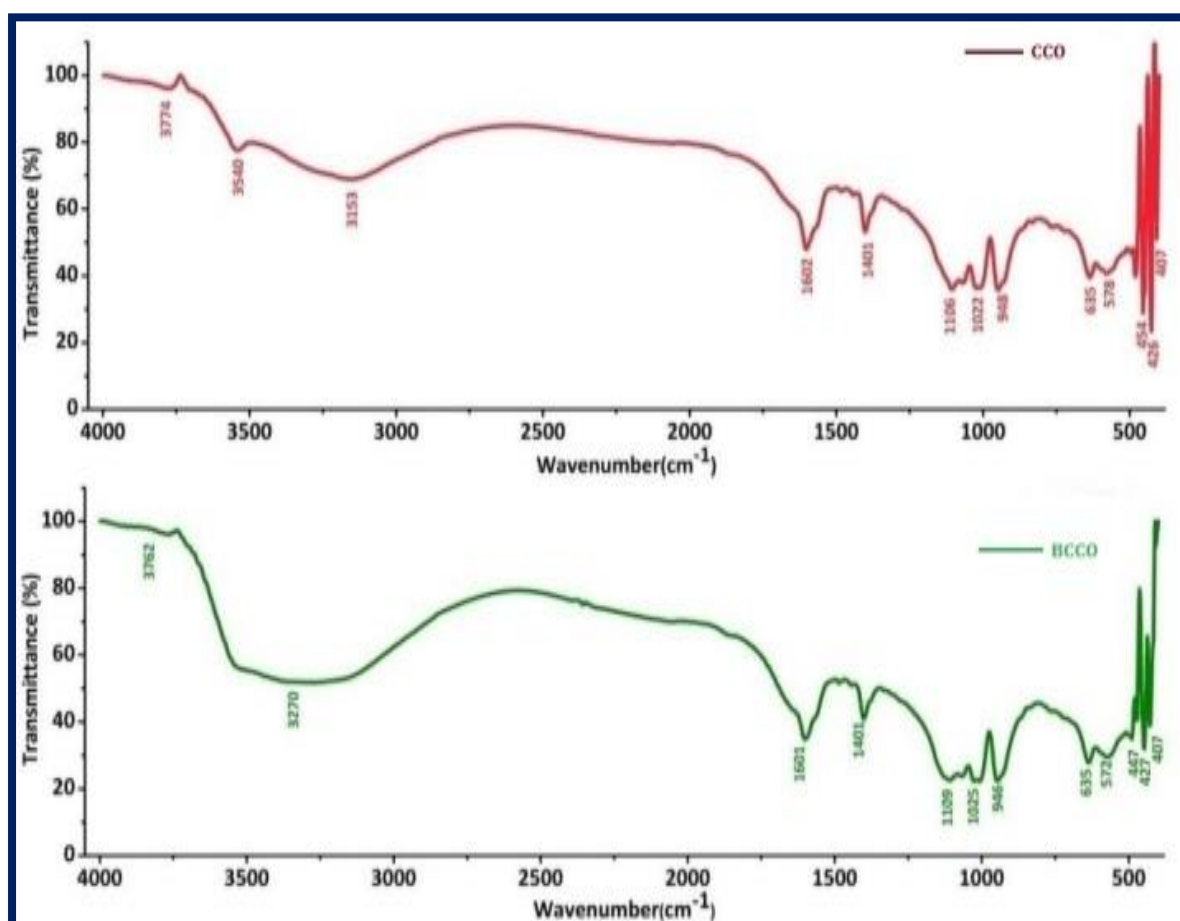


Figure 3: FTIR spectrum of the gel grown crystals

3.3 EDX analysis

Figure 4 illuminates the electron images of CCO and BCCO crystals. EDAX measurements confirmed the existence of impurity cations Ba^{+2} occupying the vacancies of some parental Cd^{+2} ions within the lattices of CCO and BCCO crystals (Figure 5). Characteristic peaks observed in the spectra establish the incorporation of elements O, C, Cu and Cd in CCO and O, C, Cu, Cd and Ba in BCCO crystals respectively. Atomic and weight percentage of elements present in the crystals are listed in Table 2.

Table 2. Atomic and weight percentages of constituents of CCO and BCCO crystals.

Crystal	Elements	Atomic %	Weight %
CCO	C	31.18	41.11
	O	62.37	109.51
	Cd	6.22	76.79
	Cu	0.22	1.55
BCCO	C	30.84	31.59
	O	61.68	84.17
	Cd	7.61	72.94
	Ba	0.01	0.08
	Cu	0.14	0.74

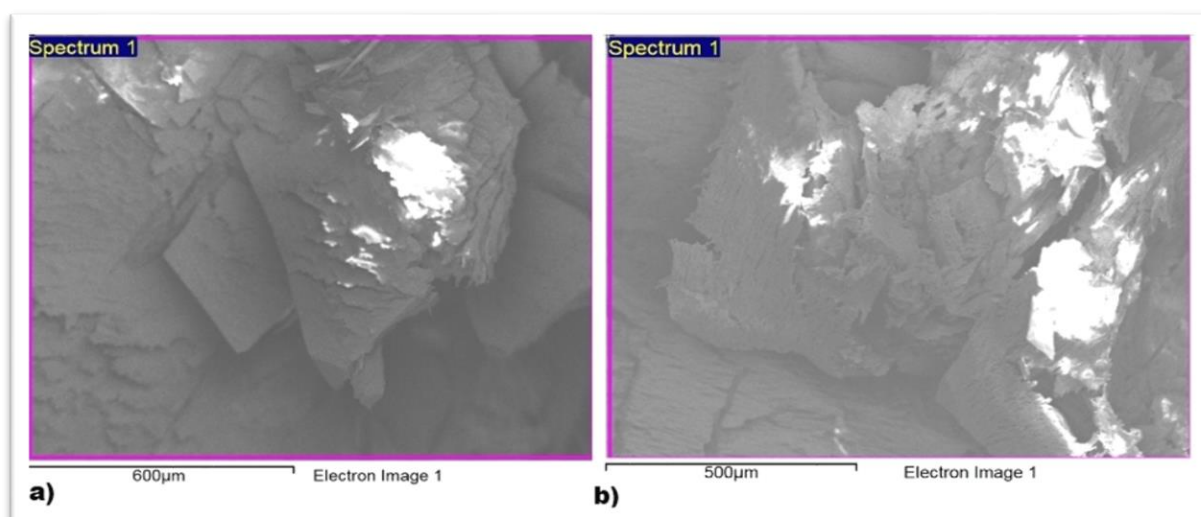


Figure 4: SEM images of (a) CCO and (b) BCCO crystals.

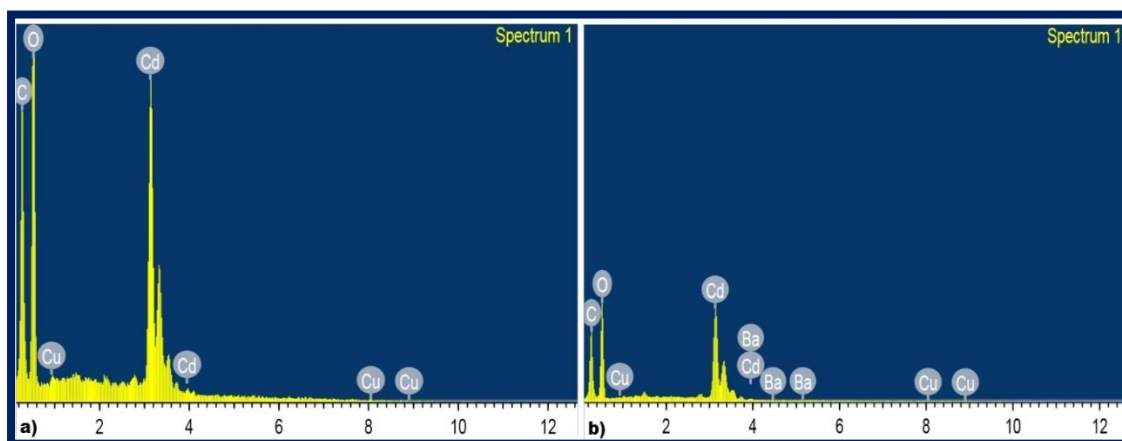


Figure 5: EDAX spectra of (a) CCO and (b) BCCO crystals.

3.4 Thermal Properties

The TG plot of CCO revealed that the decomposition occurs in two stages in the temperature range 44–350°C (Figure 6(a)). The first step of thermal decomposition occurs in the temperature range of 44–130°C with measured weight loss of 21.78% (calculated loss: 21.24%) with the loss of three water molecules. The dehydrated CCO crystal further decomposed at 240–380 °C with a weight loss of 28.57% (calculated loss: 28.318%) losing CO and CO₂ simultaneously. On heating above 380°C the crystal shows stability until 950°C. In the final stage, the material is reduced to its oxide state (>950 °C).

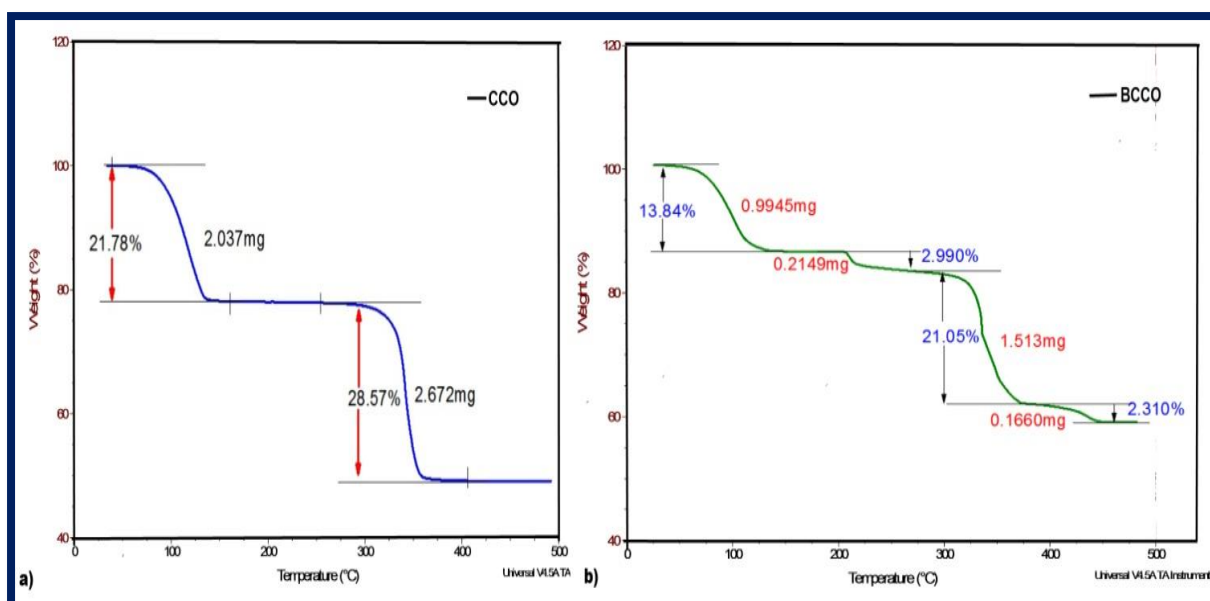


Figure 6: The TG plot of (a) CCO and (b) BCCO crystal

The TG plot of BCCO crystal is shown in Figure 6(b). The decomposition occurs in four stages in the temperature range 44–460°C. The first step of thermal decomposition occurs in the temperature range of 44–127°C with measured weight loss of 13.84% (calculated loss: 13.25%) with the loss of three water molecules. The second stage of decomposition occurs in two steps in the temperature range of 190 °C - 400 °C with a weight loss of 24.04% (calculated loss: 24.325%). Third stage of decomposition occurs in the temperature range 400–450°C with a weight loss of 2.310% (calculated loss: 2.325%).

3.5 Optical properties

Optical studies (using UV visible spectroscopy) of parental CCO and doped BCCO crystals were carried out for the wavelength range 190nm to 1000nm of the incident photons. UV visible absorption and transmittance spectra CCO and BCCO crystals are displayed in figure 7. CCO crystal shows absorption in the range 190nm–270nm (correspond to UV region) with absorption maximum (A_{\max}) of 0.07. However, BCCO crystal can absorb light in the wider range from 190nm–400nm with A_{\max} 0.30.

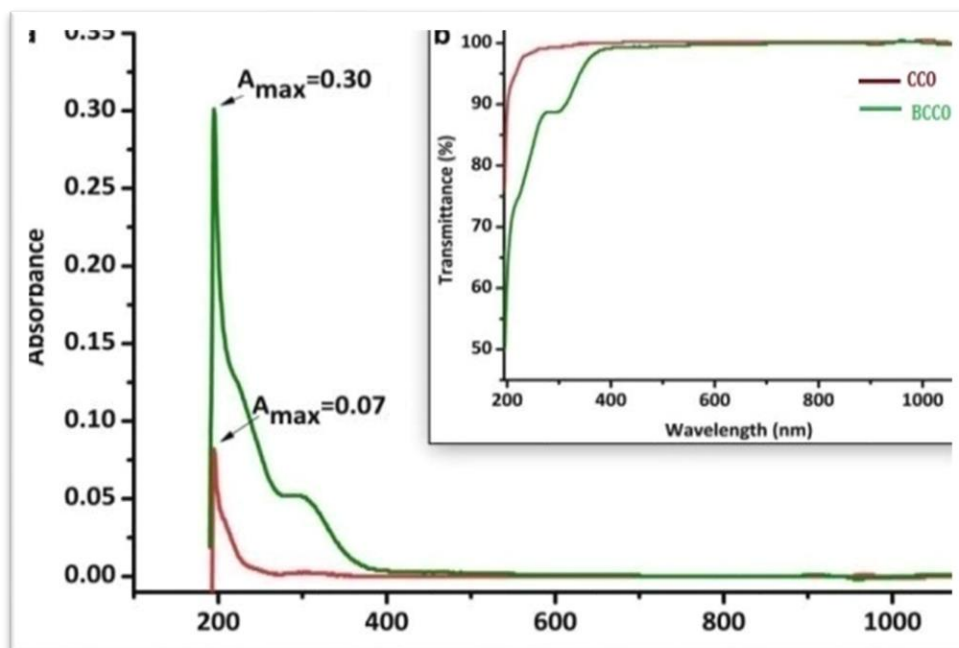


Figure 7 : UV visible absorption and transmittance spectra.

Further, for the entire visible region both the crystal shows maximum transparency. The spectra is regenerated as Tauc plot to find the energy gap (Figure 8). Band gap energies of CCO and BCCO crystals are 6.15eV and 6.09eV respectively. This elucidates the

insulating behaviour of crystals [9-10]. The difference in band gaps of the crystals suggests that two crystals are distinct. Thus reinforcement of Ba^{2+} ion with parental CCO crystal resulted in the growth of entirely new crystal (BCCO). This enumerates the success in growth and studies of BCCO crystal. One can expect more electrical conductivity in BCCO crystal due to smaller energy gap.

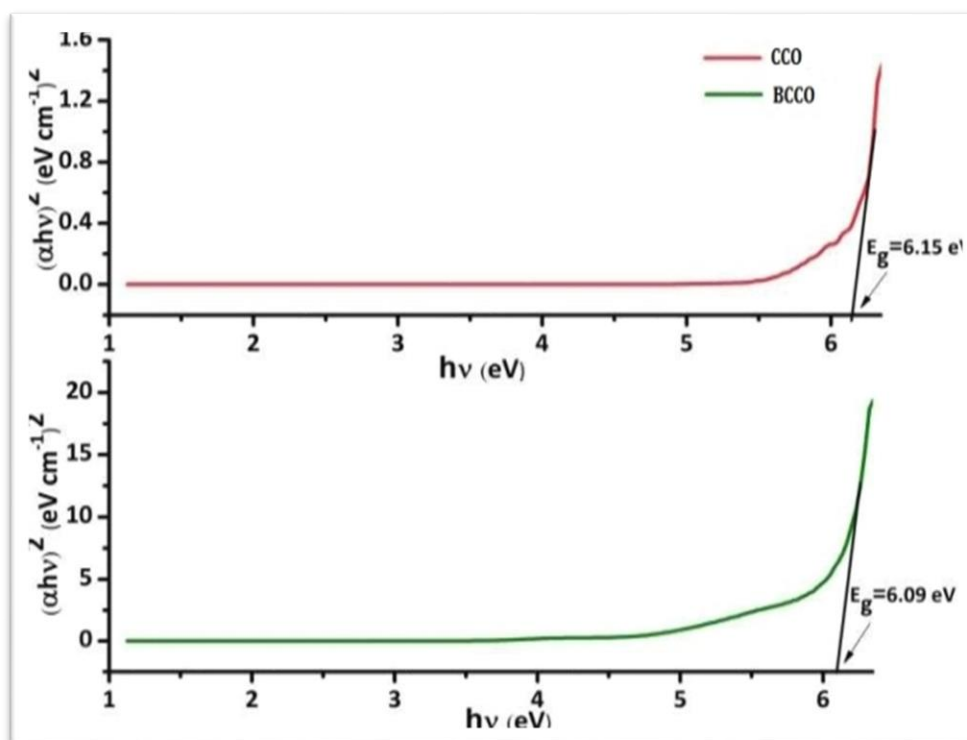


Figure 8: Tauc plot of CCO and BCCO to find the energy gap CCO and BCCO crystal

3.6 Application

The studies on properties of CCO and BCCO crystals showed high band gap energies and higher thermal stability. These results confirm that the as-grown crystals were used as dielectrics in printed circuit boards, electronic and microelectronic devices, then they would provide better electrical and physical properties.

4. Conclusion

Barium doped Copper Cadmium Oxalate single crystals were grown by the gel method. Powder XRD reveals the crystalline properties of as-grown crystal. FTIR & EDAX spectral studies confirm the presence of expected functional and metal-oxygen bonded groups of as-

grown crystal. The thermal stability were studied by the TGA/DTA supporting its application in the electronic industries. UV visible spectrophotometric studies confirm that the crystal is an insulator.

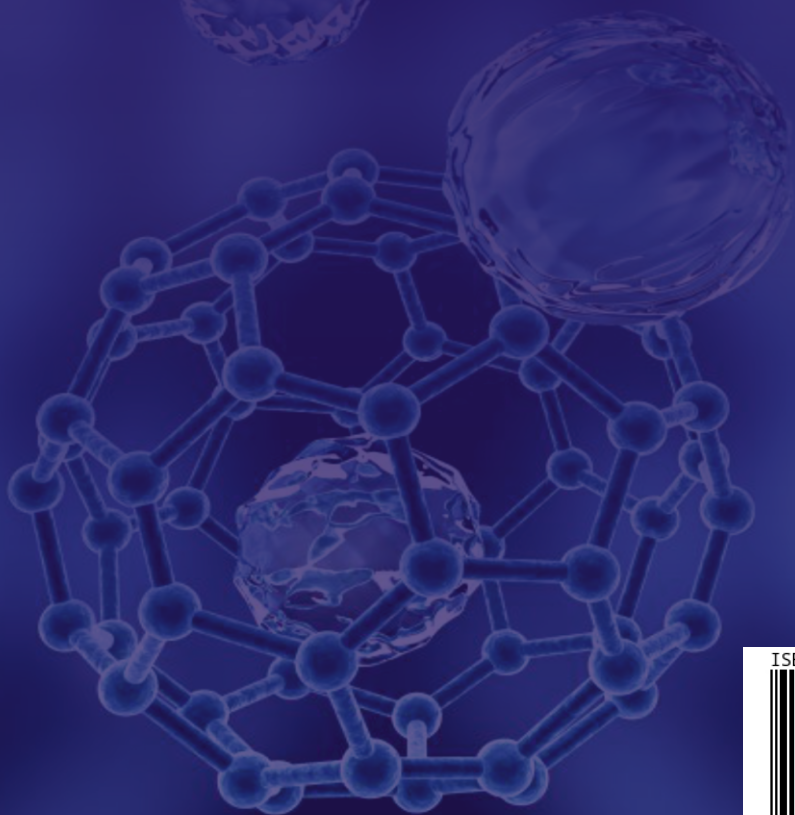
Acknowledgements

The authors are thankful to the Coordinator, DST FIST and UGC SAP, Department of Physics, Mangalore University, for providing facilities for the characterization of thin films and technical support to carry out the work.

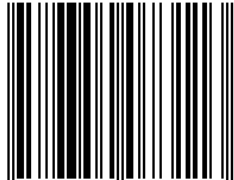
References

- [1] H. K. Henisch. Crystal growth in gels, The Pennsylvania State Univ. Press, USA **1970**.
- [2] S.M.Dharmaprakash, P. Mohan rao, Periodic Crystallization of Barium oxalate in silica hydrogel, *Bull.Mater. Sci.*, (**1986**), 8, 511.
- [3] E.D. Bacce, A.M. Pires, M.R. Davaios, M. Jafellicci Jr. “Thermal decomposition and rehydration of strontium oxalate: morphological evolution” .*Inter. J. Inorg. Mater.*3(**2001**) 443.
- [4] Daisy Selasteen F., Alfred Cecil Raj S., Alagappa Moses A., Emalda Prince F., Esther Getsy R., Elakkiya R. “Synthesis, growth and characterization of Sodium mixed Cadmium oxalate crystals.”*J. Cryst. Pro. Technol.* 6(**2016**) 11-20.
- [5] N.Jagannatha, P. Mohan Rao, Studies on Impurity Incorporation in cadmium growth of cadmium oxalate single crystals in silica gels, *Mater Chem. Phys.*, (**1998**) 52, 263.
- [6] T. P. Jyothi, H. R. Manjunath, M. K. Ravindra, M. K. Shivanand, K. M. Mahadevan, N. K. Lokanath, S. Naveen, Synthesis, Characterization and Crystal Structure Analysis of 2-(1-(4-butylphenyl)- 4,5- diphenyl-1H-imidazol-2-yl)-4-chlorophenol,*J. Applicable Chem.*,(**2018**), 7(1), 224-233.
- [7] Latha Rani N., Shivaprasad Shetty, Anil Kumar N.V., Sridhar M.A. “ Synthesis, Spectral Study and Crystal Structure Analysis of Two CoumarinDerivatives”.*J. Applicable Chem.* 7 (1)(**2018**) 59-70.
- [8] Kale M. R.,Tendolkar N. P. “Super-Capacitive Properties of Electro- Synthesized Nanocrystalline Nickel Ferrite Thin Films Deposited from Non-Aqueous Bath”. *Engineering Sciences International Research Journal* . 1 (2013)2330 – 4338.

- [9] Ignatius Korah, M.A. Cyriac Joseph, Ittyachen, Growth and structural characterization of Gadolinium Neodymium oxalate crystals grown in hydro-silica Gel, *J. Min. Mater.Char.Engin.*,(2010), 9, 1081-1086.
- [10] Raj, A.M. E, Optimized growth and characterization of cadmium oxalate single crystals in silica gel, *Sol. St. Sci.*, (2008), 10, 557-562.



ISBN 978-93-5407-311-3



9 789354 073113